Summer 1978

A Computer Model for Comparison of Flat Plate and Focusing Collectors for Solar Air Conditioning

H. B. Bucher
University of Central Florida

A COMPUTER MODEL FOR COMPARISON OF FLAT PLATE AND FOCUSING COLLECTORS FOR SOLAR AIR CONDITIONING

BY

H. B. BUCHER, JR.
B.S.E., Florida Technological University, 1973

RESEARCH REPORT

Submitted in partial fulfillment of the requirements
for the degree of Master of Science: Engineering
in the Graduate Studies Program of the College of Engineering
of Florida Technological University at Orlando, Florida

Summer Quarter
1978

ABSTRACT

Two types of solar collecting systems are frequently employed--flat plate collectors with spectrally selective windows which trap sunlight with the "greenhouse effect" and focusing systems with curved mirrors which concentrate the sun's rays on an absorbing surface. The flat plate collector is the simpler of the two designs, but cannot readily provide temperatures as high as the focusing collector. Both of these collectors are candidates for absorption cycle solar air conditioning systems. This role dictates higher temperatures than are normally required of solar collectors, particularly the flat plate design. Focusing systems of interest here are those which are fixed in orientation and require no elaborate solar tracking mount. Such collectors might be economically competitive with flat plate configurations if the higher energy "quality" or delivery temperature they can provide permitted a smaller installation than would be possible with a flat plate collector. An analysis of the two collector candidates is undertaken here to assess the merits of a fixed orientation focusing collector and a more traditional flat plate system. This analysis indicates that the focusing design is superior to the flat plate for solar air conditioning.

The study of the two designs includes selection of system configurations and the development of their mathematical descriptions.

The analytical approach was to incorporate mathematical models of the collectors into a computer program which predicts the performance of both the flat plate and focusing systems. The program has been designed to permit convenient variation of important parameters so that their effect on collector performance may be determined. The results of the collector analysis and the computer program are presented with sufficient information to permit the reader to use the program for his own analyses.

TABLE OF CONTENTS

LIST OF TABLES

LIST OF ILLUSTRATIONS

LIST OF VARIABLES

A	Diffuse Radiation Intensity Scale Factors
A_C	Flat Plate Collector Area
A_R	Area of Reflector in Focusing Collector
A_S	Area of Shadow Cast on Reflector
C	Matrix for Coordinate Transformation
COP	Air Conditioner Coefficient of Performance
C_P	Fluid Specific Heat
f	Thermostat Throttling Fraction
f_B	Transmission of Beam Radiation through Atmosphere
f_{SEL}	Spectral Selectivity Factor of Material
G	Total Radiation Power Striking a Surface
h	Effective Height of Atmosphere, Thermal Convection Film Coefficient
J	Total Radiation Power Leaving a Surface
k	Thermal Conductivity
m	Air Mass
$\dot{m}$	Mass Flow
P_B	Thermal Gain from Beam Radiation
P_D	Thermal Gain from Diffuse Radiation
$\dot{q}$	Thermal Power
Q_C	Thermal Energy Removed from Refrigerated Area

Q_H	Thermal Energy Collected
R	Earth Radius
s	Solar Ray Path Length
T	Temperature
$\overline{U}$	Unit Vector
W	Carnot Work in Reversible Air Conditioning Cycle
W_B	Beam Radiation Flux
W_D	Diffuse Radiation Intensity
W_{SC}	Solar Constant
α	Absorptivity of Material
α_D	Non-dimensional Diffuse Radiation Pattern
$\alpha\tau$	Product of α and τ
β	Angle of Incidence
γ	Normalized Earth Radius
Δ	Solar Declination Angle
ε	Emmissivity of Material
η	Angle of Rotation About an Axis of Interest
θ	Elevation Angle
λ	Collector Latitude
μ	Result of Vector Dot Product
ρ	Reflectivity of Material
σ	Stefan-Boltzmann Constant
τ	Transmissivity of Material
ϕ	Collector Tilt Angle, Radiation Flux
ψ	Aximuth Angle

Ω_E	Angular Rotation Rate of Sun with Respect to Earth's Surface
ω	Space Angle

I. INTRODUCTION

The usual application of a solar collector is the simple heating of water or air for domestic or light industrial purposes. A desirable expansion of the role of a solar energy system would be to provide air conditioning for a home or work area. This application requires thermal energy supplied at higher temperatures than other solar applications. This requirement for "high quality" energy makes the design of the solar collector used in the device crucial to the system's overall performance. Conceptually, a solar cooling mechanism is simple. A working fluid heated in a solar collector is transported to an absorption cycle air conditioning unit where it supplies the thermal energy necessary to drive the device. The air conditioning cycle is identical to that in standard gas-fired or steam-heated absorption units used for both domestic and industrial applications [1]. Heat supplied by the solar collector boils water from a solution, usually containing lithium bromide. The water vapor is then cooled and condensed to a liquid. A low pressure is maintained in the system so that the liquid water acts as a refrigerant, boiling at low temperatures [2].

In practice, several problems complicate the design of a solar air conditioning system. The boiler temperatures of ordinary absorption units are usually in the range of 90° to 120° C (200° - 250° F)[2].

Redesign of the boiler in such a system could permit operation at temperatures as low as 77° C (170° F) with considerable loss of performance [1]. Temperatures as high as this are not generally required for ordinary solar heating applications and require special consideration in the design of the collector. Another problem is the fluctuation of the thermal energy available to the unit during the day. This dictates a conservative philosophy in sizing the solar collector and complicates the control mechanisms required for satisfactory system operation. Finally, the uncertainty in the available solar energy from day to day (or hour to hour) necessitates a "back up" conventional heat source for the device [1]. Clearly, careful analysis must precede the design of a solar air conditioning system, particularly the collector. This paper addresses the effect of collector configuration on the quantity and quality of thermal energy which can be gathered for a high temperature application such as a solar air conditioner.

Two types of solar collectors are often proposed for solar energy systems--the simple flat plate collector and a focusing collector using a cylindrical parabolic mirror. These are the collector candidates considered here. Either type could be used in a solar air conditioner, but a rational choice of one candidate over another requires evaluation of their relative operating performance and cost. The analysis of the operating characteristics of a particular collector, the primary concern of this paper, involves selection of a specific configuration, choice of collector materials, and development of a mathematical description of the collector's thermal environment

and performance. Collector cost is determined by the complexity of its design, and the expense of its materials.

The flat plate collector is a simple device which employs a spectrally selective glass window to trap solar energy with the "greenhouse effect." A heat exchanger within the collector transfers the trapped energy to a suitable working fluid. The orientation of this device is not particularly critical and it traps the diffuse radiation scattered by the atmosphere as effectively as collimated radiation arriving directly from the sun. The large collecting area, exposed to the environment through the glass cover, permits high thermal losses. These losses limit the temperature which can be attained with the flat plate collector. In contrast, the focusing system is fairly complex, having a parabolic mirror which directs reflected radiation to a thermal absorber and heat exchanger located near the focal point of the reflector. While the absorber radiation properties may be spectrally selective, the primary collection mechanism is the concentration of energy on the small absorbing area. A focusing device collects very little diffuse radiation from the sky, deriving most of its energy from collimated beam radiation. Accurate orientation of the collector is very important to insure that the reflected radiation is directed at the absorber.

General construction details of the collectors considered in this analysis are shown in Figures 1 and 2. The flat plate collector configuration, illustrated in Figure 1, is a "classical" arrangement, having a single pane of window glass covering a box containing a plate of absorbant material and heat exchanger tubes [3]. The collector is

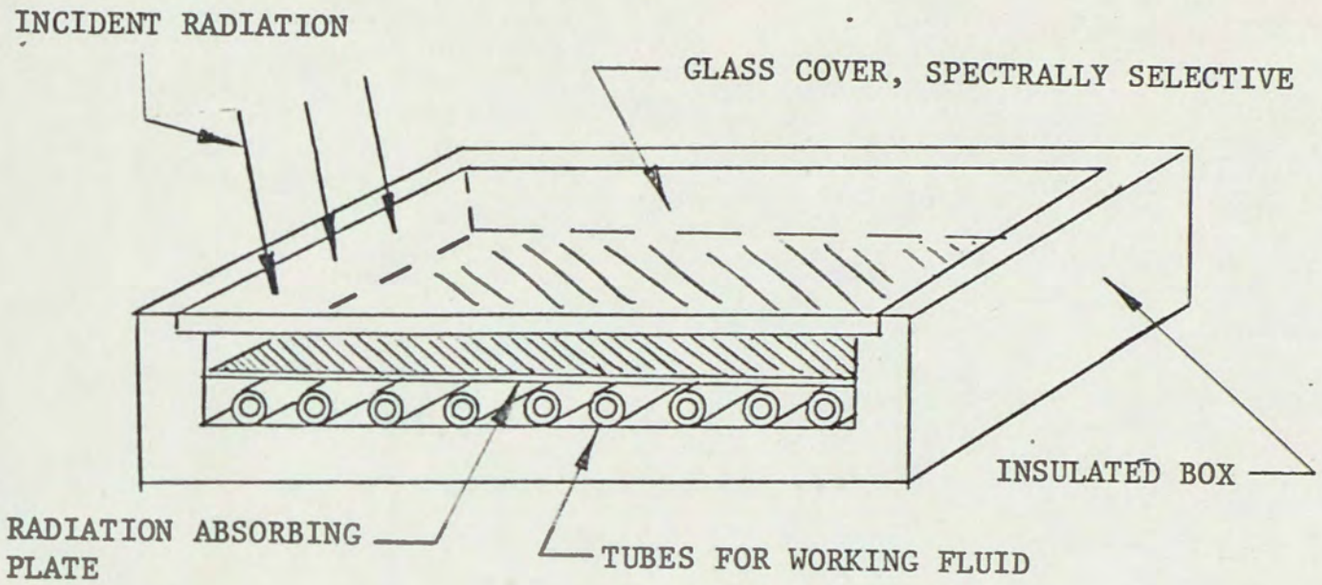

Figure 1. Flat Plate Collector Configuration Assumed for Analysis [4]

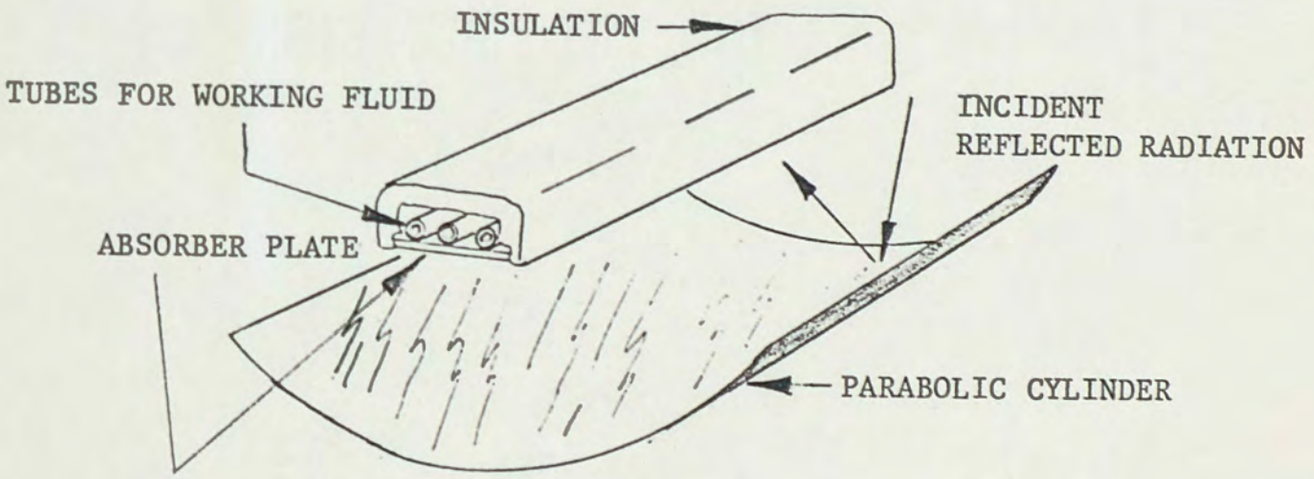

Figure 2. Cylindrical Reflector and Absorber Configuration

filled with air; no evacuation of the collector interior is assumed here. Figure 2 shows the assumed focusing collector configuration. The absorber plate and heat exchanger shown near the focal point of the reflector are similar to those inside the flat plate collector. No glass cover is provided for the absorber plate in this configuration, however.

A flat plate collector is usually oriented toward the south (if the collector is in the northern hemisphere) with its plane collecting surface elevated from the horizontal by an angle roughly equal to the latitude at which the collector is located. This causes the track of the sun to lie in the east-west plane normal to the collecting surface twice a year, at the vernal and autumnal equinoxes. At other times, the sun crosses the collector "off axis" by an amount equalling the declination of the sun. This difference between the elevations of the solar zenith and the collector normal reaches a maximum of about 23½ degrees on the shortest and longest days of the year. Collector performance is degraded somewhat by this seasonal misalignment, but not sufficiently for orientation adjustments to be considered in this analysis. If maximum thermal output is desired for a particular time of year, for example, during the summer for solar air conditioning, the collector can be oriented at an elevation angle corresponding to the solar path at that time. Such a performance boost is achieved at the expense of collector output at other times of the year.

Orientation of the focusing collector is more critical than for the flat plate. For this reason, tracking systems are often proposed

for focusing installations [3]. The cost of a tracking system to direct the collector mirror at the sun during the day is probably too high to permit such a system to be used for ordinary air conditioning applications. However, a fixed mounting for a focusing collector might make the installation economical enough to be considered. Two obvious fixed orientations are shown in Figure 3. The orientation at the top of the page places the reflector "trough" along a north-south axis. As the sun crosses the sky, the focused energy from the mirror sweeps across the plane containing the thermal absorber. For a short time each day, near solar noon, this concentrated radiation strikes the absorber and is available for collection. While this orientation "wastes" most of the thermal energy striking the reflector, it insures that at least some energy will be collected every day.

In the other orientation, the reflector trough is aligned with the east-west path of the sun and tipped so that the solar path is approximately contained in the plane of symmetry of the mirror. If the sun moves away from this plane, as its declination changes, for example, the line of focused radiation from the mirror will move away from the centerline of the absorber. If the misalignment is great enough, no concentrated radiation at all will be collected during the day. The east-west orientation is the better of the two shown in the figure from the standpoint of the amount of thermal energy it can collect, and has been chosen for analysis in this study. Its design and installation must accommodate its strict orientation requirements.

A system of this type does not track or follow the sun as it travels across the sky, but requires an occasional adjustment in

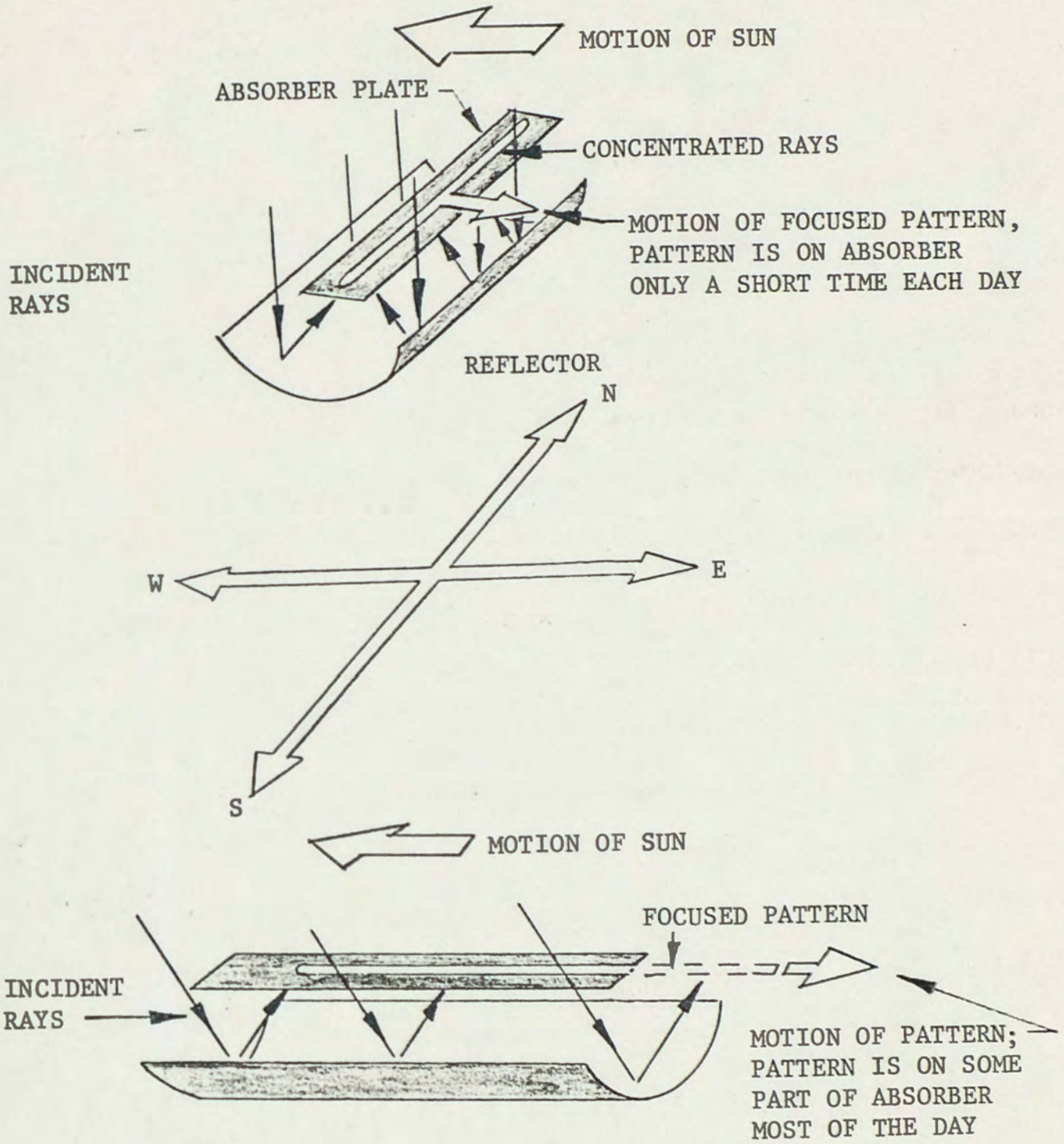

Figure 3. Fixed Focusing Collector Orientations

elevation angle to keep the solar track near the central plane of the mirror. To reduce the number of admustments required throughout the year, the absorber at the focus of the parabola is given a plane surface of appreciable width. The wider this "absorber plate" is made, the less often orientation adjustments are required for seasonal changes in the sun's track. The absorber plate casts a shadow on the parabolic reflector, however, which reduces the radiation reflected on the absorber. Hence, a trade must be made between the frequency of orientation adjustment which is desirably reduced by widening the absorber plate, and the loss in thermal energy reaching the reflector due to the absorber shadow.

The high temperatures required for the air conditioning application dictate some form of temperature regulation. The mechanism chosen for investigation is a simple thermostatic valve which regulates the flow of working fluid to control its discharge temperature. The characteristics assumed for such a device are discussed in the "Temperature Control" section of the mathematical model descriptions. For the flat plate collector, a single valve built into the heat exchanger discharge is sufficient. In the focusing system, the area of the absorber plate which is illuminated by reflected radiation moves down the length of the absorber as the sun travels across the sky during the day. To minimize losses and put the working fluid in the area of the absorber which is illuminated, the absorber heat exchanger could be divided into multiple cells functioning as individual collectors with their own temperature regulation. This configuration, illustrated in Figure 23, has been assumed for the

focusing collector analyzed. The behavior of this arrangement is described mathematically in the temperature control discussion.

The basic configuration of the flat plate and focusing collectors have been described above. The prediction of their performance requires a mathematical description of their characteristics as well as the solar environment in which they will function. The development of the mathematical models required for this is presented in subsequent sections of this report. After the descriptions of the system were derived, they were incorporated into a computer program designed to simulate collector behavior during a day's exposure to the sun. The program is documented in this report. Finally, specific values for important collector parameters were chosen to represent the configurations under investigation. The flat plate and focusing collecting systems were analyzed using the program to determine the quantity and quality of thermal energy which could be derived from both units.

II. MATHEMATICAL MODEL DEVELOPMENT

The basis for the analysis of solar collector candidates is the incorporation of mathematical descriptions of important collection processes into a computer program. The development of these descriptions is presented here, including the underlying physical principles and simplifications appropriate for the collector analysis. The result is a set of mathematical formulations, suitable for implementation in a computer program, describing the solar environment, solar and collector geometry, and the radiation properties of important collector surfaces.

Units

To simplify computations and reduce the requirement for conversion factors in intermediate calculations, metric units have been chosen for this analysis. Classical MKS units are used for most computations. Here, the meter is the unit of length, the kilogram is the mass unit, and time is measured in seconds. Time integrations are represented in hours to reduce the magnitude of the numbers. In some cases, English units are included in this paper with metric ones where this is appropriate. Useful conversion factors for quantities important in this analysis are included in Appendix V.

Solar Radiation

Solar radiation emitted from the surface of the sun consists of a spectrum of wavelengths with maximum spectral intensity in the wavelength region of 0.4 to 0.7 micrometers (μm) [3]. This area corresponds approximately to the visible spectrum, suggesting that visual evolution has taken advantage of this peak. Figure 4 illustrates solar spectral intensity above the earth's atmosphere. The curve closely resembles that of an ideal black body radiator at the temperature of the sun's surface, about 5800° K, located an equivalent distance from the earth. The spectral intensity curve of a black body at a "terrestrial" temperature of 35° C (95° F) is also shown in the figure [4]. Note the different scales for the two curves. It is evident from the figure that the radiant emission of the sun and the low temperature body are distributed in distinct spectral regions.

Spectral Models

The variation in spectral intensity with wavelength for solar or other radiation, and the properties of the absorbing surfaces oriented to collect it, are of considerable importance in the analysis of a solar collection system. For simplicity, however, the development of the mathematical model for collection presented here assumes spectrally lumped properties describing the overall response of a surface in the wavelength region corresponding to that of the incident radiation. This requires the computation of appropriate "spectral total" properties of important collector surfaces prior to their incorporation into the model. This approach simplifies the implemen-

tation of the system description in the computer program. Properties are, therefore, defined for the "short wavelength" region of the spectrum, corresponding to a surface's response to solar radiation, and the "long wavelength" region, representing behavior in the presence of radiation from low temperature or terrestrial sources [4].

The Solar Constant

As shown in Figure 4, the solar spectral intensity curve has units of watts per square meter per micrometer of wavelength. If this curve is integrated over the entire range of wavelengths, the result is a quantity with units of watts per square meter. This is the amount of energy reaching the earth from the sun per unit area per unit time, prior to any atmospheric attenuation. Although this quantity varies somewhat with transient solar activity and seasonal variations in the distance between the sun and the earth, it is constant to within about $\pm$ 3%. An average value for this spectral integral is 1353 w/m^2, based on recent satellite measurements. This power density is termed the "solar constant" [3].

Atmospheric Effects

Solar radiation striking the outer fringes of the earth's atmosphere consists of nearly parallel or collimated rays with the spectral distribution shown in Figure 4. Upon entering the atmosphere, these rays are scattered by air molecules and dust particles suspended in the air. This scattering reduces the solar energy associated with collimated light and creates a diffuse component of energy traveling in directions no longer parallel to the original rays. This

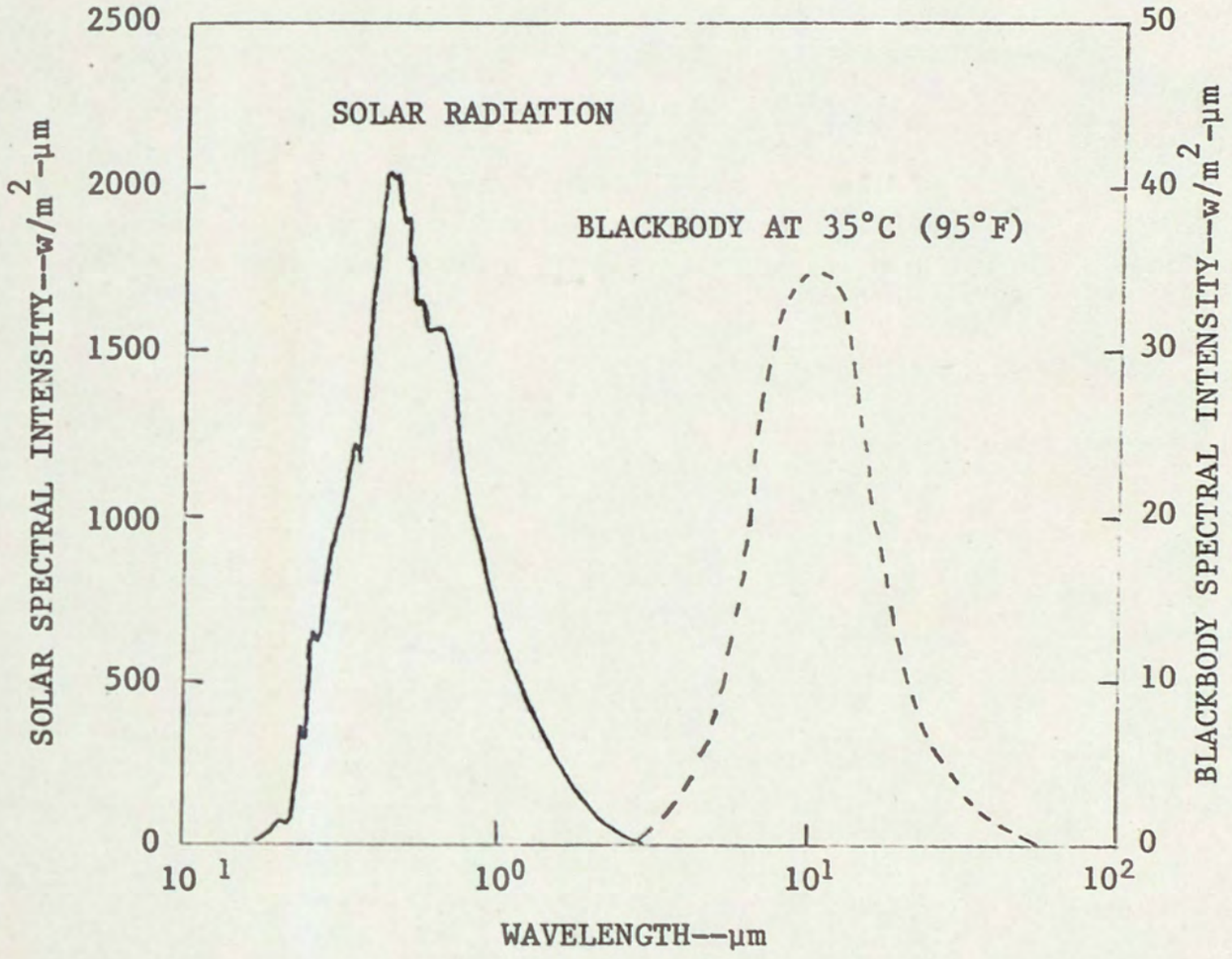

Figure 4. Spectral Distributions of Solar and Terrestrial Radiation [4]

process is illustrated in Figure 5. An additional effect on the incident radiation is the selective absorption of some of the radiation by air molecules, primarily those of water vapor and carbon dioxide. Absorption occurs at radiation frequencies corresponding to vibrational frequencies of these molecules. The absorbed energy is re-radiated by the molecules in a diffuse manner, practially eliminating any collimated component of radiation at the affected frequencies [3].

Both absorption and scattering effects display a marked dependence on wavelength. Absorption occurs mainly in the infrared region of the spectrum, at wavelengths higher than those containing most solar energy. Scattering, on the other hand, is most pronounced for radiation at short wavelengths. This explains the blue color of the sky; blue light is near the low end of the visible spectrum of wavelengths [5]. While these spectral variations are important, atmospheric diffusion will be treated in this analysis only as an overall reduction of energy associated with beam radiation and a corresponding increase in diffuse radiation intensity.

A number of simplifying assumptions have been made in the development of the atmospheric radiation model. First, it is assumed that the sky is in a state of thermal equilibrium. In this model, any radiation entering the atmosphere is either transmitted directly, scattered, or, if absorbed, is immediately re-emitted. This means that the sky stores no thermal energy. An additional assumption is that diffusing properties are uniform throughout the visible hemisphere of the sky, as is the intensity distribution of the resulting diffuse radiation. Polarization effects and anisotropic scattering due to

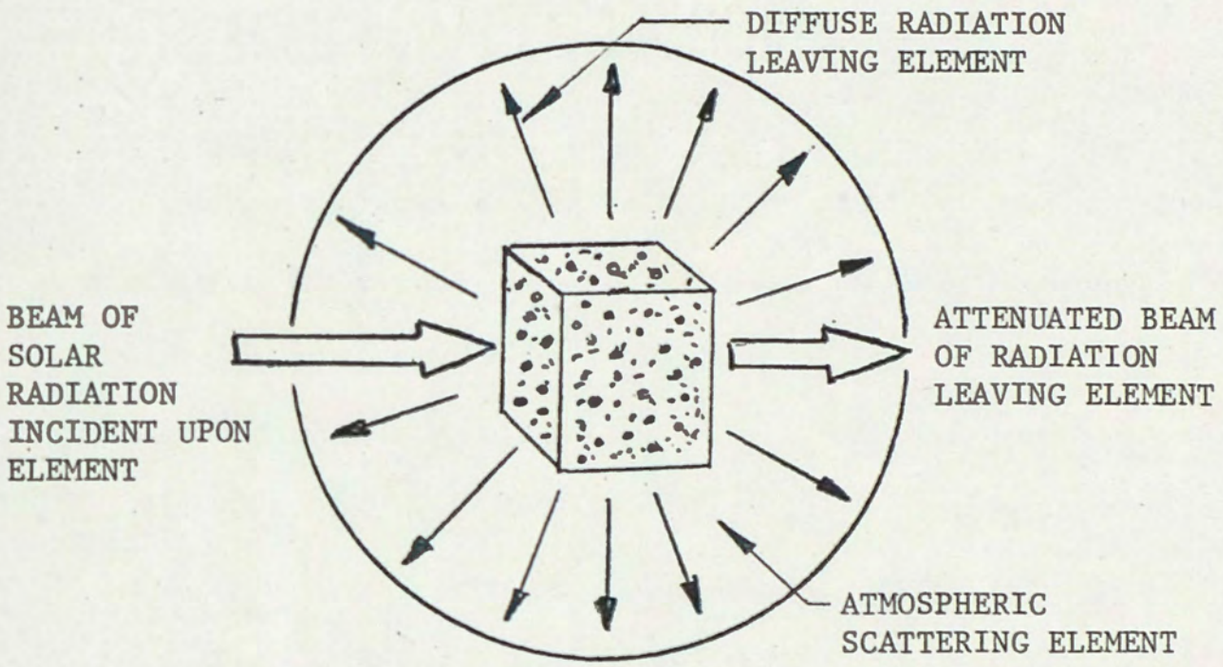

Figure 5. Creation of Diffuse Radiation in the Atmosphere

clouds or any atmospheric inhomogeneities have been neglected. The diffuse radiation intensity in a particular direction has been treated as a function only of the angle between the axis of interest and the ray representing the incoming beam of solar radiation. Thus, the locus of points making up the diffuse radiation pattern can be pictured as a surface of revolution about the incident collimated beam as shown in Figure 6. This simplification arises from the assumption of isotropic atmospheric scattering and emissive properties. Finally, the spectral properties of atmospheric diffusion have been neglected.

Absorption and scattering attenuation of a beam of light transmitted through a medium can be approximated as a drop in beam intensity varying linearly with the intensity itself and the distance traveled through the medium--

$$dW_B = W_B \, (ds/s_r)$$

Here W_B denotes the intensity of the beam radiation, ds, an incremental distance, and s_r, relaxation length which decreases as the concentration of attenuating particles in the medium increases. This is the well known relationship known as "Beer's Law" [6]. For solar radiation, the minimum path length through the atmosphere corresponds to a solar position directly over an observer on the earth's surface, or a solar elevation angle, θ, of 90°. The describing equation for attenuation along this path is,

$$dW_{Bo} = -W_{Bo} \, (dh/H)$$

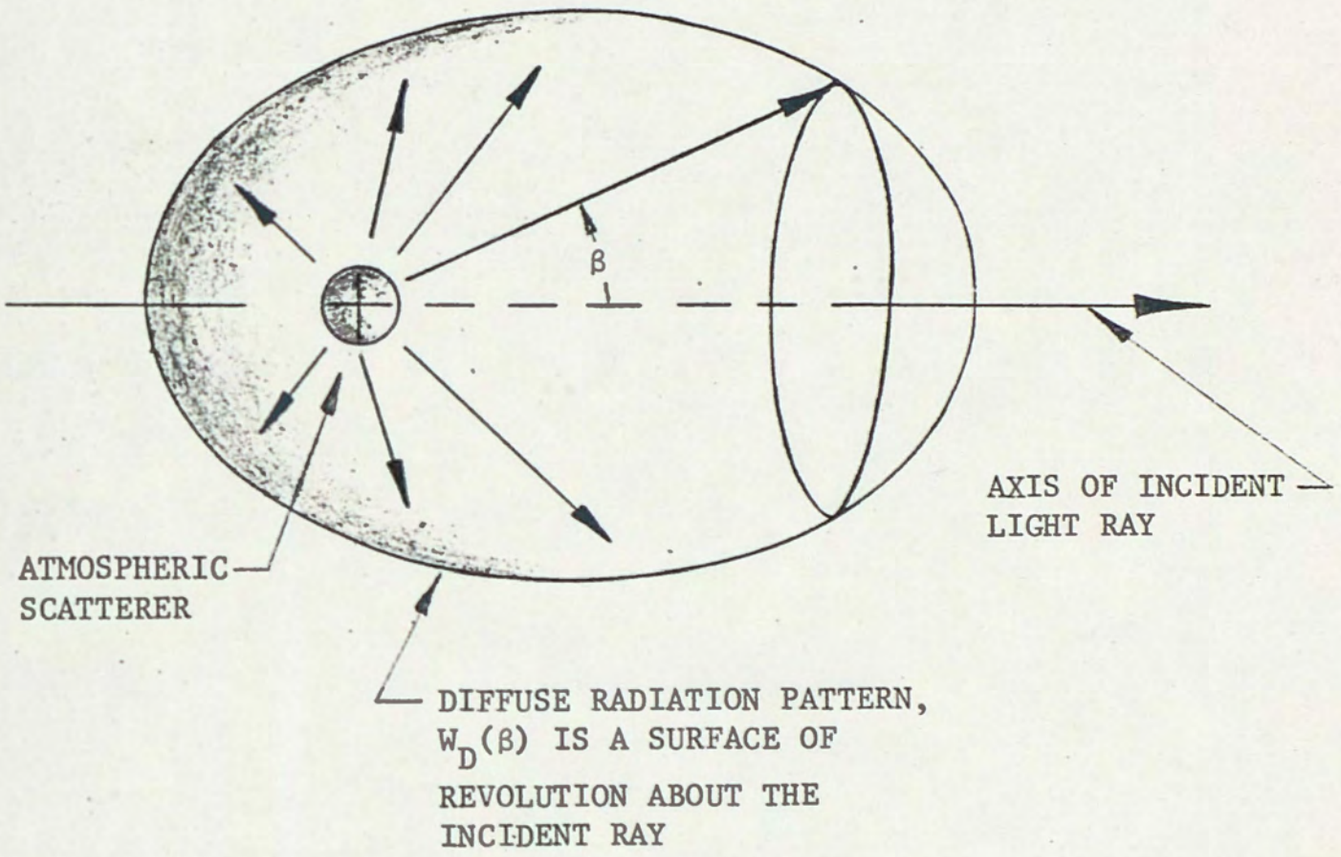

Figure 6. Assumed Atmospheric Diffuse Radiation Pattern

where dh is an incremental change in vertical position, and H is determined by the concentration of dust, water droplets, or other attenuating material. The subscript, zero, specifies this as the minimum attenuation condition.

As the solar elevation angle decreases, the solar path length increases approximately as $1/\sin\theta$, deviating from this function at low elevation angles where the earth's curvature is significant. Now,

$$dW_B = -W_B \left[(dh/\sin\theta)/H\right]$$

The quantity, $dh/\sin\theta$, is the path length of a ray of light coinciding with the change in height, dh, Manipulating the equations yields,

$$\frac{dW_B}{W_B} = \frac{1}{\sin\theta}\frac{dW_{BO}}{W_{BO}}$$

Now, both sides of the equation are integrated with appropriate limits--

$$\ln W_B - \ln W_{Bi} = (1/\sin\theta)(\ln W_{BO} - \ln W_{Bi})$$

or

$$W_B/W_{Bi} = (W_{BO}/W_{Bi})^{1/\sin\theta}$$

Here, W_{Bi} is the beam radiation intensity incident upon the atmosphere prior to any attenuation.

This is simply the solar constant previously defined. The quantity, $1/\sin\theta$, is termed the "air mass" because it describes the

variation in the mass of a column of air through which a beam of light must travel to reach the earth's surface as solar elevation angle changes [3]. The air mass is given the symbol, m. Now,

$$W_B/W_{Bi} = (W_{BO}/W_{Bi})^m$$

At low elevation angles, this expression predicts a complete extinction of beam radiation if the air mass is defined as $1/\sin\theta$. Since everyday experience indicates that at dawn and dusk considerable beam radiation survives atmospheric attenuation, there is apparently a finite limit for the air mass at low elevation angles.

An expression for the air mass predicting bounded values at low sun angles is obtained by considering the geometry of the atmosphere seen by an observer on the earth's surface as shown in Figure 7. An effective height, h, is assumed for atmospheric attenuation. The earth's radius is denoted R, and the path length of a light ray at elevation angle, θ, is s. The air mass, m, is simply s/h. Note that this is unity if the sun is directly above the observer. The path length, s, can be determined using the law of cosines. From Figure 7,

$$(R+h)^2 = R^2 + s^2 + 2Rs\cos(\theta + 90°)$$

or

$$(R+h)^2 = R^2 + s^2 + 2Rs\sin\theta$$

normalizing by h yields:

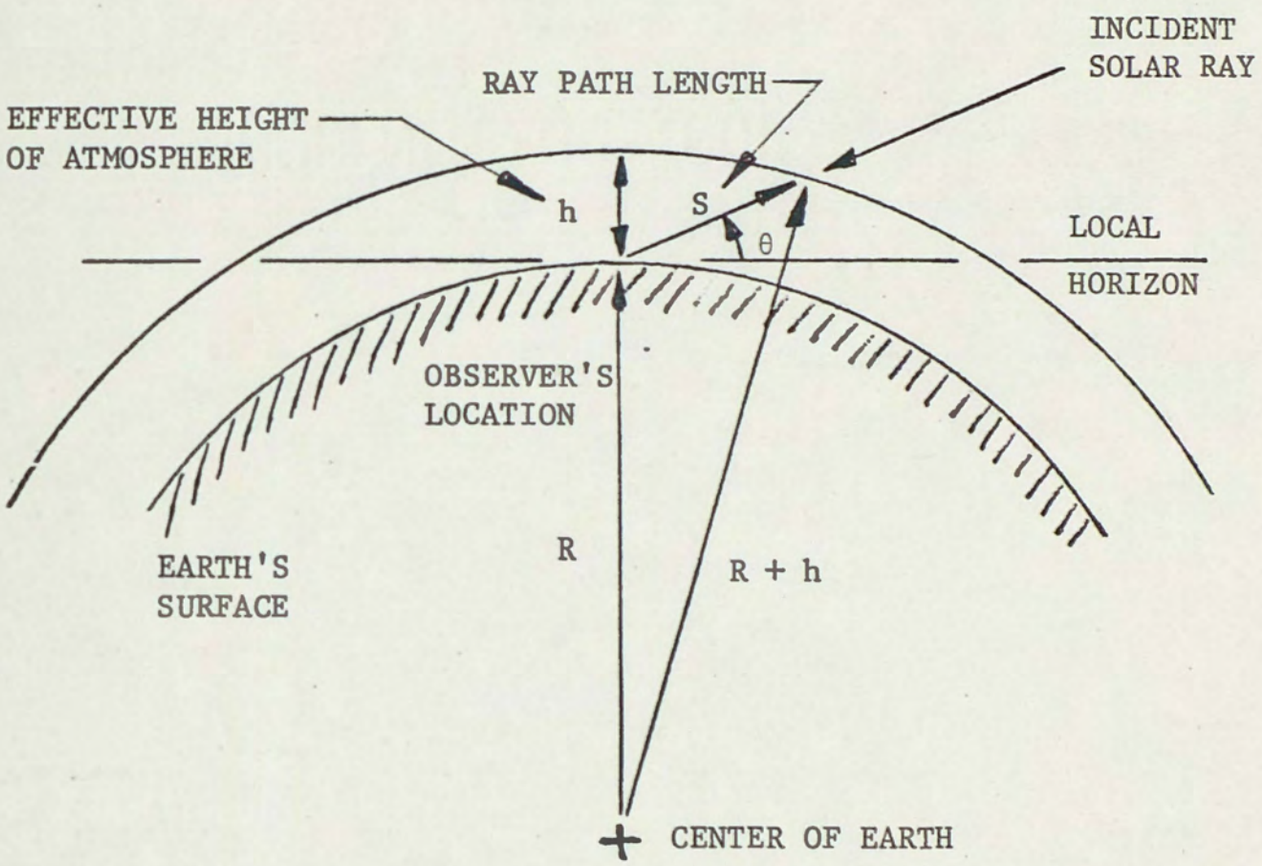

Figure 7. Air Mass Geometry with Spherical Earth

$$\left(\frac{R}{h} + 1\right)^2 = \left(\frac{R}{h}\right)^2 + \left(\frac{s}{h}\right)^2 + 2\left(\frac{R}{h}\right)\left(\frac{s}{h}\right)\sin\theta$$

Let, $\gamma = \frac{R}{h}$

$m = \frac{s}{h}$

Now,

$$(\gamma + 1)^2 = \gamma^2 + m^2 + 2\gamma m \sin\theta$$

According to the Quadratic Formula,

$$m = \frac{-2\gamma \sin\theta \pm \sqrt{4(\gamma \sin\theta)^2 + 4(2\gamma+1)}}{2}$$

Here, the positive root is chosen for a positive value of m.

$$m = \sqrt{\gamma^2 \sin^2\theta + 2\gamma + 1} - \gamma \sin\theta$$

For $\theta = 0°$, or for conditions at sunrise and sunset, the maximum air mass is found to be

$$m_{MAX} = 2\gamma + 1$$

If the portion of the atmosphere significant for solar energy attenuation is considered to extend to an altitude of 10 miles, the normalized earth radius is

$$\gamma \simeq \frac{4000}{10} = 400$$

The resulting air mass at sunrise or sunset is then,

$$m_{MAX} = 2(400) + 1 \simeq 28$$

Proper choice of the geometrical parameter γ, permits matching any experimentally determined air mass effect at low elevation angles. Note that if a very thin atmosphere is assumed (h approaches zero), the parameter, γ, approaches infinity. Under these assumptions,

$$m = \sqrt{\gamma^2 \sin^2\theta + 2\gamma} - \gamma \sin\theta$$

$$= \gamma \sin\theta \sqrt{1 + \frac{2}{\gamma \sin^2\theta}} - \gamma \sin\theta$$

Using an approximation for the square root,

$$m = \gamma \sin\theta \left(1 + \frac{1}{\gamma \sin^2\theta}\right) - \gamma \sin\theta$$

$$= \gamma \sin\theta + \frac{\gamma \sin\theta}{\gamma \sin^2\theta} - \gamma \sin\theta$$

$$= 1/\sin\theta$$

This is the expression corresponding to the assumption of a flat earth.

Once air mass is determined, the attenuation of beam radiation is found with the previously stated expression,

$$W_B/W_{Bi} = (W_{BO}/W_{Bi})^m$$

The quantity, W_B/W_{Bi} will be assigned the symbol, f_B, representing the fraction of beam radiation reaching the earth's surface. For a solar

elevation of 90°, it will be denoted, f_{BO}, representing the quotient, W_{BO}/W_{Bi}. At $\theta = 90°$, the incident beam radiation flux corresponds to the solar constant, W_{SC}. Now,

$$W_B = W_{SC}\, f_B = W_{SC}\, f_{BO}^{\,m}$$

The energy per unit area lost from the beam component of radiation is

$$W_{DT} = W_{SC}\,(1 - f_{BO}^{\,m})$$

This energy is either absorbed and re-radiated or scattered as diffuse radiation. Figure 8 shows a hypothetical diffuse radiation pattern, $W_D\,(\beta)$, seen by an observer in the sky. This distribution is consistent with the assumptions regarding atmospheric diffusion previously stated. The integration of this diffuse pattern, having units of W/m^2 steradian, over the 4π steradians representing a sphere must equal the total beam flux lost as diffuse radiation in the atmospheric attenuation process, W_{DT}. The integration is illustrated in Figure 8. Note that the diffuse radiation pattern may be described as a non-dimensional ratio, α_D, varying with total angle, β, from the incident solar ray. This specifies the shape of the distribution but not its magnitude. The determination of the intensity of the diffuse radiation resulting from beam attenuation is also shown in Figure 8. The scale factor, A, determined here, may be applied to the distribution function, α_D, to give radiation intensity. In the computer model, α_D, has been assumed constant with respect to time, but the scale factor, A, varies as the solar elevation angle changes the air mass.

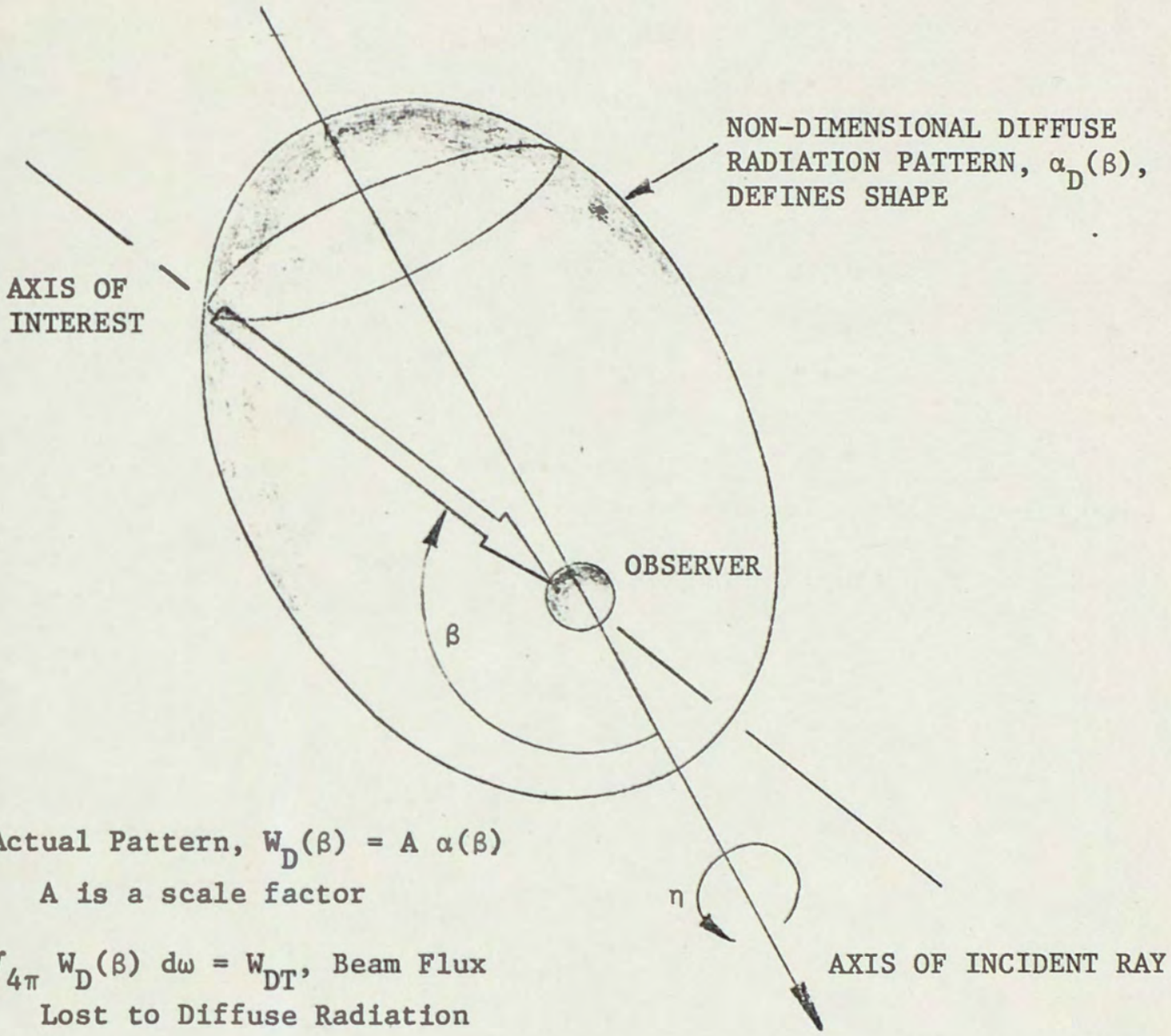

Actual Pattern, $W_D(\beta) = A\ \alpha(\beta)$

A is a scale factor

$\int_{4\pi} W_D(\beta)\ d\omega = W_{DT}$, Beam Flux Lost to Diffuse Radiation

$$A \int_0^{2\pi} \int_0^{\pi} \alpha(\beta)\ \sin\beta d\beta d\eta = W_{DT}$$

$$2\pi A \int_0^{\pi} \alpha(\beta)\ \sin\beta d\beta = W_{DT}$$

Let $B = \int_0^{\pi} \alpha(\beta)\ \sin\beta d\beta$

$$A = \frac{W_{DT}}{2\pi B}$$

Figure 8. Scaling of Non-Dimensional Distribution of Diffuse Radiation to Actual Magnitude

With these mathematical tools, the attenuation of beam radiation and propagation of diffuse radiation by the atmosphere may be represented parametrically. Note that atmospheric height, transmissivity as specified by the quantity, f_{BO}, and the spatial distribution of diffuse radiation are variables in the model.

Other Radiation Sources

Radiant energy incident upon the absorbent surface of a solar collector comes primarily from the sky, either as beam radiation directly from the sun or as diffuse radiation from all parts of the visible hemisphere. There are additional sources of radiant energy, however, which become important in the proper computation of the collector energy balance. These sources include the ground and any part of the collector structure visible to the absorbing surface.

For this analysis, the ground is treated as a black body radiator at a uniform temperature. This temperature is assumed equal to the local air temperature, T_∞, and is held constant for simplicity. The ground is treated as a flat plane extending from below the collector to the horizon. No consideration has been given to tree lines, adjacent buildings, or other structures which could extend the local horizon to higher elevation angles than the horizontal. The diffuse radiation intensity resulting from the black body emittance of the ground is simply,

$$W_{D\ ENV} = \frac{\sigma}{\pi} T_\infty^4$$

Here σ is the familiar Stefan-Boltzmann constant and $W_{D\ ENV}$ is a

uniform intensity corresponding to the radiation contribution of the local environment. It has units of w/m^2 - sr.

An additional source of radiation must be considered for the focusing collector. This is the curved reflector located below the absorbing surface. The reflector is assumed to radiate a uniform diffuse energy pattern from each point on its surface. The total emissivity, ε_R, for this radiation corresponds to the value for long wavelengths as discussed previously. The temperature of the mirror used for computation of its radiant power is assumed to be the constant "environment temperature", T_∞, used for the atmosphere and the ground. No energy balance is explicitly maintained for the mirror in this model. The diffuse intensity emanating from the reflector under these assumptions is,

$$W_{D\ REFL} = \varepsilon_R \frac{\sigma}{\pi} T_\infty^4$$

These radiation sources, while generally secondary to radiation from the sky, are important in the computation of reasonable collector temperatures under conditions of weak sky radiation. This is particularly true of the focusing collector model, which predicts very low absorber temperatures in the absence of incident radiation. In effect, the device is radiating all of its energy "into space" under these conditions. When the energy balance for the system includes environmental radiation and emission from the mirror, realistic absorber temperatures are predicted.

Geometry

Because of the importance of the geometry of the sun and a solar collector in the description of their interaction, a computer model of the thermal collection process must include geometric features. To facilitate geometric descriptions and calculation, the modeling approach taken here makes wide use of vector concepts. Vectors are used to locate points in space, establish the orientation of plane surfaces, and indicate the paths of light rays. Several coordinate systems are used in the mathematical models employed in this analysis. These permit convenient descriptions of vectors in terms of coordinates fixed to the earth, the solar collector, and the earth's polar axis for specifying the sun's position. Geometric considerations of primary importance here are the location of the sun in the sky and the orientation of the solar collector on the earth.

Solar Geometry

An observer on the surface of the earth sees the sun move across the sky from east to west each day. More subtle motion takes place on a seasonal basis as the solar track itself moves back and forth to the north and south with a yearly period. This apparent motion is due to the orientation of the earth's polar axis with respect to the solar orbital plane. The angle between the polar axis and the plane normal to a vector connecting the earth and the sun is the solar "declination." This varies from zero to about 23½° according to the approximate relationship,

$$\Delta = 23.45 \sin \left(2\pi \frac{284 + n}{365}\right) \qquad [3]$$

Here, Δ is the solar declination expressed in degrees and n is the Julian date of the day of interest. The apparent location of the sun in the sky is also a function of the observer's latitude or angular distance from the equator. A description of the sun's position in the sky must, therefore, depend upon the time of day, the solar declination, and the observer's latitude. Solar geometry is illustrated in Figure 9, with solar declination.

Coordinate Frames

To describe the apparent position of the sun as seen by a solar collector, it is convenient to resort to multiple coordinate frames and appropriate coordinate transformations. First, consider the frame shown in Figure 10. This coordinate system is fixed to the earth at the location of the collector with axes in the north, east, and down directions. Note that north is "true north", or toward the pole, and that "down" corresponds to a local plumb line. This is a frame corresponding to everyday observations and experience and is convenient for expressing solar position with the azimuth, and elevation angles, ψ_s and θ_s, shown in Figure 10. In addition, the orientation of a light ray from the sun may be expressed as a unit vector, $\bar{U}_i$, as shown in Figure 10. This coordinate system is called the "A" frame.

Another coordinate frame, now fixed to the solar collector, is shown in Figure 11. The x axis of this frame represents the orientation axis of the collector. In addition, the collector may be rotated about the x axis. A description of collector orientation angles is

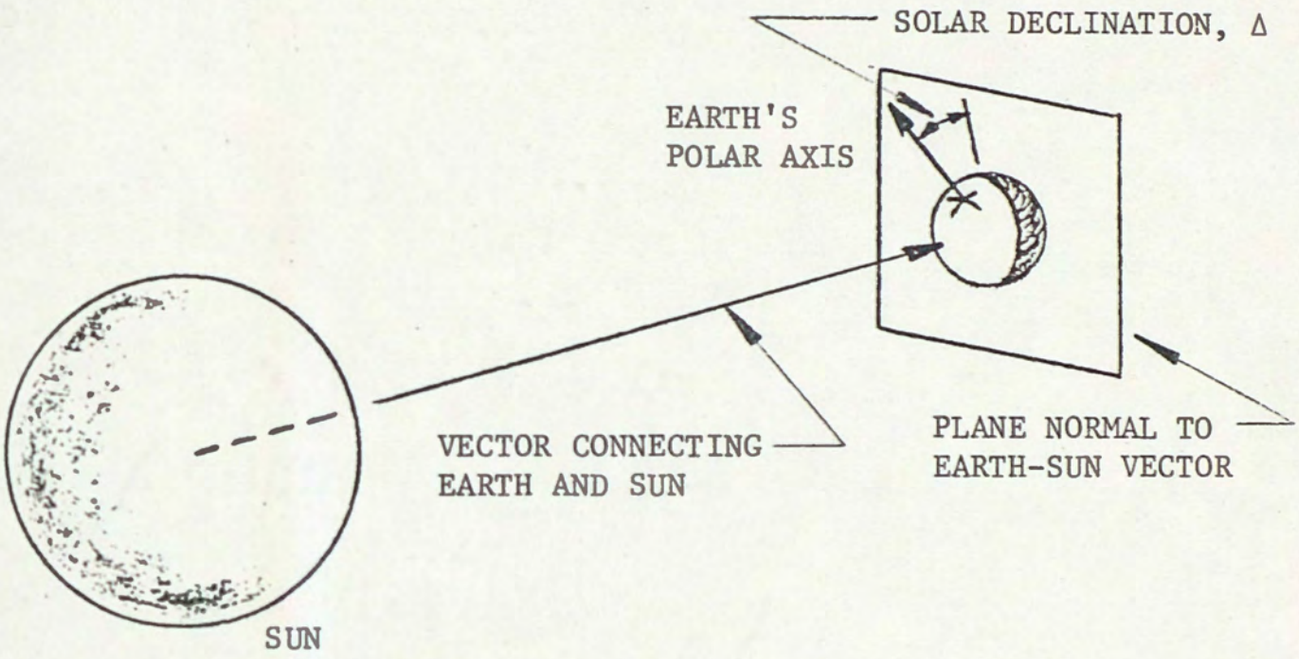

Figure 9. Geometry of Earth and Sun

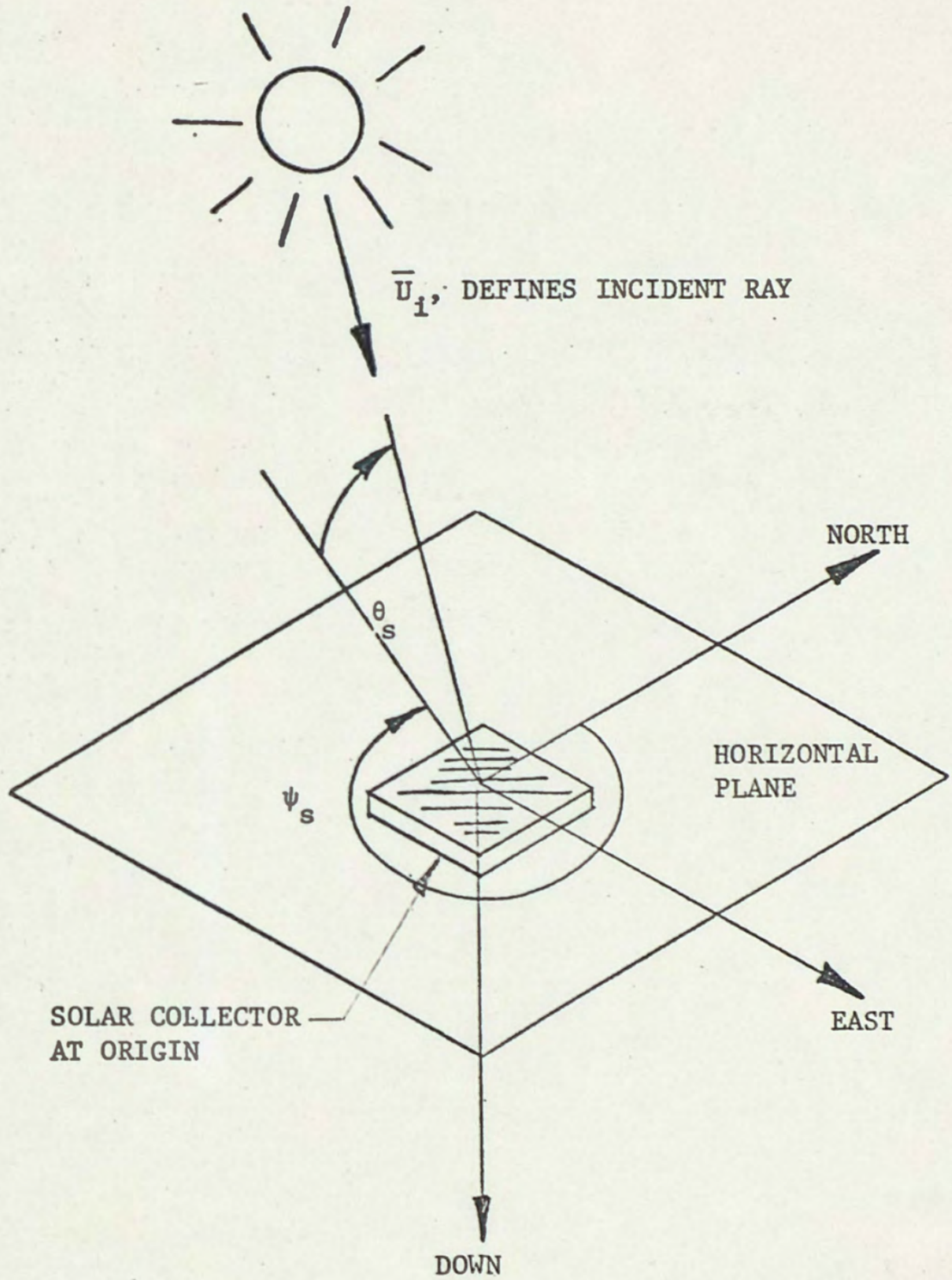

Figure 10. "A" Coordinate System and Solar Position

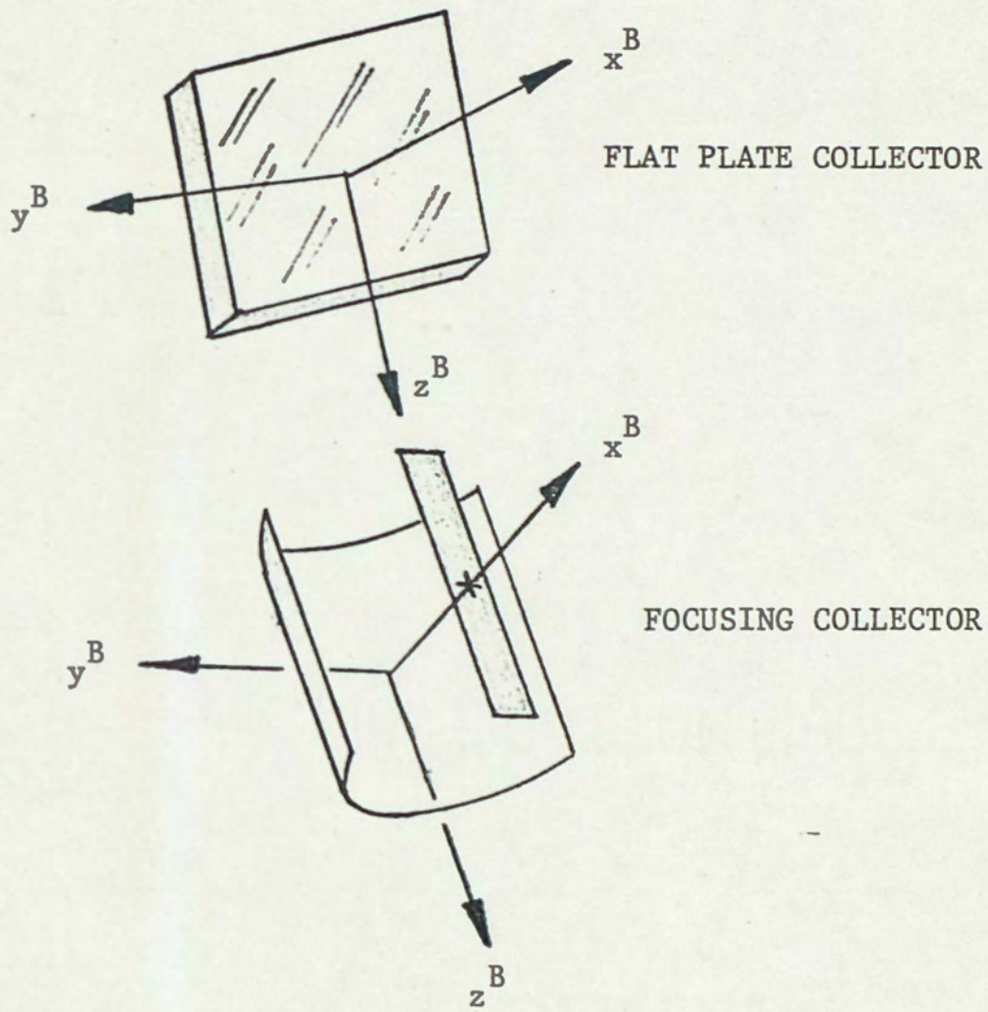

Figure 11. Collector Coordinate Systems, "B" Frames

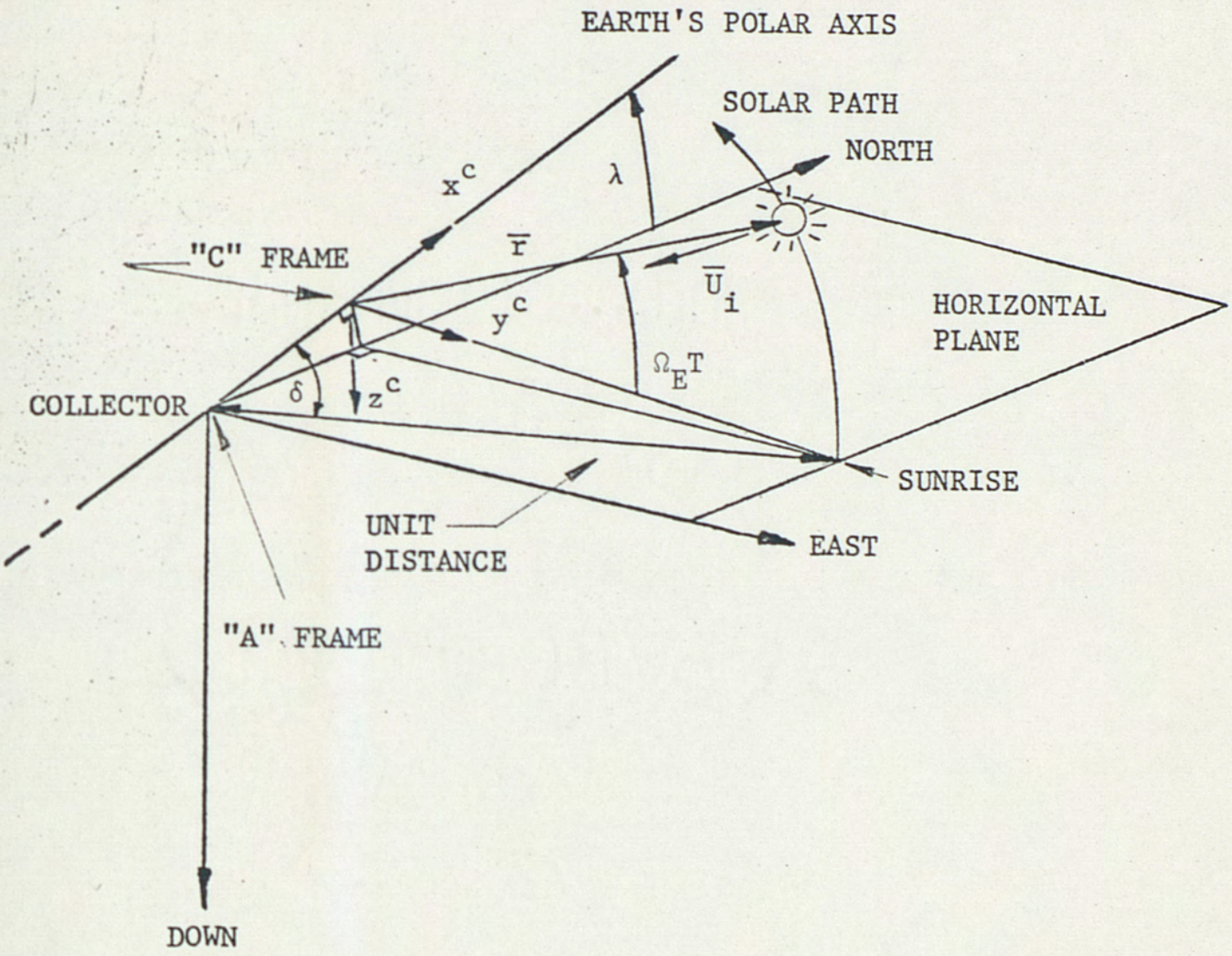

Figure 12. "C" Coordinate System and Apparent Solar Path

included in the next section of the report. Note that the parabolic shape of the cylindrical reflector is confined to the x-y plane. The collector coordinate system is designated the "B" frame.

Finally, the computation of solar position requires an additional set of axes, the "C" frame. This frame is oriented so that its x axis is aligned with the polar axis of the earth. This axis is specified by the unit vector, $\overline{U}_p$, and makes an angle with the horizontal corresponding to the geodetic latitude, λ, of the collector. The origin of the "C" frame does not coincide with the "A" frame, but is displaced along the polar axis as shown. The apparent position of the sun is a point in the y-z plane of the "C" frame, a unit distance from the origin of the "A" frame. The Y axis of the "C" frame points toward the apparent location of sunrise. Note that the orientation of the "C" frame relative to "A" is a function of latitude and declination angle. The matrix for transforming position coordinates, $C_{A/C}$, is derived from the direction cosines of the x, y, and z axes of the "C" frame expressed in the "A" frame.

The position of the sun as a function of the elapsed time from sunrise, is easily computed with the vector, $\overline{r}$, rotated relative to the y axis in the "C" frame by an amount $\Omega_E T$. Ω_E is the angular rate of the sun relative to the earth's surface and T is the time elapsed since sunrise. The sun's coordinates in the "A" frame may then be determined with the appropriate coordinate transformation. Ultimately, the unit vector describing the orientation of the incident solar radiation, $\overline{U}_i$, is desired in the collector or "B" frame to simplify computation of the reflected path or the absorption process. This

change of coordinate frames is accomplished with the appropriate matrix multiplication--

$$\overline{U}_i^{\,B} = C_{B/A}\,\overline{U}_i^{\,A}$$

Here, the superscript denotes the coordinate frame in which the vector is expressed.

Collector Geometry

The configurations of the flat plate and focusing reflector systems assumed for the development of this mathematical model were discussed in the background section. The performance of these collectors is clearly a function of their size and proportion. The flat plate collector may be represented as a plane surface of area, A_c, directed toward the sky. The area of the collector's glass face is the primary geometric variable; of secondary importance is the depth of the box below the face. This depth determines, in part, the extent of edge effects consisting of edge losses and shadows cast by the collector sides on the heat absorbing surface in the box. If the dimensions of the glass face are large compared to the depth of the box, however, these effects are small [3]. For this development, flat plate edge effects have been neglected. Further, as discussed in the description of the loss models, only "coupled" losses through the glass face are considered in the flat plate model. Hence, the geometric description of the flat plate collector is very simple. Only the area of the glass window and its orientation are needed for computation of thermal gain from solar radiation. For the computation of

conductive losses through the glass face, the thickness of the cover is also important.

More complex is the cylindrical reflector system. Here, the dimensions of the parabolic mirror and the absorber plate must be specified to predict system properties. In addition, the extent of the mirror curvature, the resulting focal length, and the distance of the absorber plate from the mirror are required. These parameters are illustrated in Figure 13. Note that the absorber plate in this system is similar to the flat plate collector described above in its characteristics. The primary difference between the two is the absence of a spectrally selective glass face on the absorber. As in the flat plate system, only coupled losses from the absorbing surface of the plate are considered in the thermal loss model. Hence, the geometric configuration of the absorber itself is not specified except for the dimensions of this surface.

The aiming of the collectors is specified with three Euler angles, ψ, θ, and ϕ, representing an azimuth swing of the collector x axis from true north, an elevation of this axis above the horizontal and, finally, a rotation of the collector about the x axis. Azimuth, elevation, and tilt angles are shown in Figure 14. Since the flat plate collector has no geometric description in the collector y-z plane other than its area, the tilt angle, ϕ, has no effect on its performance. This is determined entirely by the orientation of the normal to this area, the collector x axis. The tilt angle is important in the behavior of the focusing collector, however, because it determines the extent to which the focused solar image tracks the z

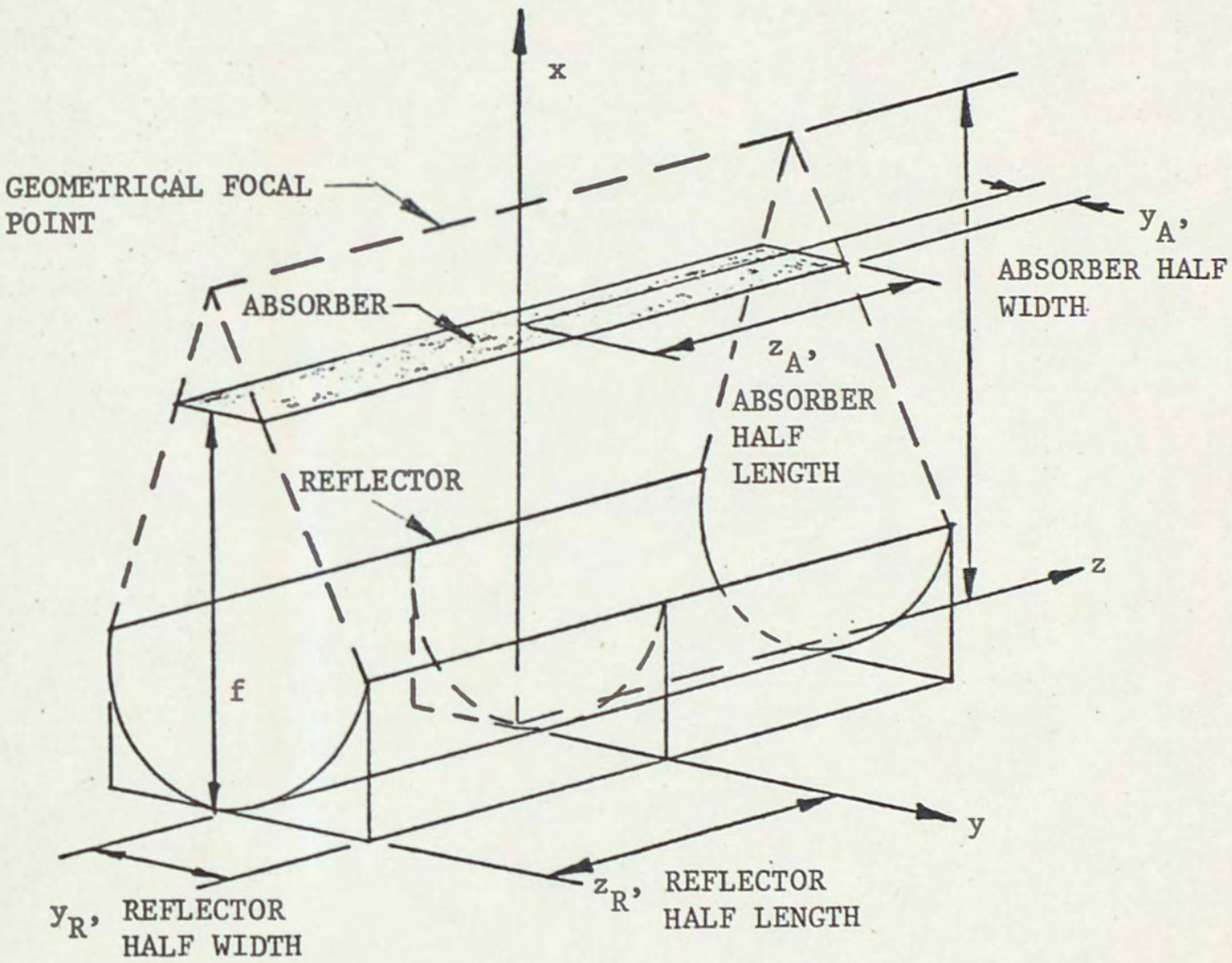

Figure 13. Focusing Collector Geometrical Parameters

At $\psi = \theta = \phi = 0°$, "A" and "B" Frames are Coincident

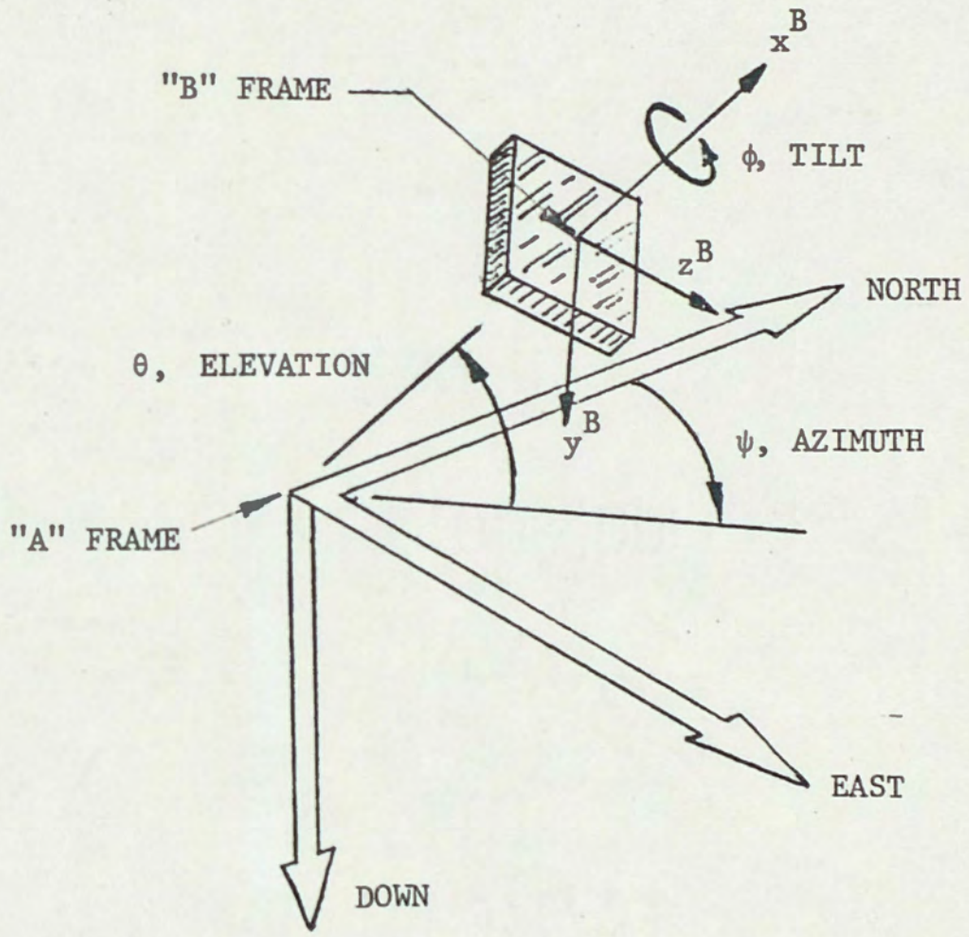

Figure 14. Euler Angles Describing Collector Orientation

axis of the absorber plate during the day.

Normally, both collectors would be oriented with an azimuth angle of 0° (due north) or 180° (south) and elevated an amount sufficient to bring the collector x axis approximately in line with the east-west path of the sun. A tilt angle of plus or minus 90° would then be required for the focusing collector to align the reflector z axis with the solar track. Note that orientation errors would generally degrade collector performance, particularly for the focusing system. The effect of perturbations to the ideal orientation angles can be studied with this model by varying these angles.

Surface Radiation Properties

The radiation properties of the materials comprising the absorbant surface of a solar collector largely determine the collector's performance. In general, these properties vary with the wavelength of the incident radiation and the angle at which an incident ray strikes the absorbing material. For this analysis, the spectral variations in surface properties have been neglected in the mathematical descriptions of the flat plate and focusing collectors. The spectrally selective properties of the glass cover of the flat plate system are considered only in terms of "short wavelength" properties for the transmission of sunlight to the interior of the collector and "long wavelength" properties for the subsequent loss of radiant energy from inside.

Typical properties of the glass cover transmission, τ, absorbence, α_c, and heat exchanger absorbence, α, are shown in Figure 15

versus the angle, β, which an incident light ray makes with an axis normal to the collector. These are short wavelength properties consistent with the spectrum of sunlight. The enrgy per unit area passing through the glass cover is the product of the incident flux and the transmittance of the glass. The energy absorbed by the plate is the product of the transmitted energy and the absorbence of the heat exchanger. The two properties may be lumped together, forming an absorbence-transmittance product which varies with incidence angle. This $\alpha\tau$ product characterizes the absorbing performance of the flat plate collector [3].

To compute the plate temperature and thermal losses, an energy balance must be maintained for the exchange between the glass cover, the absorbant plate, and the environment. This requires a description of the glass absorbtivity for the short wavelengths that characterize solar radiation as well as the emissive, reflective, and transmissive properties of the system for long wavelength radiatiōn emanating from the collector structure. The important surface properties for the flat plate collector are shown in Table I.

The two important surfaces in the focusing system are the mirror and the absorber plate. The cylindrical parabolic mirror is designed to be as reflective as possible. A typical reflectivity curve is shown for a highly polished aluminum mirror in Figure 16. This could represent a smooth glass or plastic surface with a thin film of aluminum deposited upon it. This curve shows the fraction of incident energy striking the mirror which is reflected specularly. Energy components absorbed or reflected diffusely are not included in

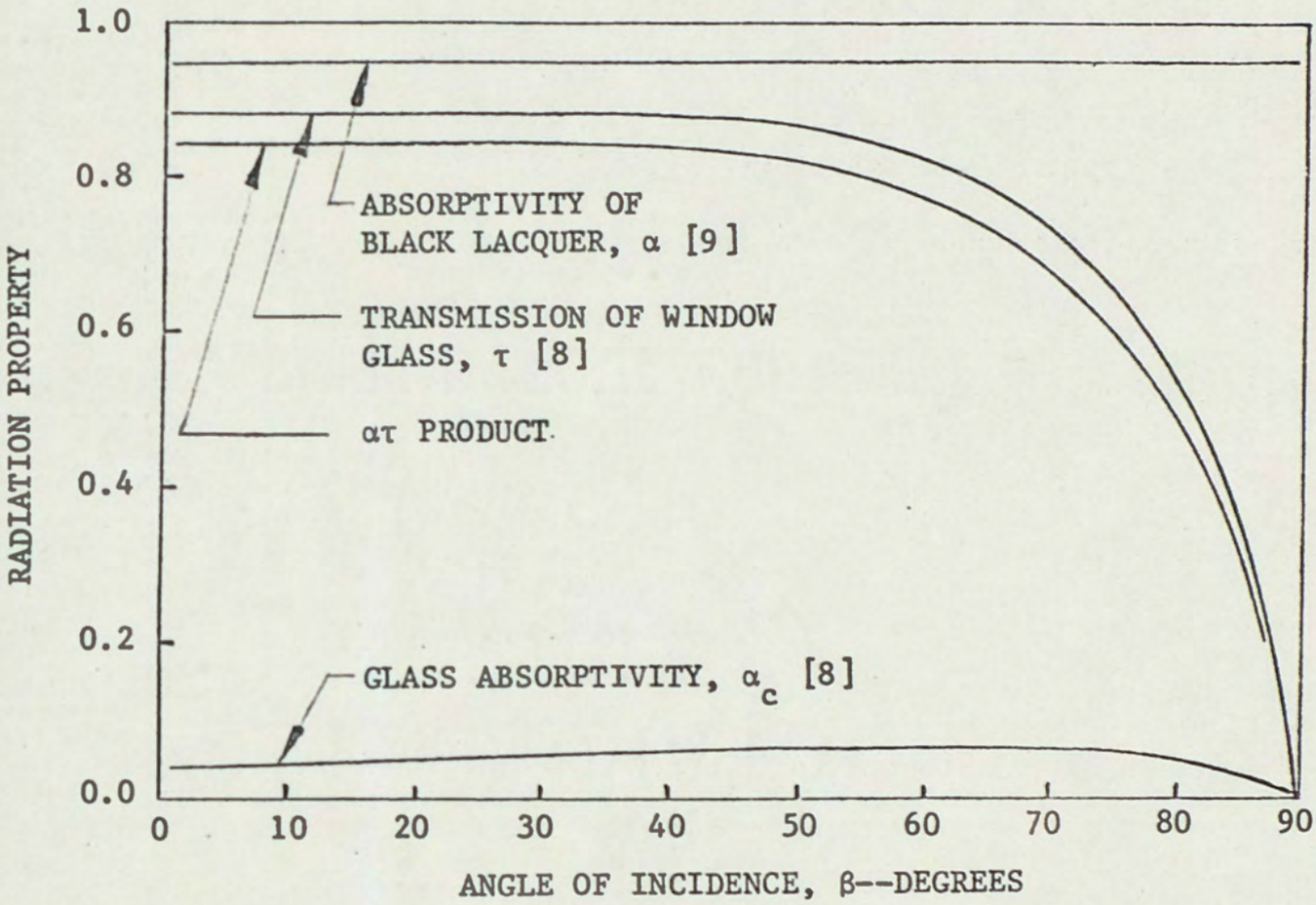

Figure 15. Typical Absorbence and Transmission Curves For Flat Plate Surfaces

the reflectivity curve. In contrast, the absorber plate is intended to absorb as much incident radiation as possible. A typical absorbence curve is also shown in Figure 16. No variation in absorbtivity with incidence angle has been assumed. A roughened surface would approximate this assumption [7]. The complexity of the reflector-absorber geometry makes a lumping of the reflectivity and absorbtivity in a single product impractical. Their effects must be considered separately as the path of a captured light ray is traced through the system.

Since this collector configuration includes no transparent cover over the absorbing surface, its radiation properties are determined solely by its absorbtivity curve. Radiation losses are characterized by the total emissivity of the surface. As in the case of the flat plate, long wavelength properties are of interest for loss computation. Energy striking the reflector which is not specularly reflected is either absorbed and then emitted, or reflected in a diffuse manner. If this energy is assumed to emanate from the mirror surface uniformly in all directions, the diffuse radiation intensity may be computed by assuming an effective mirror temperature and a hemispherical total emissivity for the reflecting material. Again, this emissivity is a long wavelength property. As discussed previously, the equivalent mirror temperature has simply been chosen to be that of the local environment.

Surface properties required for a mathematical description of the collectors are summarized in Table 1. Note that, in all cases, radiation losses involve long wavelength total properties. Energy

TABLE 1

COLLECTOR SURFACE PROPERTIES

Collector	Property		Symbol	Wavelength Region
Flat Plate	Absorbance-Transmission Product		$\alpha\tau$	Short (Solar)
	Cover Absorptivity		α_C	Short
	Hemispherical Total:	Cover Emissivity	ε_C	Long (Terrestrial)
		Cover Reflectivity	ρ_C	
		Cover Transmissivity	τ_C	
		Plate Emissivity	ε_P	
		Plate Reflectivity	ρ_P	
	Spectral Selectivity Factor For:*	$\alpha\tau$ Product	f_{SEL}	Long/Short
		Cover Absorptivity	f_{SELC}	
Focusing	Mirror Reflectivity		ρ	Short
	Absorptivity		α	Short
	Hemispherical Total Absorber Emissivity		ε_{HT}	Long
	Mirror Emissivity		ε_R	Long
	Spectral Selectivity Factor*		f_{SEL}	Long/Short

*Ratio of Longwave Property to Shortwave Property

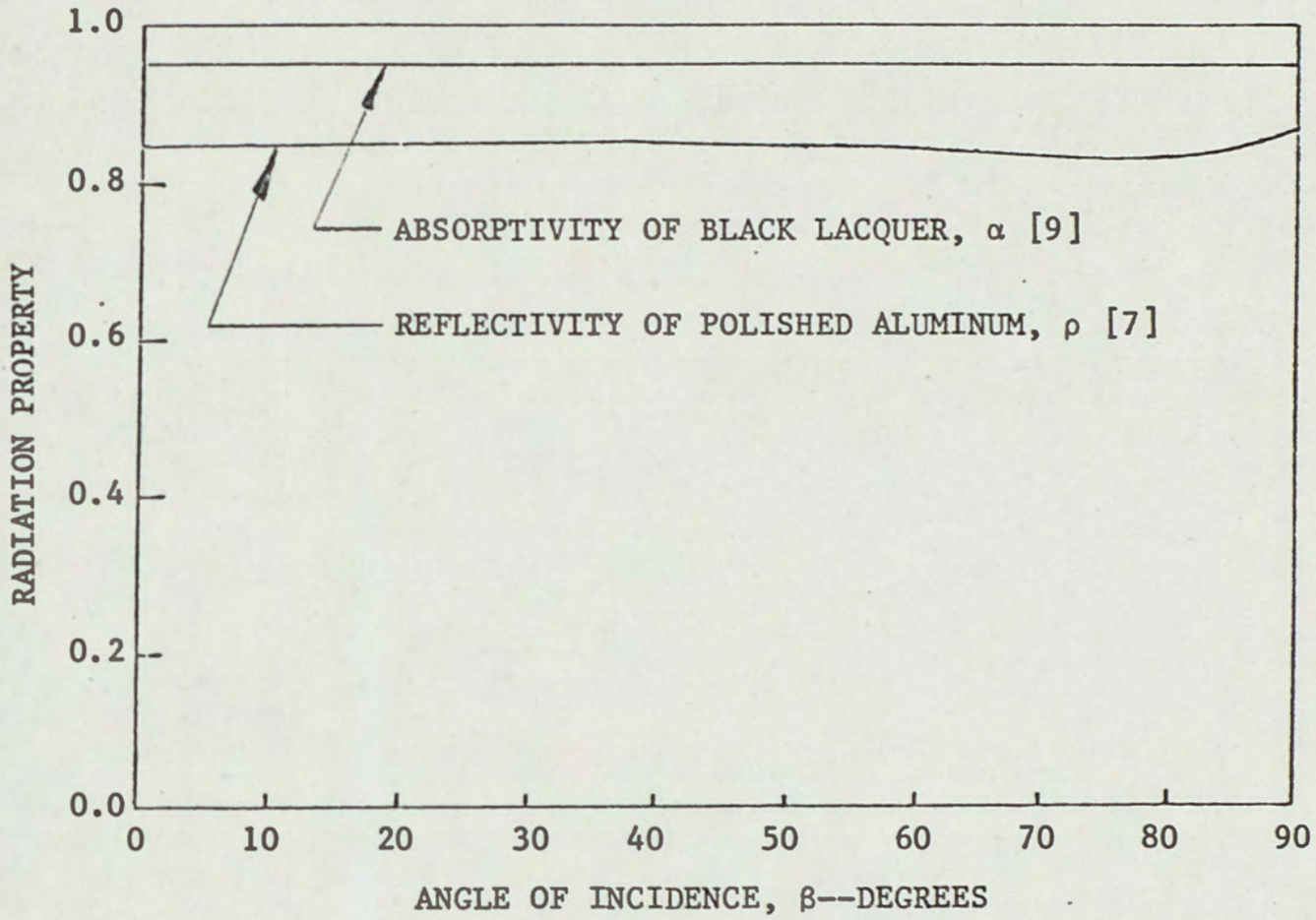

Figure 16. Typical Absorbence and Reflectivity Curves for Focusing Collector Surfaces

gain computations generally use short wavelength properties varying with incidence angle. An exception is in the description of the capture of diffuse terrestrial radiation by the collecting surfaces. Here, a "selectivity factor", f_{SEL}, is applied to the short wavelength curves to account for the long wavelengths of local radiation.

Collector Energy Gain

A solar collector traps radiant energy of two types--collimated beam radiation traveling along a direct path from the sun to the collector, and diffuse radiation from all parts of the sky. In addition, diffuse radiation is emitted from the ground and the collector structure itself. The collector design determines the efficiency with which these radiation components are absorbed. In this discussion, "thermal gain" will be used to denote the energy absorbed by the collector prior to any system losses.

For the flat plate collector, the energy absorbed by both the collector heat exchanger and the glass cover must be determined for correct computation of the system energy balance. Figure 17 shows a flat plate collector aimed toward the sky with its normal specified by the unit vector, $\overline{U}_n$. The horizon is shown as a dotted horizontal line. An incident ray of light, designated by the unit vector, $\overline{U}_i$, strikes the collector surface at the angle, β, with respect to the normal. If W_B, having units of watts/m^2, is the beam radiation flux normal to the path defined by $\overline{U}_i$, then,

$$dP_B = W_B \, (-\overline{U}_i \cdot \overline{U}_n) \, \alpha\tau(\beta) dA$$

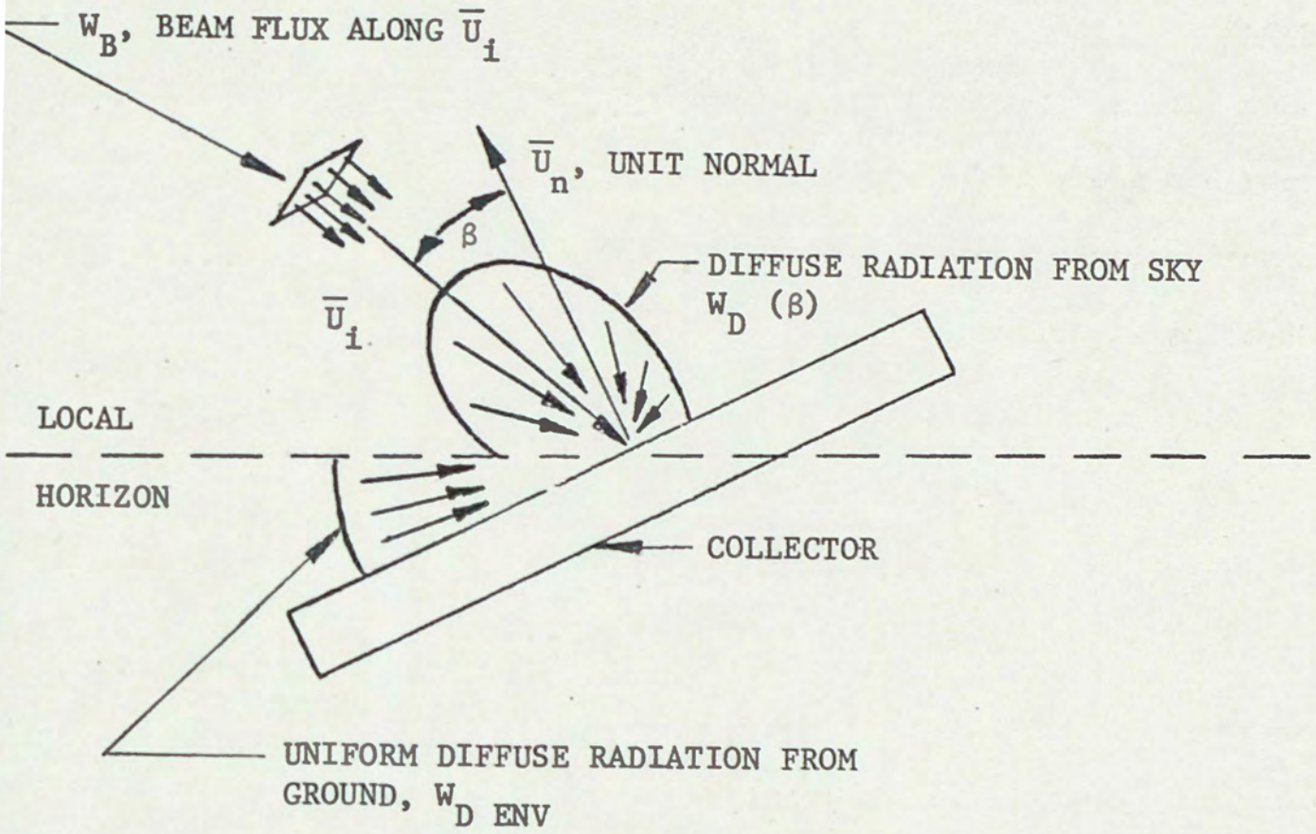

Figure 17. Radiation Environment of Flat Plate Collector

where dP_B is the thermal power from beam radiation absorbed by the collector area element, dA. A similar expression describes the power collected by the glass cover, dP_{BC}. For this computation, the cover absorbtivity, $\alpha_c(\beta)$ is substituted for the $\alpha\tau$ product.

Note that the dot product, $\overline{U}_i \cdot \overline{U}_n$, accounts for the projection of the area element into a plane normal to the path of the incident light ray. The minus sign is necessary for a positive result because $\overline{U}_i$ and $\overline{U}_n$ oppose each other as defined in the figure. To simplify the expression for dP_B, a new quantity, μ, is defined for the dot product.

Let

$$\mu = \begin{cases} -\overline{U}_i \cdot \overline{U}_n, & \text{if } \overline{U}_i \cdot \overline{U}_n < 0 \\ 0, & \text{if } \overline{U}_i \cdot \overline{U}_n \geq 0 \end{cases}$$

This definition is consistent with the characteristic of the collector that it is largely unaffected by radiation striking it from behind. The angle, β, is simple $\cos^{-1}(\mu)$. The thermal power gain associated with beam radiation is now,

$$P_B = \int_{A_C} W_B \, \mu \, \alpha\tau(\beta) \, dA = W_B \, \mu \, \alpha\tau(\beta) \, A_C$$

where A_C is the collector surface area. Again, a similar expression is used for the glass cover.

It is evident from the figure that diffuse radiation components from both the sky and the ground also strike the collector face. This diffuse radiation has intensity, W_D, with the units w/m^2 - sr. To

compute the thermal gain from this incident light, the diffuse radiation intensity must first be integrated over the hemisphere surrounding the collector face giving a flux with units of w/m^2, and then over the collector area to finally provide the gain in watts. Figure 18 shows the quantities used in the space angle integration. Vectors are expressed in the collector (B) frame for convenience. In the figure, $\overline{U}_i$ specifies the orientation of the incident light ray as before, $\overline{U}_n$ is the collector normal, and $\overline{U}$ is a unit vector of varying orientation which represents the centerline of the differential space angle, $d\omega$. Angles β and η specify the relative orientation of $\overline{U}$ and $\overline{U}_n$. β_D is the angle which $\overline{U}$ makes with $\overline{U}_i$.

Let

$$\mu = \begin{cases} \overline{U} \cdot \overline{U}_n, \text{ if } \overline{U} \cdot \overline{U}_n > 0, \\ 0, \text{ if } \overline{U} \cdot \overline{U}_n \leq 0, \end{cases}$$

$$\mu_D = \begin{cases} -\overline{U} \cdot \overline{U}_i, \text{ if } \overline{U} \cdot \overline{U}_i < 0 \\ 0, \text{ if } \overline{U} \cdot \overline{U}_i \geq 0 \end{cases}$$

$$\beta = \cos^{-1}(\mu),$$

$$\beta_D = \cos^{-1}(\mu_D),$$

$$\text{and, } d\omega = \sin\beta d\beta d\eta$$

The component of radiant flux associated with a space angle element incident upon the collector is now written

$$d\phi = W_D \mu \, d\omega$$

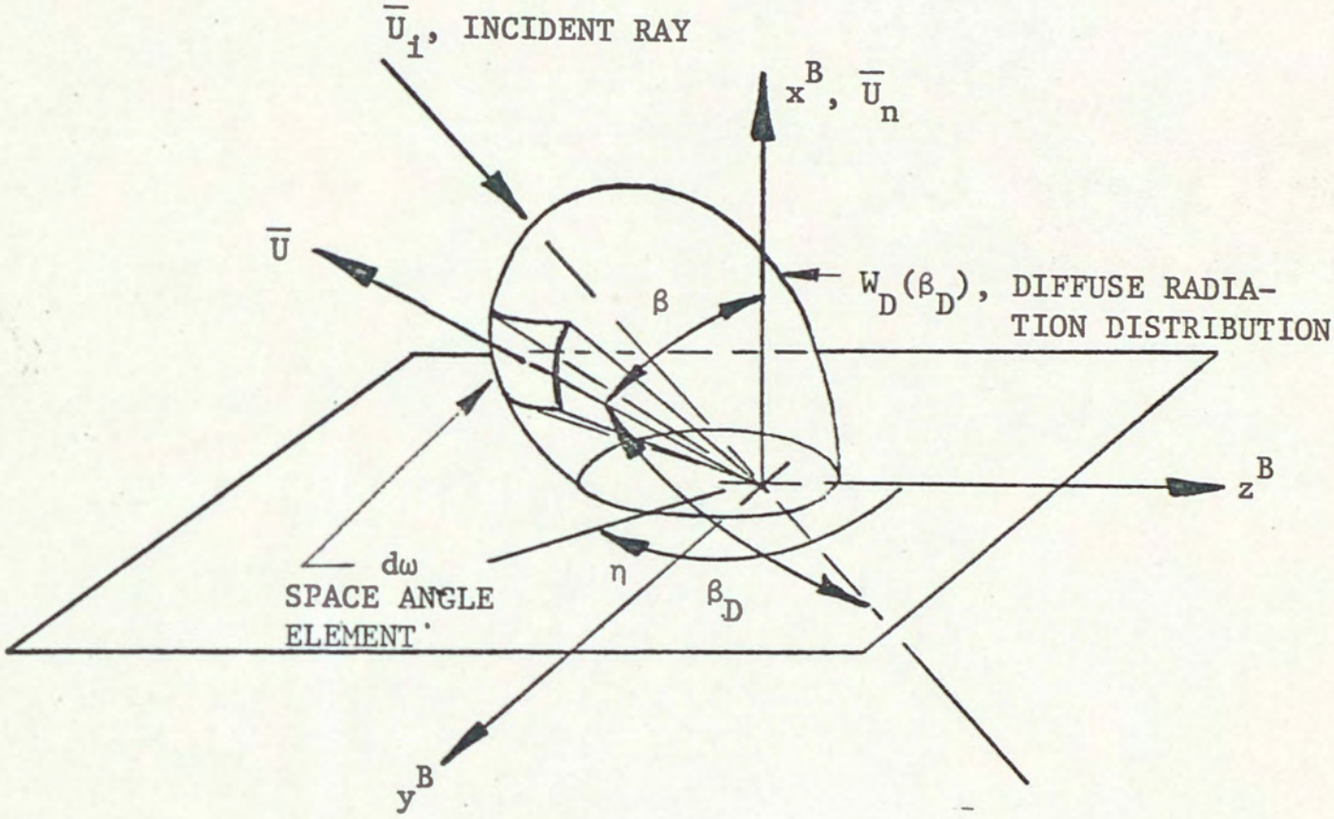

Figure 18. Space Angle Integration of Diffuse Radiation

The incremental absorbed radiation is then,

$$d\phi_A = W_D \mu \alpha\tau(\beta) d\omega$$

This must be integrated over the hemisphere visible to the collecting surface. The total absorbed power from diffuse radiation is obtained simply by integrating the absorbed flux over the collector area.

$$P_D = \int_{A_C} [\int_{2\pi} d\phi_A] dA$$

The total thermal power absorbed or gained by the collector plate is just the sum of the beam and diffuse gains.

$$\dot{q}_{INP} = P_B + P_D$$

The thermal power absorbed by the glass cover, $\dot{q}_{INP}$, is also computed with these equations using the appropriate absorptivity. In general, losses will substantially reduce the thermal energy available for useful heat exchange.

Note that in the course of the space angle integration, the variable vector, $\overline{U}$, points at both the sky and the ground. The value used for the diffuse intensity, W_D, is determined by the orientation of $\overline{U}$. Hence,

$$W_D = \begin{cases} W_D(\beta_D), & \text{if } \overline{U} \text{ points toward the sky,} \\ W_{D\ ENV}, & \text{if } \overline{U} \text{ points toward the ground.} \end{cases}$$

The sky radiation, $W_D(\beta_D)$, is treated only as a function of the angle,

β_D, as explained in the discussion of atmospheric diffusion. The quality, $W_{D\ ENV}$, is just an assumed "environmental" radiation emitted by the ground. This was described in the section dealing with radiation sources other than the sun and sky.

A focusing collector is shown in Figure 19 with a radiation distribution similar to that specified for the flat plate. The geometry of this system is more complex than for a flat plate collector. Here, the intersection of an incident light ray, $\overline{U}_i$, with the parabolic mirror must be described, and it must be determined if a reflected ray, $\overline{U}_r$, strikes the absorber plate. If the reflected ray is intercepted by the absorber, that process must be described just as in the case of the flat plate. In addition, the thermal gain from diffuse radiation striking the absorber must be computed.

The radiation absorbed from collimated sunlight is determined by integrating the contribution of area elements, dA_R, making up the parabolic mirror. The integration is complicated by the fact that the absorber plate casts a shadow on the reflector. Area elements within this shadow contribute nothing to the beam radiation falling on the absorber. The reflector area elements, dA_R, represent components of the reflecting surface area. For convenience, these elements are described in terms of their projection into the y-z plane of the collector coordinate frame. The element, dA_R', is the projection of dA_R in this plane. The orientation of the unit normal, $\overline{U}_{nR}$, of element, dA_R, relative to the collector x axis determines the magnitude of the projection. The path of a reflected light ray is computed from the orientation of the incident ray and the unit normal, $\overline{U}_{nR}$.

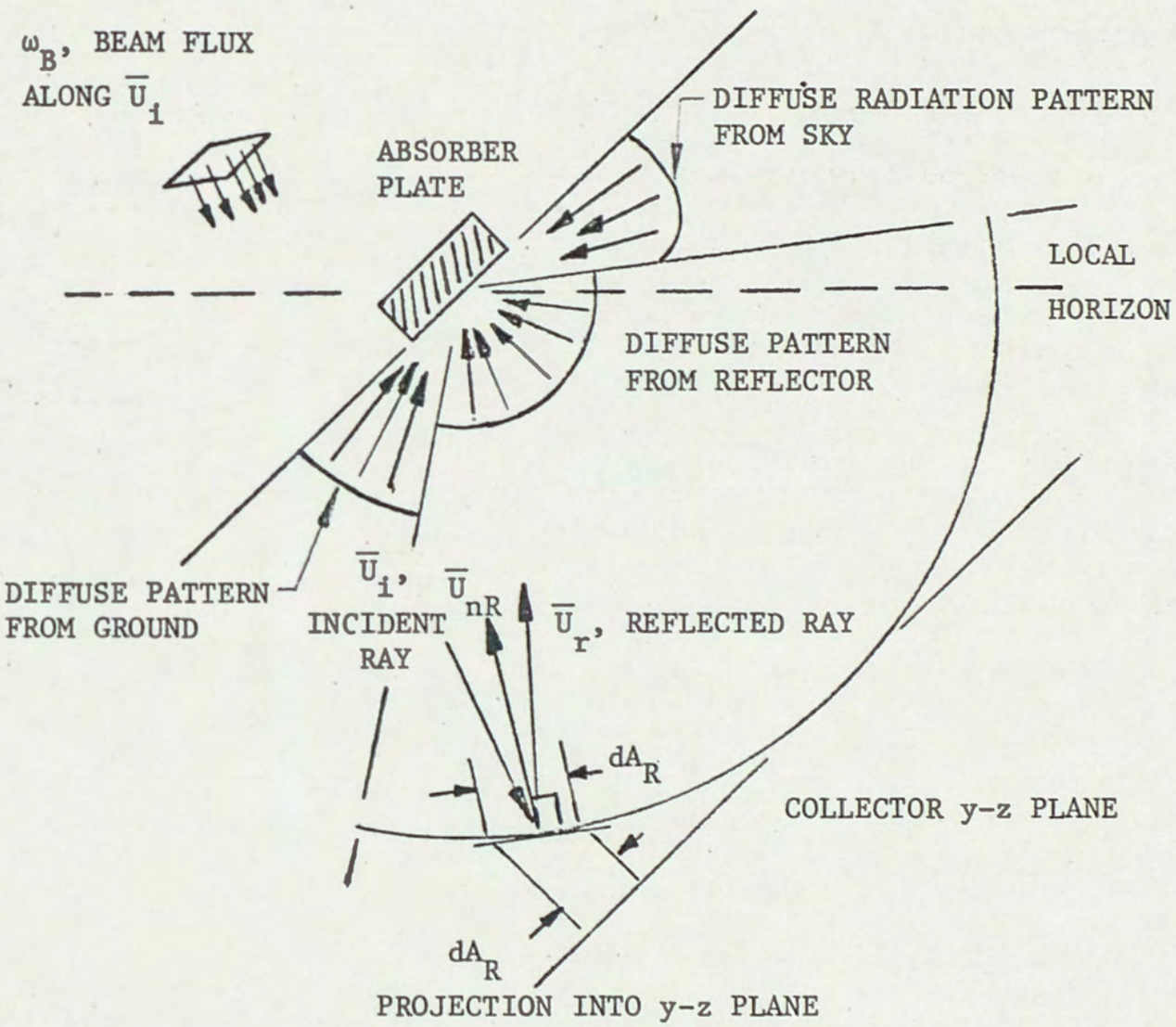

Figure 19. Radiation Environment of Focusing Collector

Techniques for computing a vector unit normal to the parabolic surface and a vector reflection from it are shown in the appendices.

For each area element in the reflector, a unit normal is calculated--

$$\overline{U}_{nR} = \frac{1}{\zeta}\begin{bmatrix} 1 \\ -2Ky \\ 0 \end{bmatrix}, \quad \text{where } \zeta = \quad 1 + (2Ky)^2$$

Now, $dA_R = \zeta dA_R'$. Note that dA_R' represents an area in the y-z plane.

Let

$$\mu_R = \begin{cases} -\overline{U}_{nR} \cdot \overline{U}_i, & \text{if } \overline{U}_{nR} \cdot \overline{U}_i < 0, \\ 0, & \text{if } \overline{U}_{nR} \cdot \overline{U}_i \geq 0. \end{cases}$$

The reflected ray from the area element is,

$$\overline{U}_r = \overline{U}_i + 2\mu_R \overline{U}_{nR}$$

The angle between the incident (and reflected) ray and the area normal is,

$$\beta_R = \cos^{-1}(\mu_R)$$

The reflected thermal power from the area element is now computed.

$$dP_B = W_B \mu_R \rho(\beta_R) \zeta dA_R'$$

Here, W_B is the beam radiation flux normal to $\overline{U}_i$ having units of w/m^2, and ρ is the reflectivity of the mirror.

Let

$$\mu_A = \begin{cases} -\overline{U}_{nA} \cdot \overline{U}_r, & \text{if } \overline{U}_{nA} \cdot \overline{U}_r < 0, \\ 0, & \text{if } \overline{U}_{nA} \cdot \overline{U}_r \geq 0, \end{cases}$$

$$\text{and, } \beta_A = \cos^{-1}(\mu_A)$$

$\overline{U}_{nA}$ is a unit vector normal to the absorber plate which points toward the reflector. The absorbed thermal power from beam radiation contributed by each reflector area element is defined as follows:

$$dP_B = \begin{cases} \alpha(\beta_A)\, dP_R, & \text{if the reflected ray strikes the absorber,} \\ 0, & \text{if the reflected ray misses the absorber} \end{cases}$$

The total thermal gain from beam radiation is,

$$P_B = \int (A_R' - A_S') \, dP_B$$

The areas, A_R' and A_S', are, respectively, the projected areas of the reflector and the shadow cast by the absorber plate in the collector y-z plane.

The thermal gain from diffuse radiation for the focusing collector is derived, in part, from components emitted from this sky and the ground, as in the case of a flat plate. These components strike the absorber plate from around the periphery of the parabolic reflector. In addition, the mirror itself emits radiation for which the intensity is determined by the mirror emissivity and temperature. These are the major contributors. There is also some diffuse radiation from the sky

and the local environment which reaches the absorber plate after being reflected by the parabolic mirror. The mathematical description of that capture process is complicated, however, and predicts virtually no thermal gain from this source.

The inefficiency of the focusing system in collecting diffuse radiation is illustrated in Figure 20. An incremental space angle, $d\omega$, is shown emanating from the absorber located near the focal point of the mirror. The "reflection" of this angle is a mapping process which redirects the angle toward the sky. Integration of diffuse radiation falling in or "trapped by" reflected space angle elements over the hemisphere of the visible sky determines the collected diffuse energy. The initial angle, $d\omega$, is shown as a four-sided pyramid whose corners are rays intersecting the mirror as shown. The reflected rays continue to diverge in the collector z direction, but have been made nearly parallel in the y direction by the reflection or mapping process. The resulting wedge encloses no space angle because the area of its base does not vary as the square of its height as in the case of the pyramid. Hence, there is no space angle directed toward the sky to permit the capture of diffuse radiation. For this reason, reflected diffuse radiation is not considered a source of thermal energy in this analysis.

The computation of the absorption of diffuse light from the major contributors is handled as in the case of the flat plate, except that the mirror emission must be considered in addition to ground and sky radiation. For the focusing system, the unit vector, $\overline{U}$, and the associated space angle, $d\omega$, are defined within the hemisphere around

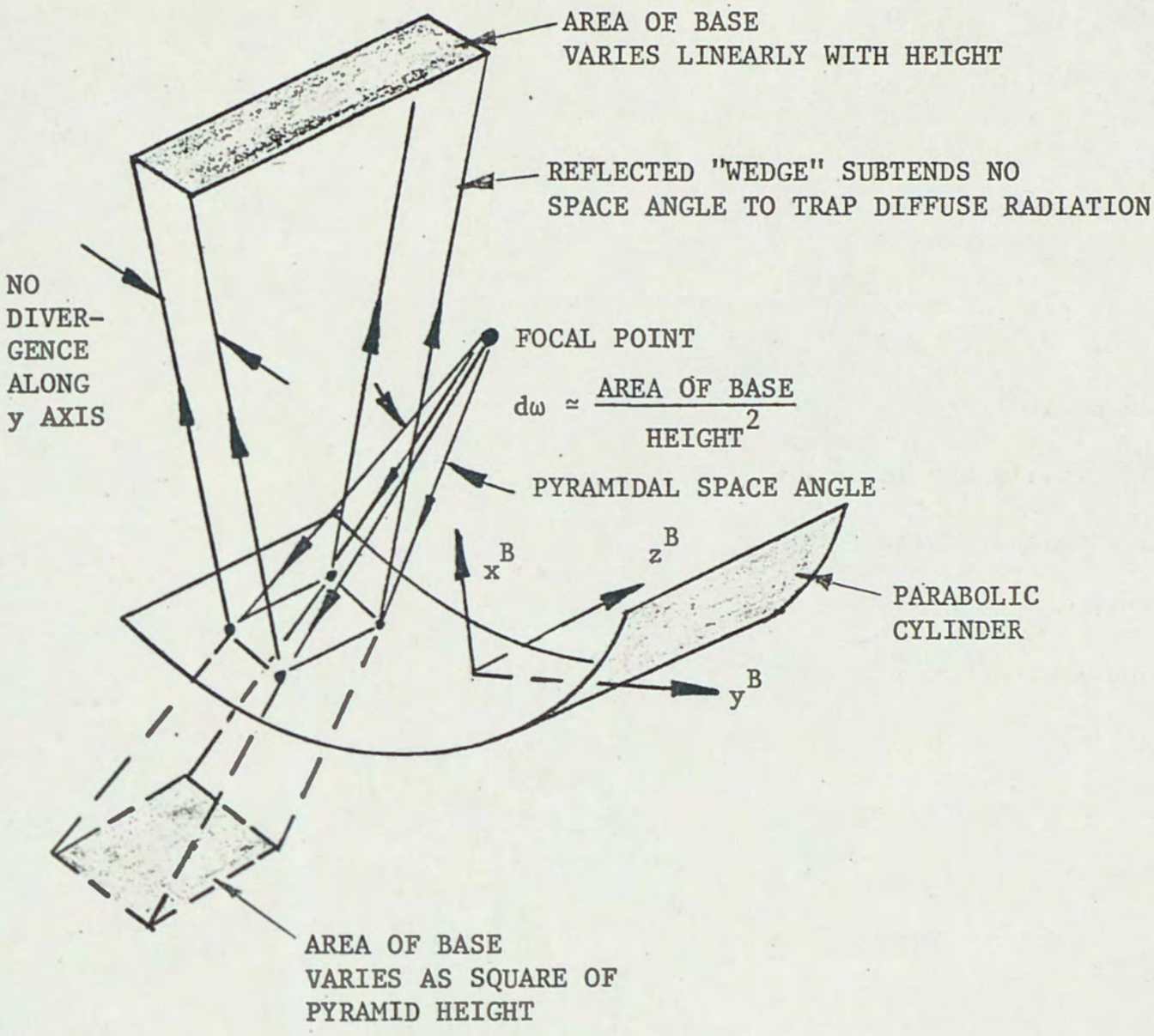

Figure 20. Inefficiency of Parabolic Reflector in Collecting Diffuse Radiation

the absorber surface. The quantities, μ, μ_D, β, and β_D, are defined as before. Now, the incident flux from a particular orientation of $\overline{U}$ is written,

$$d\phi = W_D \mu d\omega \quad \text{where} \quad W_D = \begin{cases} W_{D\ REFL}, & \text{if } \overline{U} \text{ points toward the reflector,} \\ W_D(\beta_D), & \text{if } \overline{U} \text{ points toward the sky,} \\ W_{D\ ENV}, & \text{if } \overline{U} \text{ points toward the ground.} \end{cases}$$

The absorbed flux is,

$$d\phi_A = W_D \mu \alpha(\beta) d\omega$$

where α is the absorbtivity of the absorber plate.

The total absorbed power from diffuse radiation requires integration with respect to space angle and area.

$$P_D = \int_{A_A} \left[\int_{2\pi} d\phi_A \right] d_A$$

In this expression, A_A is the absorber surface area. As in the case of the flat plate collector,

$$\dot{q}_{IN} = P_B + P_D,$$

$\dot{q}_{IN}$ representing total absorbed thermal power prior to any losses.

Temperature Control

Since the air conditioning application anticipated for the collectors under analysis requires thermal energy of high quality, some means of temperature control must be provided in the system. The

easiest means of maintaining a desired temperature would be to regulate the flow of working fluid or coolant through the heat exchanger in the collector. This would involve a throttle valve retarding coolant flow when the incident radiant flux was low and opening to admit extra coolant as this flux increased. The mechanism envisioned here is a simple thermostat which first permits fluid flow at a predetermined temperature, the set point, and, as fluid temperature increases, opens an amount proportional to this temperature rise. Eventually, the coolant flow area reaches the maximum permitted by the geometry of the device, and no further opening is possible.

If fluid flow is assumed to vary linearly with the flow area, a simple characteristic for the device is derived. This is illustrated in Figure 21 where fluid mass flow is plotted versus collector temperature. No flow of coolant is permitted below the set point, T_o. Above this value, the flow rate linearly ramps to a maximum at temperature, T_{oo}. At higher temperatures, no further variation in flow occurs and no temperature control is possible. If the sloping portion of the characteristic is sufficiently steep, the collector heat exchanger will be "flooded" with coolant as soon as the temperature exceeds T_o, and any deviation from the set point will be slight. Clearly, this control technique discards some solar energy in that no energy is collected at temperatures below the set point. It also aggravates system losses by throttling the working fluid to keep the temperature high. This is the price paid for temperature regulation, and is a necessary characteristic of any system designed to supply thermal energy of specified quality.

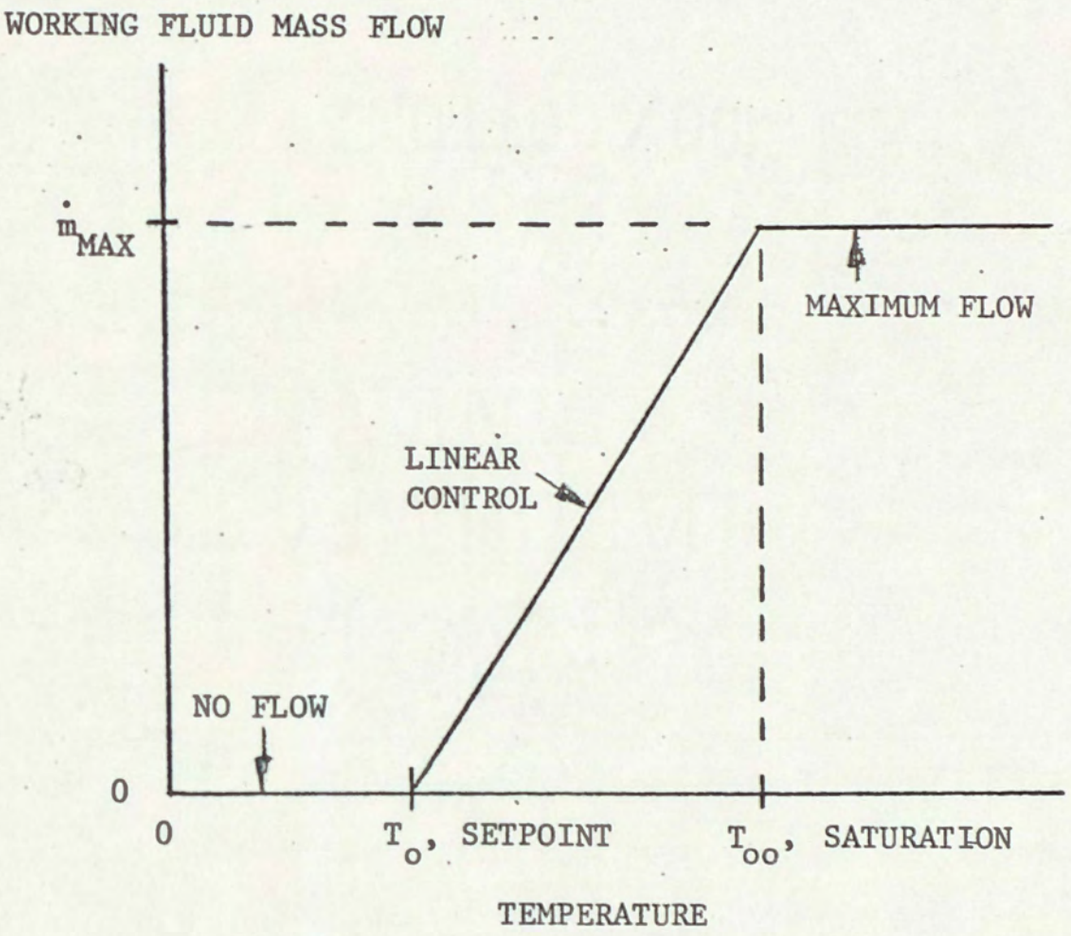

Figure 21. Assumed Thermostat Characteristic

A simplified schematic diagram of this conceptual thermostat is shown in Figure 22. The temperature sensitive valve is assumed immersed in the coolant emerging from the absorbing section of the collector so that its flow area closely reflects the delivery conditions of the fluid. The similarity of this device to the thermostat in automotive cooling systems is evident. Perhaps an automotive device could be used for such an application; in any case, it suggests a form which the collector thermostat might take.

The operation of a flat plate collector with the thermostat is fairly simple. Some time after sunrise, the temperature of the collector will rise sufficiently to open the thermostat and permit the working fluid to start circulating. Presumably a switch starting a circulating pump will close at this time also. As the radiation flux incident upon the collector increases during the morning, the temperature of the working fluid rises slightly, causing the thermostat to open further to permit more fluid flow. In the afternoon, this process will reverse itself. The thermal power collected by the working fluid (and the flow rate of the fluid itself) resembles a sine wave if plotted against time of day with the peak thermal gain at solar zenith. The temperature of the working fluid remains constant at a value corresponding to that of the coolant reservoir until the thermostat opens. The delivery temperature then jumps to the set point value and remains there with only small excursions until the thermostat closes in the afternoon. The effect of passing clouds or overcast conditions would be to reduce the working fluid flow rate and the thermal power collected. There will be very little disturbance to the

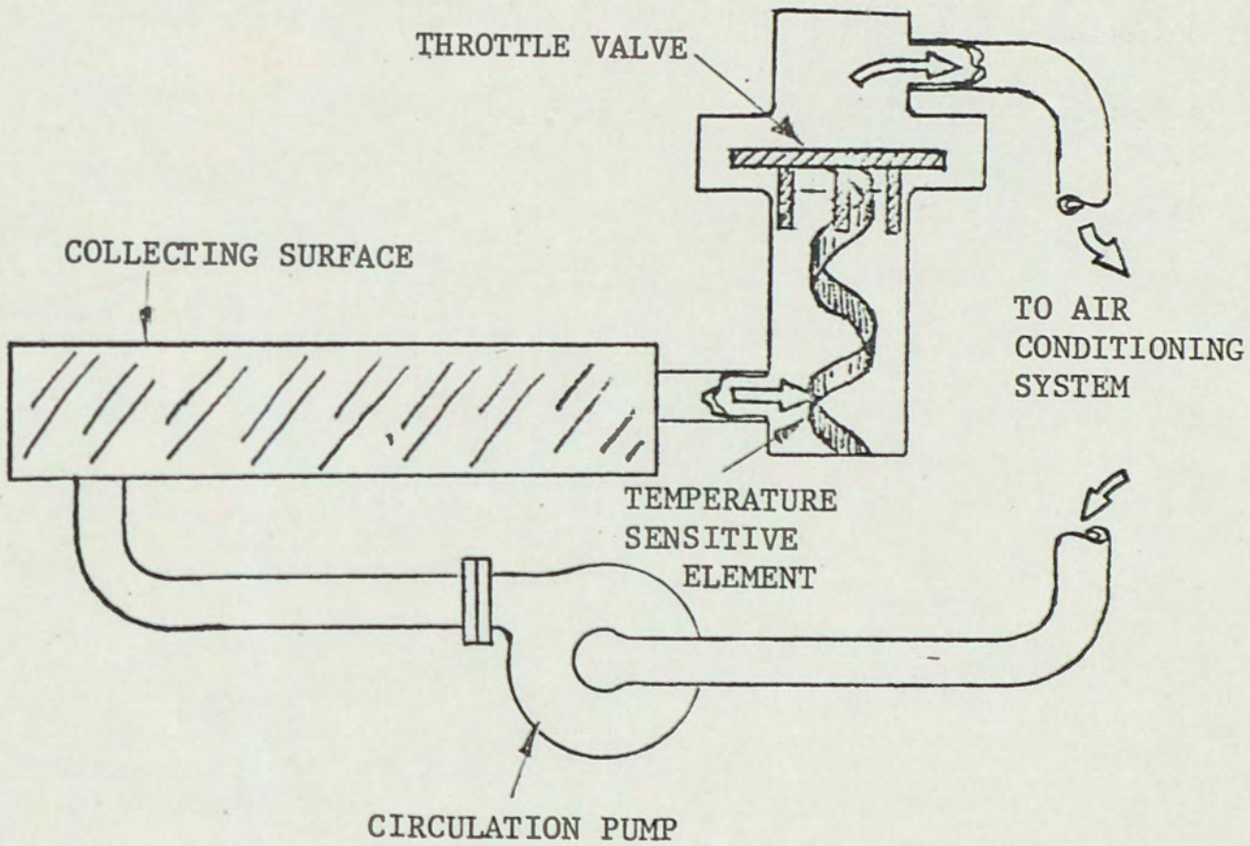

Figure 22. Collector Thermostat Concept

fluid temperature due to these effects, however.

The face of the flat plate collector is always uniformly illuminated during the day; in contrast, the radiation flux falling on the absorber plate in the focusing system varies considerably down the length of the device as the sun moves across the sky. The motion of the portion of the absorber plate illuminated by beam radiation is illustrated in the Introduction in Figure 3. To reduce losses and increase the working fluid delivery temperature in this system, it would be desirable to admit fluid only to the illuminated portion of the absorber. An approximate method for accomplishing this is to subdivide the absorber into a series of individual cells, each containing its own thermostat. Then only those cells receiving sufficient solar energy to open their thermostats will permit coolant flow. Within each cell, the flow is regulated so that the desired fluid delivery temperature is maintained. The absorber cells are manifolded for parallel input and output from a single pump as shown in Figure 23. In this system, the total fluid mass flow is a function of all the cell temperatures and the total thermal power is the sum of the contributions of each cell.

The operation of the focusing collector with this heat exchanger and temperature control arrangement is similar to that of the flat plate with a single thermostat. Here, a number of cells are functioning independently as a series of miniature "flat plates". As in the case of the flat plate system, the fluid delivery temperature is tightly controlled throughout the day. With the modular arrangement, however, a plot of thermal power over the course of a day's operation

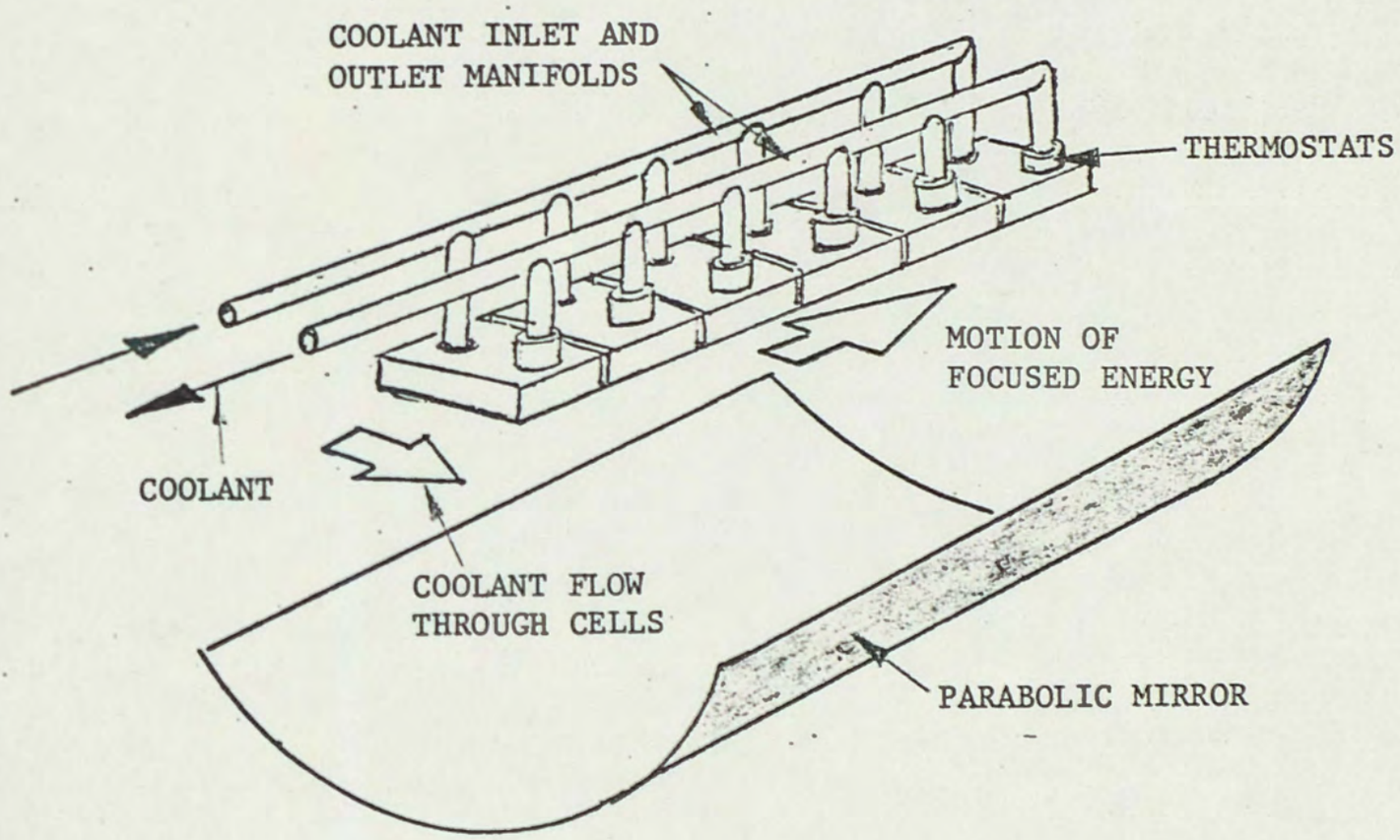

Figure 23. Absorber Cells in Focusing Collector

would generally reveal a sequence of "steps" or rapid changes in collected power coinciding with the abrupt opening and closing of thermostats as the illuminated portion of the absorber plate shifted across the cells.

Collector Energy Balance and Losses

In the solar collector heat exchanger, the thermal energy absorbed by the collecting surface heats a working fluid which transports it to the appropriate location. The heat absorbed by the working fluid represents the useful or net thermal energy absorbed by the device. This contrasts the "gross" energy or thermal gain of the collector which includes all of the energy absorbed by the collector plate. The difference between the two quantities is the energy lost from the plate through thermal conduction, convection, and radiation. These losses represent heat transfer through the walls of the heat-absorbing section of the collector, including the absorbent face.

Suitable design and generous use of thermal insulation can reduce losses through the absorber housing to an arbitrary level. Losses through the absorbent face of the system, however, are determined by the mechanism of heat absorption inherent in the collector design. Obviously, it is not possible to insulate the collecting face of the system if any energy is to be absorbed. Therefore, losses through the face must be accepted as part of the operating characteristics of the collector. Since the absorber face losses are a direct function of the thermal gain of the device, they are called "coupled" losses [10]. Losses through the other sides of the absorber section

are arbitrarily reduceable and are, therefore, "uncoupled". Only coupled losses are considered here because they represent the most significant loss component in a well-designed system. Also collector performance predictions considering only coupled losses indicate the "limiting case" of collector efficiency.

Computation of net thermal power and working fluid delivery temperature derived from an incident radiation flux requires consideration of the radiation properties of the absorbent surface, the glass cover, the thermal properties of the fluid, and the temperature control mechanism of the collector. For the following development, it will be assumed that the energy absorbed by the collector heat exchanger and the cover have been computed by the means outlined in the energy gain section. Other assumptions are that the working fluid undergoes no phase change in the collector, that its specific heat, C_p, is constant, and, finally, that the delivery temperature of the fluid is equal to that of the heat exchanger surface. Coupled losses for a flat plate collector and the radiation exchange between the plate and the glass cover are shown in Figure 24. Here, T_p is the temperature of the collector heat exchanger plate as well as the working fluid discharge, T_c is the temperature of the glass cover, and T_∞ is the outside air temperature.

Loss mechanisms include a convection-conduction path and a radiation path. Thermal energy is convected via the air inside the collector from the collector plate to the glass cover. The film coefficient for convection inside the system is denoted h_i. Thermal losses then propagate through the glass cover having conductivity, k,

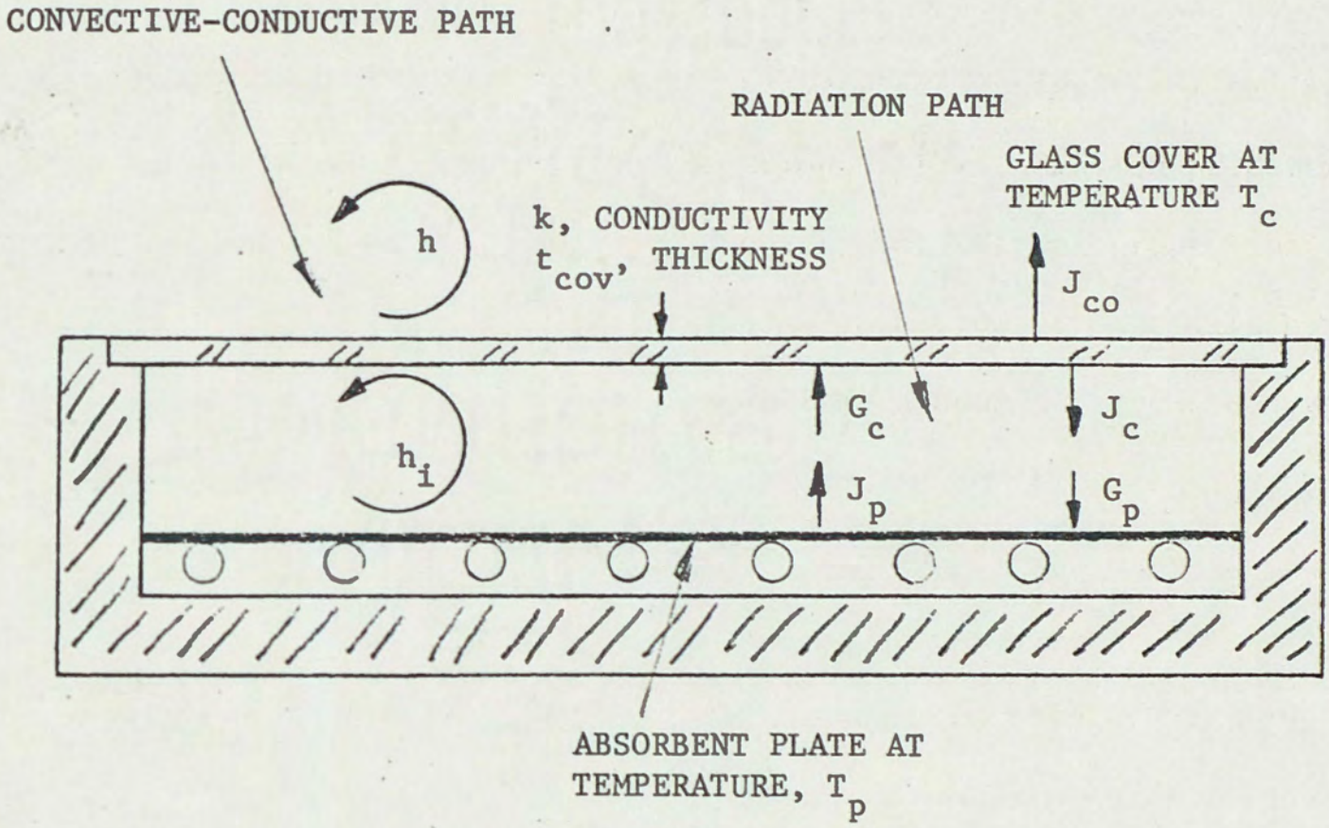

Figure 24. Loss Paths in Flat Plate Collector

and thickness, t. Finally, energy lost via this path is convected from the outer surface of the glass cover with a film coefficient, h. The radiation path starts with emission from the collector plate and requires transmission through the glass cover. In addition, the emission of the glass cover and the exchange of this radiation with the absorbent plate must be considered. In the figure, the symbol "J" denotes thermal energy leaving a surface, and "G" denotes energy striking a surface. Since the thermal input to the device is specified by the equations described previously, only the emissive exchange between the glass cover and the absorbent plate will be considered. The energy contribution of incident or trapped solar energy is neglected here.

With these starting assumptions, the following quantities are defined:

$\dot{q}_{INP}$	thermal power from incident flux absorbed by the plate
$\dot{q}_{INC}$	thermal power from incident flux absorbed by the glass cover
$\dot{q}_{NET}$	net thermal power after losses
$\dot{q}_{CP}$	loss through convection and conduction
$\dot{q}_{CC}$	net loss through convection and conduction from cover
$\dot{q}_{RAD}$	radiation loss from plate
$\dot{q}_{RADC}$	net radiation loss from cover
$\dot{m}$	working fluid mass flow
C_p	working fluid specific heat

$\dot{m}_{MAX}$ maximum mass flow permitted by thermostat

T_{IN} working fluid inlet temperature

T_{OUT} working fluid delivery temperature

A_C collector area

h_i' lumped convective-conductive loss coefficient for plate-cover exchange

h' lumped convective-conductive loss coefficient for cover-environment exchange

J_P radiant power leaving plate, excluding solar wavelengths

G_P radiant power striking plate, exluding solar flux

J_C radiant power leaving glass cover from interior surface, excluding solar flux

G_C radiant power striking glass cover on interior surface, excluding solar wavelengths

J_{CO} radiant power leaving glass cover from exterior surface, excluding solar wavelengths

ε_P hemispherical total plate emissivity

ρ_P hemispherical total plate reflectivity

ε_C hemispherical total cover emissivity

ρ_C hemispherical total cover reflectivity

τ_C hemispherical total cover transmissivity

The convective-conductive loss path is described with two coefficients reflecting the characteristics of the path,

$$h_i' = h_i + k/2t$$

$$h' = h + k/2t$$

The temperatures of the plate and the cover, convective losses, and radiation losses must be determined simultaneously. The following seven equations are written for the system:

(1) $$\dot{q}_{NET} = \dot{q}_{INP} + G_P - J_P - h_i' A_C (T_P - T_C)$$

(2) $$J_{CO} = \dot{q}_{INC} + G_C - J_C + h_i' A_C (T_P - T_C) - h' A_C (T_C - T_\infty)$$

$$J_P = \varepsilon_P A_C \sigma T_P^4 + \rho_P G_P \qquad [9]$$

$$J_C = \varepsilon_C A_C \sigma T_C^4 + \rho_C G_C \qquad [9]$$

$$J_{CO} = \varepsilon_C A_C \sigma T_C^4 + \tau_C G_C$$

$$G_P = J_C$$

$$G_C = J_P$$

The last five equations are solved for J_P, J_C, and J_{CO} in terms of the temperatures T_P and T_C.

$$J_P = \left(\frac{1}{1-\rho_P\rho_C}\right) \varepsilon_P A_C \sigma T_P^4 + \left(\frac{\rho_P}{1-\rho_P\rho_C}\right) \varepsilon_C A_C \sigma T_C^4$$

$$J_C = \left(\frac{\rho_C}{1-\rho_P\rho_C}\right) \varepsilon_P A_C \sigma T_P^4 + \left(\frac{1}{1-\rho_P\rho_C}\right) \varepsilon_C A_C \sigma T_C^4$$

$$J_{CO} = \left(\frac{\tau_C}{1-\rho_P\rho_C}\right) \varepsilon_P A_C \sigma T_P^4 + \left(\frac{1+\rho_P\tau_C-\rho_P\rho_C}{1-\rho_P\rho_C}\right) \varepsilon_C A_C \sigma T_C^4$$

The convective loss terms are,

$$\dot{q}_{CP} = h_i' A_C \, (T_P - T_C)$$

$$\dot{q}_{CC} = h' A_C \, (T_C - T_\infty) - \dot{q}_{CP}$$

The net radiation energy lost from the plate is the difference between J_P and G_P (or J_C).

$$\dot{q}_{RAD} = J_P - J_C = \left(\frac{1-\rho_C}{1-\rho_P\rho_C}\right) \varepsilon_P A_C \sigma T_P^4 - \left(\frac{1-\rho_P}{1-\rho_P\rho_C}\right) \varepsilon_C A_C \sigma T_C^4$$

The net radiant energy leaving the glass cover is the sum,

$$J_{CO} + J_C - G_C \text{ (or } J_P)$$

This is expressed as,

$$\dot{q}_{RADC} = J_{CO} - \dot{q}_{RAD}$$

The fraction of maximum fluid mass flow, f, permitted by the thermostat is determined by the thermostat model,

$$0, \text{ if } T_P < T_O,$$

$$f = \frac{T_P - T_O}{T_{OO} - T_O}, \text{ if } T_O \leq T_P < T_{OO},$$

$$1, \text{ if } T_{OO} \leq T_P.$$

Now,

$$\dot{m} = f\dot{m}_{MAX}$$

and,

$$\dot{q}_{NET} = (C_P\dot{m})\ (T_P - T_{IN}).$$

Note that the net thermal power and the loss terms are functions of the plate temperature, T_P, and the cover temperature, T_C. Equations 1 and 2 are solved for these temperatures. This gives the delivery temperature of the working fluid and the net thermal energy absorbed.

Since the radiation terms make the equations non-linear, they are most easily solved iteratively with a computer. For the iterative approach, plate and cover temperatures are assumed and residuals R_P and R_C are computed for the energy balance.

$$R_P = \dot{q}_{NET} - \dot{q}_{INP} + \dot{q}_{CP} + \dot{q}_{RAD}$$

$$R_C = -\dot{q}_{INC} + \dot{q}_{CC} + \dot{q}_{RADC}$$

Both residuals must be reduced to zero in the solution of the equations. For simplicity, the following substitutions are made:

$$F_{RP1} = \left(\frac{1-\rho_C}{1-\rho_P\rho_C}\right)\ \varepsilon_P A_C G$$

$$F_{RC1} = \left(\frac{1-\rho_P}{1-\rho_P\rho_C}\right)\ \varepsilon_C A_C G$$

$$F_{RP2} = \left(\frac{\tau_C}{1-\rho_P\rho_C}\right)\ \varepsilon_P A_C G$$

$$F_{RC2} = \left(\frac{1+\rho_P\tau_C-\rho_P\rho_C}{1-\rho_P\rho_C}\right)\ \varepsilon_C A_C G$$

Now,

$$R_P = fC_P\dot{m}_{MAX}\,(T_P-T_{IN}) - \dot{q}_{INP} + h_i'A_C\,(T_P-T_C) + F_{RP1}\,T_P^{\,4} - F_{RC1}\,T_C^{\,4}$$

$$R_C = -\dot{q}_{INC} + h'A_C\,(T_C-T_\infty) - h_i'A_C\,(T_P-T_C) + F_{RP2}\,T_P^{\,4} + F_{RC2}\,T_C^{\,4}$$

$$-F_{RP1}\,T_P^{\,4} + F_{RC2}\,T_C^{\,4}.$$

The change in R_P and R_C with T_P and T_C may be estimated with partial derivatives. if ΔT_P and ΔT_C are small errors in the temperature estimates, then,

$$\begin{bmatrix} R_P \\ R_C \end{bmatrix} \simeq \begin{bmatrix} \frac{\partial R_P}{\partial T_P} & \frac{\partial R_P}{\partial T_C} \\ \frac{\partial R_C}{\partial T_P} & \frac{\partial R_C}{\partial T_C} \end{bmatrix} \begin{bmatrix} \Delta T_P \\ \Delta T_C \end{bmatrix}$$

The determinant of the matrix of partial derivatives is

$$DET = \frac{\partial R_P}{\partial T_P}\frac{\partial R_C}{\partial T_C} - \frac{\partial R_C}{\partial T_P}\frac{\partial R_P}{\partial T_C}$$

The matrix is inverted and the equation solved for the temperature errors.

$$\Delta T_P = \left(\frac{\partial R_C}{\partial T_C} R_P - \frac{\partial R_P}{\partial T_C} R_C\right) /DET$$

$$\Delta T_C = \left(-\frac{\partial R_C}{\partial T_C} R_P + \frac{\partial R_P}{\partial T_P} R_C\right) /DET$$

The partial derivatives are defined as follows:

$$\frac{\partial R_P}{\partial T_P} = \left(\frac{T_P - T_{IN}}{T_O - T_{OO}} + f\right) C_P \dot{m}_{MAX} + h_i' A_C + 4F_{RP1} T_P^3$$

The term,

$$\frac{T_P - T_{IN}}{T_O - T_{OO}},$$

is

$$\frac{\partial f}{\partial T_P}.$$

$$\frac{\partial R_P}{\partial T_C} = -h_i' A_C - 4F_{RC1} T_C^3$$

$$\frac{\partial R_C}{\partial T_P} = -h_i' A_C + 4F_{RP2} T_P^3 - 4F_{RP1} T_P^3 = -h_i A_C + 4(F_{RP2} - F_{RP1}) T_P^3$$

$$\frac{\partial R_C}{\partial T_C} = h' A_C + h_i' A_C + 4F_{RC2} T_C^3 + 4F_{RC1} T_C^3$$

$$= (h' + h_i') A_C + 4(F_{RC2} + F_{RC1}) T_C^3$$

The values of T_P and T_C used in the equations are estimates of these temperatures. The temperature estimates are adjusted by the corrections determined in the matrix inversion,

$$T_P = T_P - \Delta T_P$$

$$T_C = T_C - \Delta T_C.$$

These are the temperature estimates for the next iteration. By looping through these equations, the correct values of T_P, T_C, and $\dot{q}_{NET}$ are approached. The iterations cease when the temperature error estimates ΔT_P and ΔT_C drop below a specified tolerance.

Coupled losses for the focusing system are shown in Figure 25. Here, loss paths result from convection from the exposed surfaces of the cell absorber plates and emission of radiation from these surfaces. The energy balance equation is simpler than that for the flat plate, because there is no exchange with a glass cover. Here, however, the energy balance must be computed for each cell in the collector system. Since there are no glass covers on the cells, the convective loss path is described only with the film coefficient, h, and the radiative path with the hemispherical total emissivity, ε_{HT}, of the absorber surface. Now the terms in the energy balance equation must be subscripted to denote a specific cell. Cell areas are denoted, A_i. The absorber will be assumed to consist of "N" cells, each having a temperature, T_{pi}.

Let

$$e_i = \begin{cases} 0, & \text{if } T_{pi} < T_O, \\ T_{pi} - T_O, & \text{if } T_O \leq T_{pi} < T_{OO}, \\ T_{OO} - T_O, & \text{if } T_{OO} \leq T_{pi}, \end{cases}$$

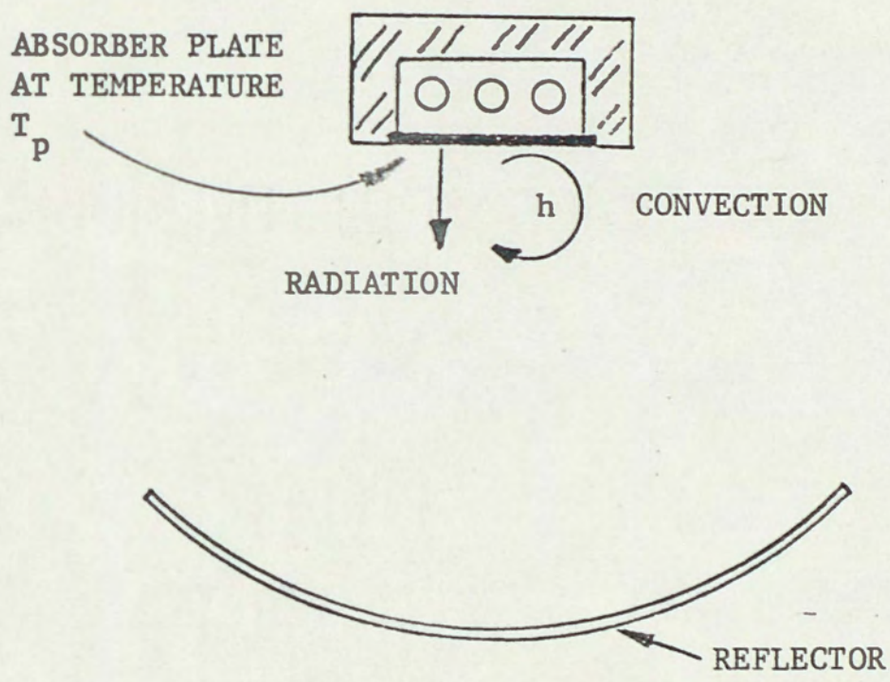

Figure 25. Loss Paths in Focusing Collector

$$E = \sum_{i=1}^{N} e_i,$$

and

$$f_i = \frac{e_i}{E}.$$

f_i is the fraction of total working fluid mass flow, $\dot{m}_{TOT}$, allocated by the temperature control system to cell, "i".

$$\dot{m}_{TOT} = [E/N\ (T_{OO}-T_O)]\ \dot{m}_{MAX}$$

The denominator of this expression is a proportionality constant representing the condition in which all of the cell thermostats are fully open.

Now,

$$\dot{q}_{NET\ i} = f_i\ (C_p \dot{m}_{TOT})\ (T_{pi}-T_{IN}),$$

and the convective and radiation loss terms are simply,

$$\dot{q}_{c\ i} = hA_i\ (T_{pi}-T_\infty)$$

and

$$\dot{q}_{RAD\ i} = A_i \varepsilon_{HT} \sigma T_{pi}^4.$$

A set of N simultaneous equations must be solved for the energy balance.

$$\dot{q}_{NET\ i} - \dot{q}_{IN\ i} + \dot{q}_{c\ i} + \dot{q}_{RAD\ i} = 0,\ i = 1,\ N.$$

Equation residuals are computed as in the case of the flat plate,

$$R_i = f_i\ (C_p \dot{m}_{TOT})\ (T_{pi}-T_{IN}) + hA_i\ (T_{pi}-T_\infty) + A_i \varepsilon_{HT} \sigma T_{pi}^4,$$

The equations are differentiated with respect to the temperatures, T_{pi}.

$$\Delta R_i = f_i\ (C_p \dot{m}_{TOT})\ \Delta T_{pi} + C_p \dot{m}_{TOT}\ (T_{pi}-T_{IN})\ \Delta f_i + hA_i \Delta T_{pi}$$

$$+ 4\ A_i\ \varepsilon_{HT}\ \sigma\ T_{pi}^3\ \Delta T_{pi}$$

or,

$$\Delta R_i = [C_p \dot{m}_{TOT}\ (f_i + \frac{T_{pi}-T_{IN}}{T_{OO}-T_O}) + hA_i + 4A_i \varepsilon_{HT} \sigma T_{pi}^3]\ \Delta T_{pi}$$

The temperature corrections for each cell are computed with the derivative.

$$\Delta T_{pi} = R_i / (\Delta R_i / \Delta T_{pi})$$

New temperatures are then estimated with these corrections,

$$T_{pi} = T_{pi} - \Delta T_{pi}.$$

A convergence test stops the iterations as in the previous discussion.

The net total thermal power collected is determined as simply:

$$(\dot{q}_{NET})_{TOT} = \sum_{i=1}^{N} \dot{q}_{NET\ i}.$$

The working fluid delivery temperature is then found to be,

$$T_{OUT} = \frac{(\dot{q}_{NET})_{TOT}}{C_p \dot{m}_{TOT}}.$$

Collector Figure of Merit

Two parameters are of interest in assessing the performance of a solar collector intended for an air conditioning application--the quantity of solar energy collected and the temperature at which it can be delivered to the system. The comparison of two collector candidates is simplified if a single figure of merit encompassing both these parameters can be used. Since the purpose of an air conditioner is to remove heat from an area while maintaining a lowered temperature, the quantity of heat which can be removed would seem to be a good measure of the effectiveness of the system. A prediction of heat removal for an actual air conditioner involves many practical considerations dependent upon the design of that particular device. The approach taken here is to assume an ideal, reversible air conditioning cycle, and predict system performance accordingly. It will be assumed that the relative performance of collector candidates in driving the ideal system reflects their relative performance in an actual installation.

The absorption refrigeration cycle is fairly complex with several phase changes and solution concentrations "in the loop".

The cycle can be analyzed thermodynamically in a straightforward manner, however, Figure 26 shows a purely theoretical model of an absorption cycle. Heat from the solar collector, Q_H, is supplied the air conditioner at temperature T_H'. The high temperature point in the reversible cycle, the boiler, is at temperature, T_H. Some irreversibility is involved in the transfer process, but this is not considered part of the ideal cycle. Q_C is the heat drawn from the cooled area maintained at temperature, T_C. All waste heat from the device is dumped to the local environment at the ambient temperature, T_A. In this model, a Carnot engine drives an ideal refrigerator, a Carnot engine "running backward". The Carnot engine operates between the temperatures T_H and T_A, while the refrigerator operates between T_C and T_A.

The coefficient of performance (COP) of this cycle is defined to be the ratio Q_C/Q_H. This can be rewritten,

$$COP_i = (Q_C/W) \times (W/Q_H)$$

where W is the work done by the hypothetical Carnot engine. The quantity, Q_C/W, is the usual definition of refrigerator COP; W/Q_H is the efficiency of the heat engine. For the ideal case,

$$Q_C/W = \frac{T_C}{T_A - T_C}$$

and

$$W/Q_H = \frac{T_H - T_A}{T_H} .$$

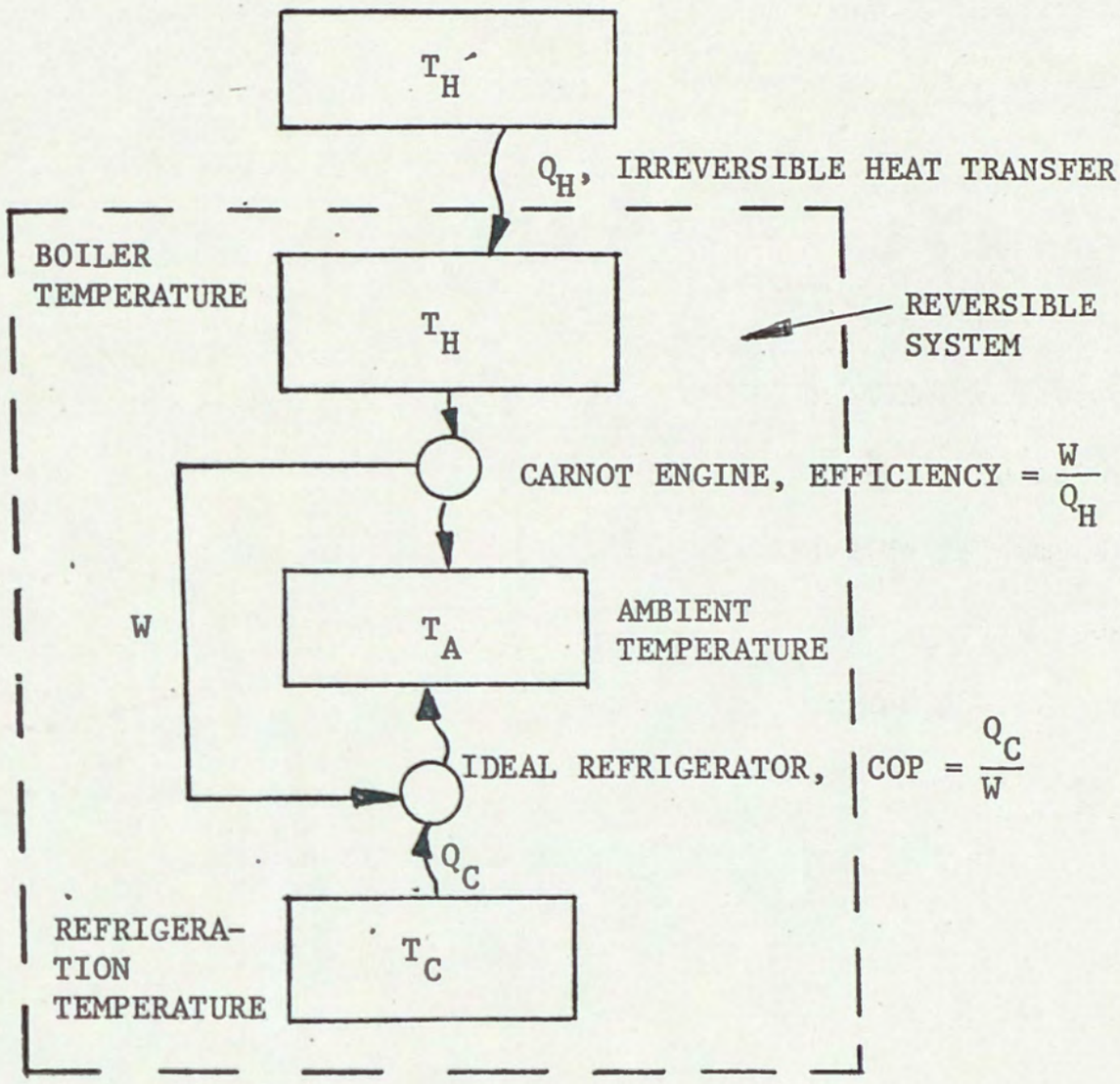

Figure 26. Thermodynamic Model of Ideal Absorption Cycle Supplied by Solar Collector

Thus, the ideal coefficient of performance is,

$$COP_i = \left(\frac{T_C}{T_A - T_C}\right)\left(\frac{T_H - T_A}{T_H}\right).$$

The ideal quantity of heat removed from the refrigerated area by the system is,

$$Q_C = Q_H\,(COP_i). \qquad [2]$$

This expression will be used as the definition of the collector figure of merit in subsequent performance comparisons.

Note that this definition separates important system characteristics into distinct groups. As would be expected, the figure of merit varies linearly with the quantity of energy, Q_H, supplied by the solar collector. Energy quality is reflected in the ideal COP. Here, the term,

$$\frac{T_C}{T_A - T_C},$$

represents the portion of the COP which is determined by the collector temperature T_H', since this limits the driving temperature, T_H [2]. It is apparent that Q_C can be increased by increasing the supplied thermal energy or by increasing the ideal coefficient of performance. For two systems to be equivalent, it is only necessary for their Carnot works,

$$Q_H \left(\frac{T_H - T_A}{T_H}\right),$$

to be equal, provided the temperatures T_C and T_A are the same for both units. This implies that a trade off can be made between Q_H and T_H for equal performance. This is exactly the choice afforded by the flat plate and focusing collector configurations.

III. COMPUTER PROGRAM DESCRIPTION

The mathematical models developed in the preceeding section have been implemented in a FORTRAN computer program. The program predicts the behavior of either of the collector systems under study at a specified latitude and time of year. The program steps through a simulated day at discrete time intervals and determines the local solar environment surrounding the collector. The amount of energy captured by the collector from the environment and the delivery temperature of the system working fluid are computed for each time interval. All of the important parameters identified in the mathematical model section are inputs to the program. Thus, any of these parameters can be varied easily to represent any configuration consistent with the geometry and spectral characteristics assumed in the model development.

Only one type of collector is simulated by the program in a particular run. The choice of the collector is specified as an input. Obviously, a primary function of the program is to present collector data representing the operation of both collector systems for comparison. In addition, the flexibility afforded by the program permits other types of analyses. These include studies of collector geometry and sizing, collector materials, the aiming of the collector, and the sensitivity of collector performance to either manufacturing or aiming

tolerances. In addition, the effect of variations in collector thermostat set points or working fluid specific heat and flow rate can be evaluated.

In the following description of the program, some knowledge of FORTRAN by the reader has been assumed. The overall structure of the program is discussed, including important subroutines and variables. The program implementation of some of the mathematical models are explained in detail, where the complexity of the implementation warrants this. A complete listing of the program is included in Appendix VI. Note that comment cards have been placed in the listing at crucial points to help explain the program flow.

Program Structure

The computer program consists of a main program and a number of subroutines, each of which performs a specific function based on the development of the mathematical models described previously. Figure 27 shows the hierarchy of major subroutines. Input and output functions are performed in the main program, as well as initialization and overall control of program flow. The subroutines at the next lower level are called TIME, SOLPOS, FLPLC, and CYLRF. Subroutine TIME generates times at a specified interval throughout the simulated day. Times are available in the form of seconds from midnight, used for the computation of solar position, and, in the more familiar form of hours, minutes, and seconds, for printout. Times are represented as integers in the program, and are quantized to the nearest second. The position of the sun throughout the day is provided by subroutine

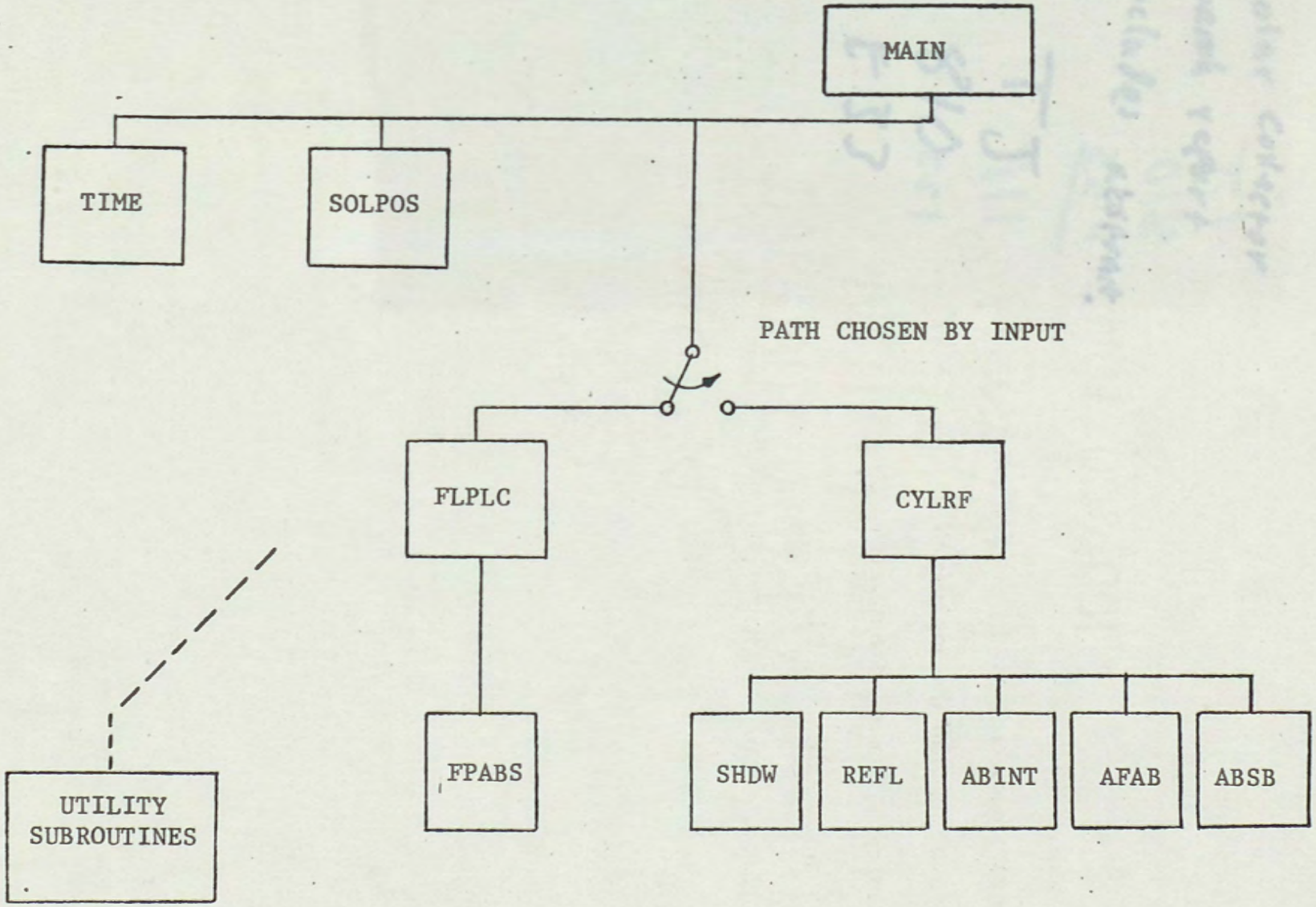

Figure 27. Subroutine Hierarchy in Computer Program

SOLPOS, using the times specified by TIME. This position is defined so that noon always coincides with solar zenith. Solar azimuth and elevation angles are provided by SOLPOS as well as the components of the unit vector, $\overline{U}_i^A$, describing the orientation of an incident light ray in the "A" coordinate frame.

After the position of the sun is determined by SOLPOS, the subroutine representing the collector chosen for analysis is called. This is either FLPLC, if the flat plate collector is specified or CYLRF, if the cylindrical reflector model is chosen. The flat plate subroutine is simple, computing the solar energy gain from beam and diffuse radiation in a single step, without the need for any division of the plate into multiple area elements. Flat plate collector losses, working fluid mass flow and overall energy balance are computed in subroutine FPABS at the next level.

In contrast, the focusing system subroutine has many supporting routines to perform the more complex operations necessary to establish thermal energy gain. These include SHDW, REFL, ABINT, AFAB, and ABSB. Subroutine SHDW determines the boundary of the shadow cast by the collector absorber plate on the parabolic reflector. REFL computes the orientation of a light ray reflected by the mirror given its original orientation and its point of intersection with the mirror. Once this orientation is specified, the point of intersection of the reflected ray with the plane containing the absorber plate is found in subroutine ABINT.

The reflector is divided into a specified number of rectangular area elements. The corners of each of these reflector elements are

"mapped" into the absorber plane with subroutine ABINT. A four-sided figure results from this mapping operation. Only the portion of this figure intersecting the absorber plate boundary represents any energy contribution to the system. The fraction of area of the mapped figure intersecting the absorber boundary is computed by subroutine AFAB. The thermal power contained in the beam of rays reflected from each mirror area element is multiplied by the fraction determined by AFAB to give the power from that element actually striking the absorber plate. Finally, losses, working fluid mass flow, and the collector energy balance for the focusing system are computed in subroutine ABSB.

In addition to the major subroutines described above, a number of utility subroutines are available for specific functions and may be called anywhere in the program. These subroutines are listed in Table 2 with a short description. Note that vector dot and cross product subroutines are available as well as a vector rotation or coordinate transformation subroutine. Several standard FORTRAN functions, those for the square root, arcsine, and arcosine, have been modified to prevent arguments which are outside of the function ranges from causing abnormal program endings. For example, the arcsine of 1.0001 is simply treated as 90°. The linear interpolation subroutine is used to specify collector surface radiation properties as a function of incidence angle as well as the diffuse radiation pattern. This subroutine requires a tabular input of the independent and dependent variables for each function.

Variable names in the program have generally been made similar

TABLE 2

UTILITY SOFTWARE SUPPORTING MAJOR SUBROUTINES

Subroutine Name	Function
ROT	Vector Rotation or Coordinate Transformation
CROSS	Vector Cross Product
DOT	Vector Dot Product
ANGLE	Converts Cartesian to Polar Coordinates
DCBA	Defines $C_{B/A}$, Matrix for "A" to "B" Frame Transformation
RANK	Ranks Array in Ascending Order
LINT	Linear Interpolation of Tabular Data
SQRTI	Square Root with Negative Arguments Set to Zero
ACOS1	Arcosine with Arguments Limited to $\pm$ 1
ASIN1	Arcsine with Arguments Limited to $\pm$ 1

to the corresponding symbols in the formulas derived in the mathematical model development. Important variables are included in Table 3. with their description and units. Input and output variables are denoted by an "I" or "O" in parentheses. Dimensioned variables are shown with the number of elements assigned them in parentheses. Note that the maximum numbers of points permissible for describing functions with tables corresponds to the number of elements shown. Variables are transferred throughout the program with several COMMON blocks. These blocks are divided into categories including collector geometry, surface properties, and the local thermal environment. The major COMMON blocks in the program and the data they contain are listed in Table 4.

Reflector-Absorber Model

Because of the complexity of the focusing collection process, a detailed description of the software implementation of the reflector energy capture is provided here. First, the reflector is divided into a series of uniform strips or bands running parallel to the collector z axis as shown in Figure 28. These are the area elements described in the energy gain section. The division is always such that a band is centered on the reflector z axis. The remainder of the reflector is then divided into an equal number of strips on each side of the center one. The number of strips on each side is an input parameter, M_R; the total number of strips is simply, $2M_R + 1$. The intersections of the four corners of the shadow cast by the absorber plate with the reflector are found with subroutine SHDW. The outline on the shadow is also

TABLE 3

IMPORTANT PROGRAM VARIABLES

Variable	Units	Description
(I) NAT	-	Number of Flat Plate $\alpha\tau$, α_C Tabular Entries
(I) BTFP (10)	deg.	Table of Incidence Angles for $\alpha\tau$, α_C
(I) ALCOV (10)	-	Table of α_C
(I) AT (10)	-	Table of $\alpha\tau$ Product
(I) FSEL	-	Selectivity Factor for $\alpha\tau$ Product
(I) FSELC	-	Selectivity Factor for α_C
(I) EP	-	Plate Emissivity (Long Wave)
(I) RHP	-	Plate Reflectivity (Long Wave)
(I) EC	-	Cover Emissivity (Long Wave)
(I) RHC	-	Cover Reflectivity (Long Wave)
(I) TAUC	-	Cover Transmissivity (Long Wave)
(I) CNCOV	m	Cover Thickness
(I) NRH	-	Number of Reflector ρ Tabular Entries
(I) BTAR (10)	deg.	Table of Incidence Angles for ρ
(I) RHO (10)	-	Table of ρ
(I) EHTR	-	Reflector Emissivity (Long Wave)

TABLE 3--Continued

Variable	Units	Description
(I) NAL	-	Number of Absorber α_A Tabular Entries
(I) BTAB (10)	deg.	Table of Incidence Angles for α_A
(I) ALPH (10)	-	Table of α_A
(I) EHT	-	Absorber Emissivity (Long Wave)
(I) FSLAB	-	Selectivity Factor for α_A
(I) SOLC	w/m^2	Solar Constant
(I) FBZ	-	Atmospheric Transmission for Sun Overhead
(I) AMASZ	-	Air Mass at Sunrise, Sunset
(I) NDF	-	Number of Diffuse Radiation Pattern Entries
(I) BETD (20)	deg.	Table of Angles for Diffuse Pattern
(I) AWD (20)	-	Table of Non-Dimensional Diffuse Intensities
(I) H	w/m^2-°C	External Film Coefficient
(I) HI	w/m^2-°C	Internal Film Coefficient (Flat Plate)
(I) TINF	°C	Local Ambient Temperature
(I) CP	J/Kg-°C	Working Fluid Specific Heat
(I) XMDI	Kg/hr	Maximum Working Fluid Mass Flow
(I) AC	m^2	Flat Plate Collector Area
(I) TCOV	m	Glass Cover Thickness

TABLE 3--Continued

Variable	Units	Description
(I) MR	-	Number of Reflector Area Elements on Each Side of Center
(I) YR	m	Reflector Half-Width
(I) ZR	m	Reflector Half-Length
(I) YA	m	Absorber Half-Width
(I) NA	-	Number of Absorber Cells on Each Side of Center
(I) ZA	m	Absorber Half-Length
(I) FZ	m	Reflector Geometrical Focal Length
(I) F	m	Distance of Absorber from Reflector Base
(I) XLATI	deg.	Collector Latitude
(I) AZI	deg.	Collector Azimuth
(I) ELI	deg.	Collector Elevation
(I) TILTI	deg.	Collector Tilt
(I) NDAY	-	Julian Date of Day Simulated
(I) IDTI	sec.	Time Interval for Integration
(I) JPRINT	-	Frequency of Printout (Every $J^{\underline{th}}$ Time Interval)
(I) ISW	-	Choice of Collector--1 = Flat Plate, 2 = Focusing
(I) TZ	°C	Thermostat Setpoint Temperature
(I) TZZ	°C	Temperature of Maximum Fluid Flow

TABLE 3--Continued

Variable	Unit	Description
(I) TIN	°C	Working Fluid Inlet Temperature
DECL	rad.	Solar Declination
DELT	rad.	Complement of Declination
ITIME	sec.	Time from Midnight in Seconds
(0) JTIME (3)	hr, min, sec	Time from Midnight in Hours, Minutes, and Seconds
UIA (3)	-	Unit Vector of Incident Solar Ray in "A" Frame
UIB (3)	-	Unit Vector of Incident Solar Ray in "B" Frame
CBA (9)	-	Matrix for Coordinate Transformation from "A" to "B" Frame
UNR (3)	-	Unit Vector Normal to Reflector
UNA (3)	-	Unit Vector Normal to Absorber
RS1 (3)		
RS2 (3)	m	Cordinates of Corners or Absorber Shadow on Reflector
RS3 (3)		
RS4 (3)		
P1 (3)		
P2 (3)	m	Coordinates of Corners of Reflector Area Elements Projected into Absorber Plane
P3 (3)		
P4 (3)		

TABLE 3--Continued

Variable	Unit	Description
AMASS	-	Air Mass
NW	-	Desired No. of Space Angle Elements for Hemisphere
NN	-	Actual No. of Space Angle Elements for Hemisphere
DW	Ster.	Magnitude of Space Angle Element
UST (3)	-	Unit Vector Specifying Orientation of Space Angle Element
(0) AZ	deg.	Solar Azimuth
(0) EL	deg.	Solar Elevation
(0) XMD	Kg/hr	Working Fluid Mass Flow
(0) CPMD	w/°C	Working Fluid Specific Heat - Mass Flow Product
(0) POUT	w	Thermal Power Transferred to Fluid
(0) TOUT	°C	Delivery Temperature of Fluid
(0) PSURF	w	Thermal Power Striking Absorbent Face of Collector
(0) EOUT	Kw/hr	Thermal Energy Collected Since Sunrise
(0) ESURF	Kw/hr	Thermal Energy Striking Absorbent Face Since Sunrise
(0) WB	w/m^2	Incident Beam Radiation Flux
(0) WDT	w/m^2	Beam Flux Lost to Diffuse Radiation
(0) TPL	°C	Flat Plate Temperature
(0) QDINF	w	Thermal Power Absorbed by Plate

TABLE 3--Continued

Variable	Unit	Description
(0) CONVF	w	Convection Loss from Plate
(0) RADF	w	Radiation Loss from Plate
(0) FF	-	Flat Plate Thermostat Throttling Fraction
(0) TC	°C	Glass Cover Temperature
(0) QDINC	w	Thermal Power Absorbed by Cover
(0) TP (21)	°C	Absorber Cell Temperatures
(0) QDIN (21)	w	Absorber Cell Thermal Power Input
(0) FI (21)	-	Absorber Cell Thermostat Throttling Fractions
(0) CONV (21)	w	Absorber Cell Convection Losses
(0) RAD (21)	w	Absorber Cell Radiation Losses
(0) QDNET (21)	w	Thermal Power Transferred to Fluid in Absorber Cells

TABLE 4

IMPORTANT COMMON BLOCKS

Common Block	Data Contained
SOLP	Solar Position Parameters
VECT	General Purpose Vectors
GEOM	Geometric Parameters for Flat Plate and Focusing Collectors
SURFP	Surface Radiation Properties and Curves
STRAD	Space Angle Data for Diffuse Radiation Description/Integration
THERM	Thermostat Parameters
QNET	Delivery Condition of Working Fluid

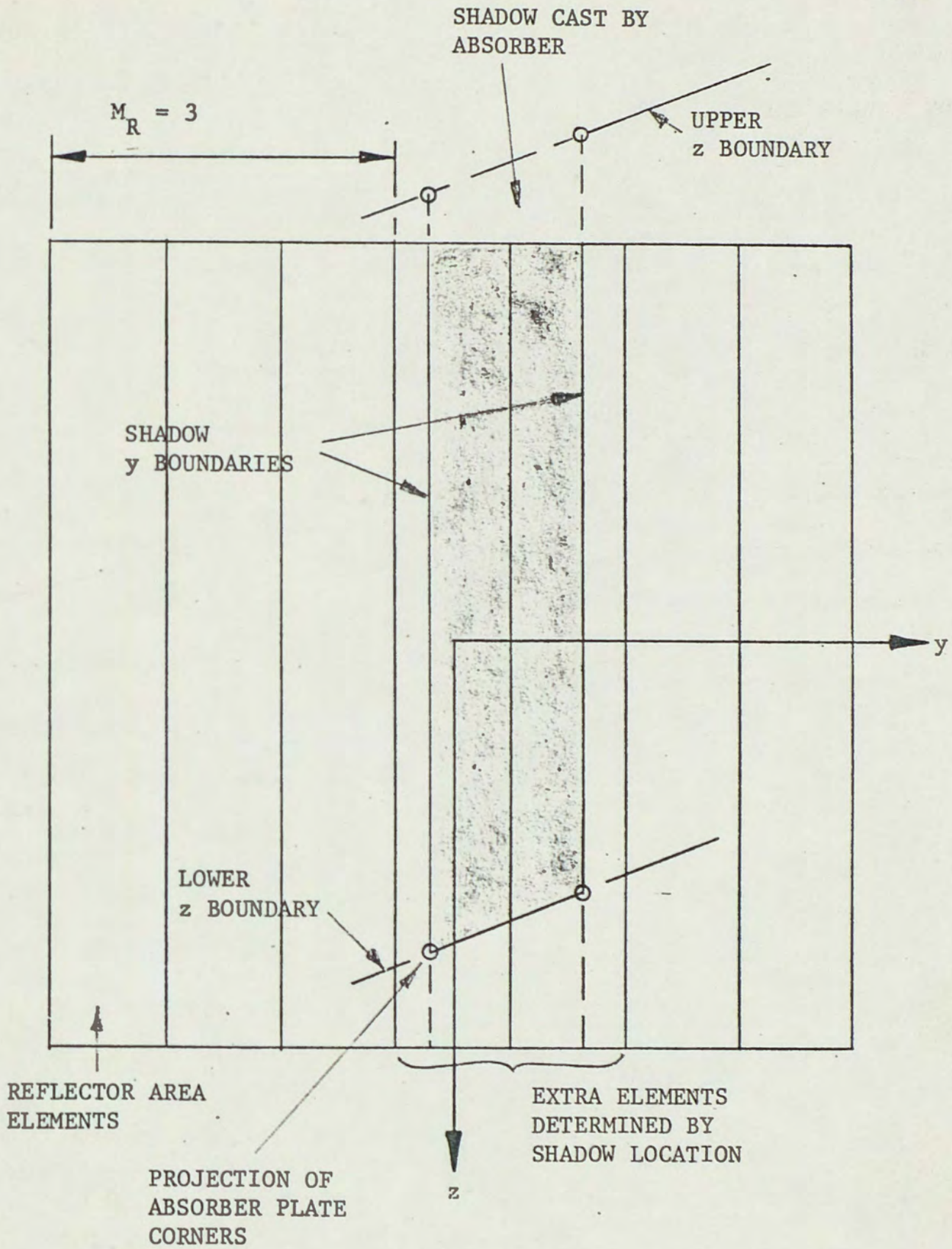

Figure 28. Reflector Area Elements Used in Computer Program

shown in the figure. The shadow boundaries parallel to the z axis define additional area elements--those between the shadow "Y-Boundaries" and the previously defined strip edges. In addition, elements are established corresponding to areas above or below the shadow "Z-Boundaries". These area elements are all shown in the figure.

The orientations of light rays reflected from each corner of these area elements are determined in subroutine REFL. Using these orientations, the corners of the elements are projected or mapped into the plane containing the absorbant face of the absorber plate with subroutine ABINT. A typical projection is shown in Figure 29 with the absorber boundary. Straight lines are assumed to connect the four projected corners. The shaded area in the figure represents that part of the light reflected by the mirror area element which strikes the absorber. The fraction of the total projected area of each reflector element intersecting the absorber is computed in subroutine AFAB. This is used to determine the amount of energy actually striking the absorber.

The absorber is also divided into area elements as shown in the figure. These represent the individual heat exchanger cells discussed previously. As in the case of the reflector elements, the absorber cells are positioned so that a center cell coincides with the center of the collector. An equal number of cells, specified by the input parameter, N_A, are placed on each side of the center cell along the collector z axis. The total number of cells is then, $2N_A + 1$.

Since an energy balance must be maintained for all these cells,

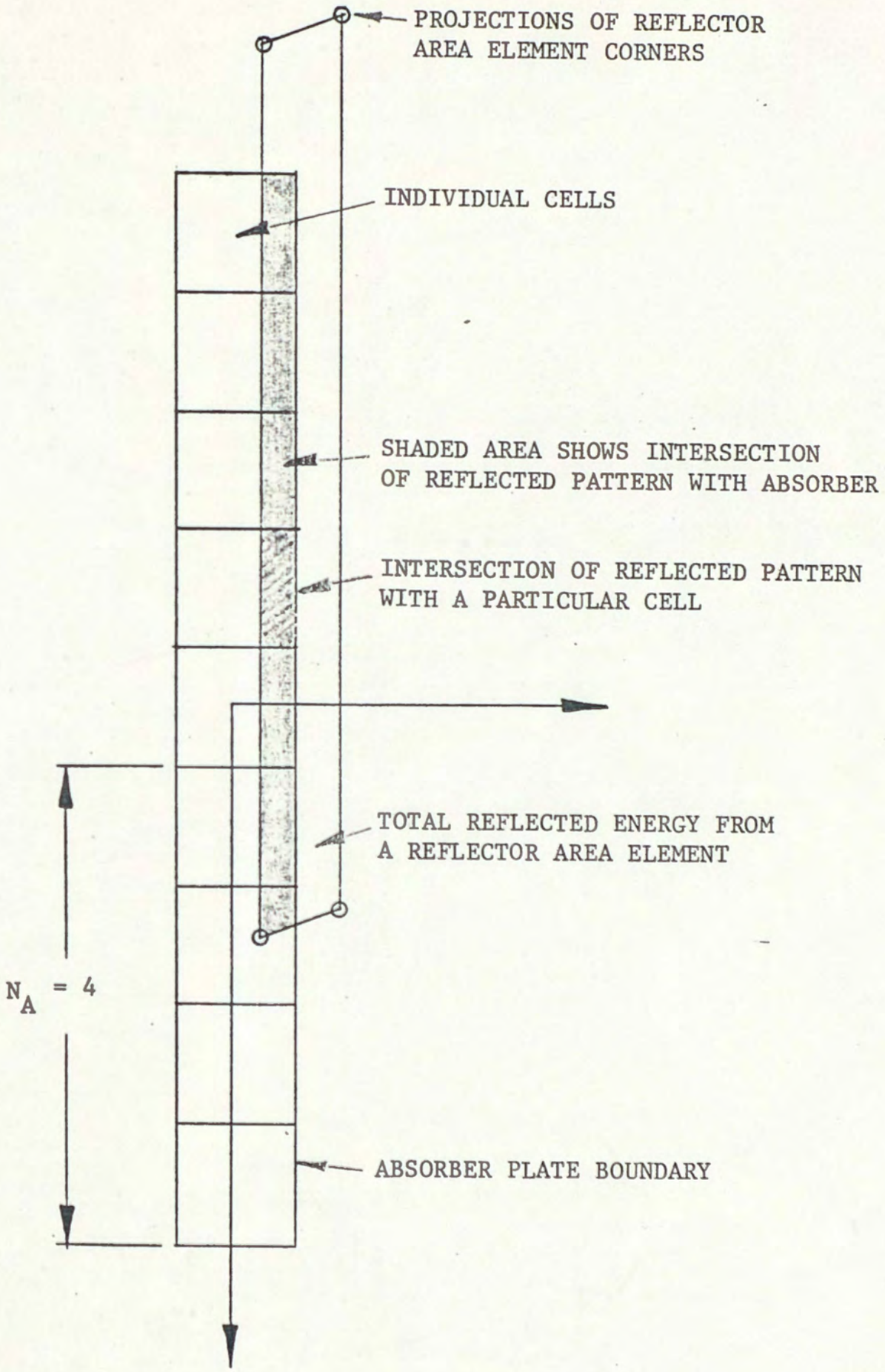

Figure 29. Intersection of Reflected Pattern with Absorber Cells

the fractional intersection of each projected area element of the reflector with each absorber cell must be computed. In the program, a "do loop" specifies each reflector area element, while a nested loop steps through all the absorber cells. Obviously, if the projected reflector element completely misses the absorber boundary, no incident energy is computed for any of the cells.

Note that as the specified station of the absorber plane approaches the focal point of the parabolic mirror, the projected reflector areas shrink to line segments having no width in the Y-direction. This is due to the focusing of the reflected rays by the mirror, and reaches the limiting case when the absorber is placed exactly at the reflector focal point. Here, computational problems in the program are avoided by simply assuming a small width for projected area elements in the event that this situation arises. Imperfect collector optics and the finite angular size of the solar disk prevent such a complete focusing of incident light in an actual reflecting system.

Space Angle Representation

Space angle elements are required for the integration of diffuse radiation intensity over the hemisphere visible to a collecting surface. In the program, these elements are specified by subroutine STER. The subroutine is initialized in the first call made in the program. The number of elements desired to represent a hemisphere, N_ω, is specified in this call. The geometry assumed in the subroutine is shown in Figure 30. The subroutine computes a series of discrete

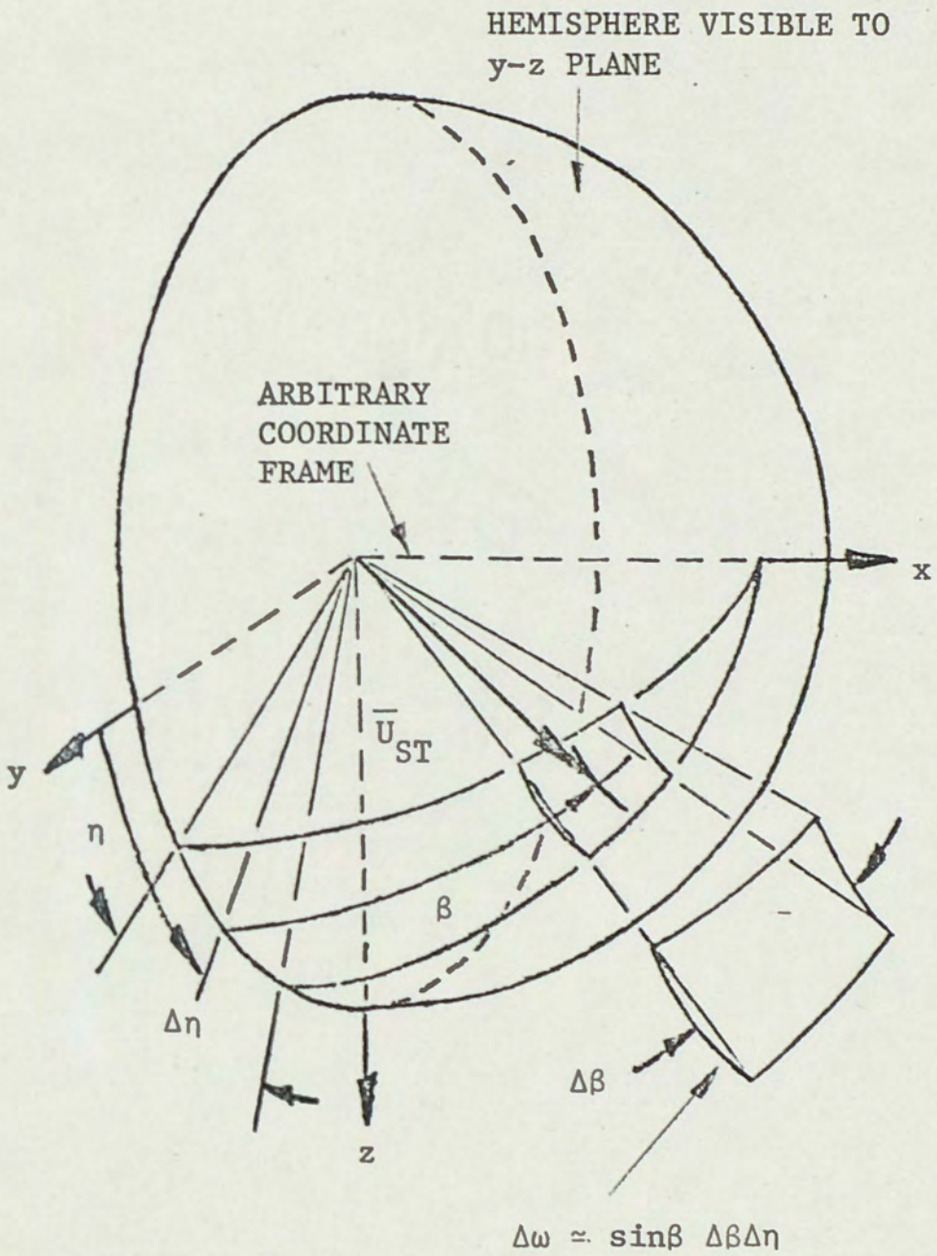

Figure 30. Division of Hemisphere into Finite Space Angle Elements

values of the angles β and η, which specify space angle elements, $\Delta\omega$. The actual number of elements computed, N_N, is approximately equal to the desired number specified in the initializing subroutine call. Differences between the desired and actual number of elements are due to the quantization of the hemisphere into a finite number of elements and computational limitations in defining them.

After the initialization, a call to STER may be placed in a do loop with the index specifying the number of calls equal to the number of space angle elements, N_N, defined in the initialization. As each call is made, the subroutine steps through the previously determined sequence of space angle elements, and returns values for the angles, β and η, a corresponding unit vector $\overline{U}_{ST}$, and the magnitude of the element, $\Delta\omega$. The vector, $\overline{U}_{ST}$, represents the centerline of the space angle element and is directed radially outward. No particular coordinate frame has been assigned subroutine STER. The coordinates implicit in the subroutine may be assumed to coincide with any chosen frame, for example, the collector or "B" frame. In the event that more than one coordinate system representation of the vector is required, the appropriate transformation of $\overline{U}_{ST}$ must be made. No change in the magnitude, ΔW, results from a coordinate transformation.

Inputs

The program employs list directed input for all of the numerical parameters. This input mode requires no special formatting of the input data. Numbers may be punched on the input cards in any columns as long as their proper order is maintained. Numbers must be separated

by at least one blank space or a comma. The inputs are divided into two categories--those specified only once at the start of each execution of the program, and those specified for each stacked run. The "one time inputs" consist of the parameters describing collector surface properties, geometry, the thermal environment, and the working fluid. These include values for both the flat plate collector and the cylindrical reflector. Thus, a data deck is assembled which fully describes both systems and is used for simulation of either of the collectors.

The repeated inputs include a title card (read with an alphanumeric format), and numerical parameters specifying the orientation of the collector, its latitude, and the time of year. In addition, the desired time interval, used by the program to "step" through the day, the frequency of printed output, the collector system to be simulated and the thermostat parameters are repeated inputs. Table 5 shows the necessary arrangements of the input data deck with the input parameters which were defined in Table 3. Note that the inputs for multiple runs are simply repeated for each run. If no changes from the previous run are required on a given card, a "slash" (/) may be punched on the card. This causes the appropriate READ statement to be skipped so that there is no change in the affected parameters. A slash may also be punched in the middle of a data field, following the last number to be changed. This stops the input of data for that READ statement so that only those numbers preceeding the slash are affected. Run termination is accomplished by placing a title card punched "end" in the left most columns after the last run desired in the program

TABLE 5

ARRANGEMENT OF INPUT DATA DECK

Card	Variables
1	NAT
2*	BTFP (up to 10 values)
3*	ALCOV (up to 10 values)
4*	AT (up to 10 values)
5	FSEL, FSELC
6	EP, RHP, EC, RHC, TAUC
7	CNCOV
8	NRH
9*	BTAR (up to 10 values)
10*	RHO (up to 10 values)
11	EHTR
12	NAL
13*	BTAB (up to 10 values)
14*	ALPH (up to 10 values)
15	EHT, FSLAB
16	SOLC
17	FBZ, AMASZ
18	NDF
19*	BETD (up to 20 values)
20*	AWD (up to 20 values)
21	H, HI
22	TINF
23	CP
24	XMDI
25	AC, TCOV
26	MR, YR, ZR
27	YA, NA, ZA

TABLE 5--Continued

Card	Variables
28	FZ, F
29	TITLE (up to 80 columns)
30**	XLATI, AZI, ELT, TILTI, NDAY
31	IDTI, JPRINT, ISW, TZ, TZZ, TIN

*Continue as necessary

**Repeat for each stacked run

execution.

Output

The output of this program consists of a set of descriptive parameters printed at specified time intervals throughout the day. The set of output parameters consists of several lines of print which appear regardless of the type of collector chosen for simulation, and one or more lines below these which differ depending upon the collector system specified. Typical blocks of output data are shown in Tables VI and VII, showing printout for both the flat plate and cylindrical reflector systems. The top line gives the time of day as hours, minutes, and seconds, and the azimuth and elevation angles of the sun at that time. The next line gives the mass flow of coolant or working fluid through the collector in Kg/hr, the product of mass flow and specific heat, $\dot{m}C_p$, in W/°C, the thermal power and temperature delivered by the collector in watts, and the thermal power falling on the absorbent face of the collector in watts. Below this line are listed the thermal energy delivered by the collector since sunrise, the energy which fell on the absorbent collector face since sunrise, both in Kw-hr, and the thermal fluxes associated with beam and diffuse radiation. The sum of the last two quantities is the solar constant.

Parameters peculiar to the specific collector modeled include the thermal energy absorbed by the collector, the convective and radiation losses deducted from this input power, the temperature of the absorbent face, and the amount of thermostat throttling of the

working fluid. For the flat plate collector, these parameters are listed in a single line along with the glass cover temperature and power absorbed by the cover. This format is shown in Table 5. If the focusing collector is simulated, a line is printed for each of the important parameters. The numbers in each line are the values corresponding to the individual absorber cells modeled for the focusing collector. Typical values are shown in Table 6.

TABLE 6

SAMPLE OUTPUT FOR FLAT PLATE COLLECTOR

10 SQUARE METER FLAT PLATE COLLECTOR JUNE 22 SETPOINT=80C

HR:MN:SC		AZ	EL			
XMD	CPMD	POUT	TOUT	PSURF		
EOUT	ESURF	UB	UDT			
TPL	QDINF	CONUF	RADF	FF	TC	QDINC
-12:30: 0		234.9	81.6			
338.31	393.48	2633.	82.	9199.		
6.994	45.752	846.	504.			
82.	7376.	1442.	3301.	0.338	33.	708.
-12:40: 0		242.9	79.7			
332.51	386.73	2577.	82.	9133.		
7.429	47.279	844.	506.			
82.	7318.	1442.	3299.	0.333	33.	708.
-12:50: 0		248.6	77.7			
325.82	378.82	2584.	82.	9049.		
7.852	48.794	841.	509.			
82.	7243.	1442.	3297.	0.325	33.	707.

TABLE 7

SAMPLE OUTPUT FOR FOCUSING COLLECTOR

```
////////////////////////////////////////////////////////////
10 SQUARE METER FOCUSSING COLLECTOR  JUNE 22  SETPOINT-100C
////////////////////////////////////////////////------------
 - - - - - - -HR:MN:SC        AZ          EL
      XRD          CPRD          POUT          TOUT          PSURF
     EOUT         ESURF            UB           UDT

   TP---1       2       3       4       .       .       .       .       .
 QDIN---1       2       3       4       .       .       .       .       .
   FI---1       2       3       4       .       .       .       .       .
 COMV---1       2       3       4       .       .       .       .       .
  RAD---1       2       3       4       .       .       .       .       .
QDNET---1       2       3       4       .       .       .       .       .
////////////////////////////////////////////////------------

 - - - - - - -12:30: 0        234.9          81.6
   219.44       255.23          2843.          101.          7079.
    7.397       22.314           846.          504.

   100.    101.    101.    101.    101.    101.    101.    101.    101.    101.    101.
   359.    549.    545.    542.    540.    541.    540.    542.    545.    548.    553.
 0.0351  0.0979  0.0967  0.0957  0.0950  0.0953  0.0950  0.0957  0.0967  0.0976  0.0991
    77.     78.     78.     78.     78.     78.     78.     78.     78.     78.     78.
   190.    192.    192.    192.    192.    192.    192.    192.    192.    192.    192.
    93.    280.    276.    273.    270.    271.    270.    273.    276.    279.    283.

 - - - - - - -12:40: 0        242.9          79.7
   211.83       246.37          2751.          101.          6947.
    7.864       23.483           844.          506.

    95.    101.    101.    101.    101.    101.    101.    101.    101.    101.    101.
   250.    587.    541.    538.    536.    537.    536.    538.    541.    544.    549.
   0.0     0.1135  0.0989  0.0979  0.0971  0.0974  0.0971  0.0979  0.0989  0.0999  0.1014
    71.     78.     78.     78.     78.     78.     78.     78.     78.     78.     78.
   180.    192.    192.    192.    192.    192.    192.    192.    192.    192.    192.
     0.    317.    272.    269.    266.    267.    266.    269.    272.    275.    279.

 - - - - - - -12:50: 0        248.8          77.7
   211.06       245.47          2742.          101.          6800.
    8.321       24.628           841.          509.

    56.    101.    101.    101.    101.    101.    101.    101.    101.    101.    101.
   142.    623.    536.    533.    531.    532.    531.    533.    536.    539.    544.
   0.0     0.1253  0.0976  0.0965  0.0958  0.0961  0.0958  0.0965  0.0976  0.0986  0.1001
    28.     78.     78.     78.     78.     78.     78.     78.     78.     78.     78.
   114.    193.    192.    192.    192.    192.    192.    192.    192.    192.    192.
     0.    362.    267.    264.    261.    262.    261.    264.    267.    270.    274.
```

IV. FLAT PLATE AND FOCUSING COLLECTOR COMPARISON

A comparison of specific flat plate and focusing collector configurations has been made using the computer program. For this comparison, several basic ground rules were observed. The collector candidates were given the same projected area with which to capture sunlight. This permitted a direct comparison of their net energy gains for an indication of their relative efficiencies. In addition, reasonable operating temperatures for the two systems were assumed. Since the flat plate collector is inherently a lower temperature device than the focusing collector, it would not be fair to assume equal operating temperatures (and absorption cycle boiler temperatures) for the two systems. Temperatures were chosen which reflected the capabilities of the collectors. A central Florida location (Latitude=28.5°) was assumed for the collectors, and the performance comparison was based on operation on the longest day of the year, June 22. Finally, the comparison was confined to operation on a clear day in still air.

Geometry

The collectors were given projected areas of $10m^2$. This size was deemed reasonable for a modular component in a small air conditioning installation. The collector configurations are shown in Figure

31. Note that the shape of the flat plate collector is not important in this analysis; only its area affects performance. The glass cover was assumed to be ordinary window glass about 6 mm (¼ inch) thick. The focusing collector was given an oblong shape, 5 m by 2 m, and a focal length of 2 m, so that it could begin to collect energy at solar elevation angles as low as 22°. The absorber plate has been made the same length as the reflector in this system. The "half-width" of the absorber plate was chosen to be 10% of the focal length of the mirror. This half-width subtends an angle of roughly 6° with respect to the base of the reflector. Since the solar declination changes at a maximum rate of somewhat less than 3° per week [3], this width should be sufficient to require orientation adjustment no more often than once per week. Also, a considerable defocusing of the concentrated energy due to poor reflector optics would be permissible before any energy was lost between weekly adjustments with this absorber width. To simulate some defocusing, the absorber plate was placed 1.9 m from the base of the reflector. This corresponds to 95% of the geometrical focal length of the parabola. The absorber plate was divided into eleven thermostatically controlled cells to minimize losses.

Collector orientation is illustrated in Figure 32, with appropriate solar zenith elevations. The collectors were both aimed south (azimuth=180°) with the elevation angles shown in the figure. The flat plate collector was assumed to be fixed in orientation at an elevation corresponding to solar zenith at the equinox. The focusing collector was aimed directly along the solar zenith elevation

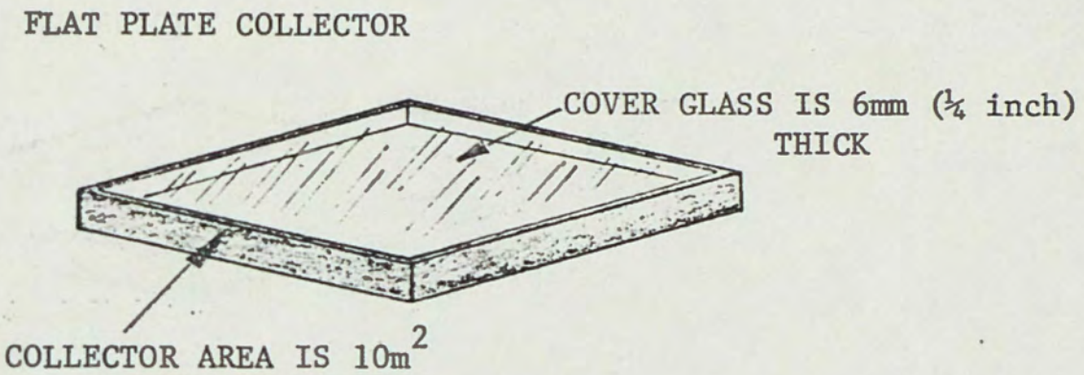

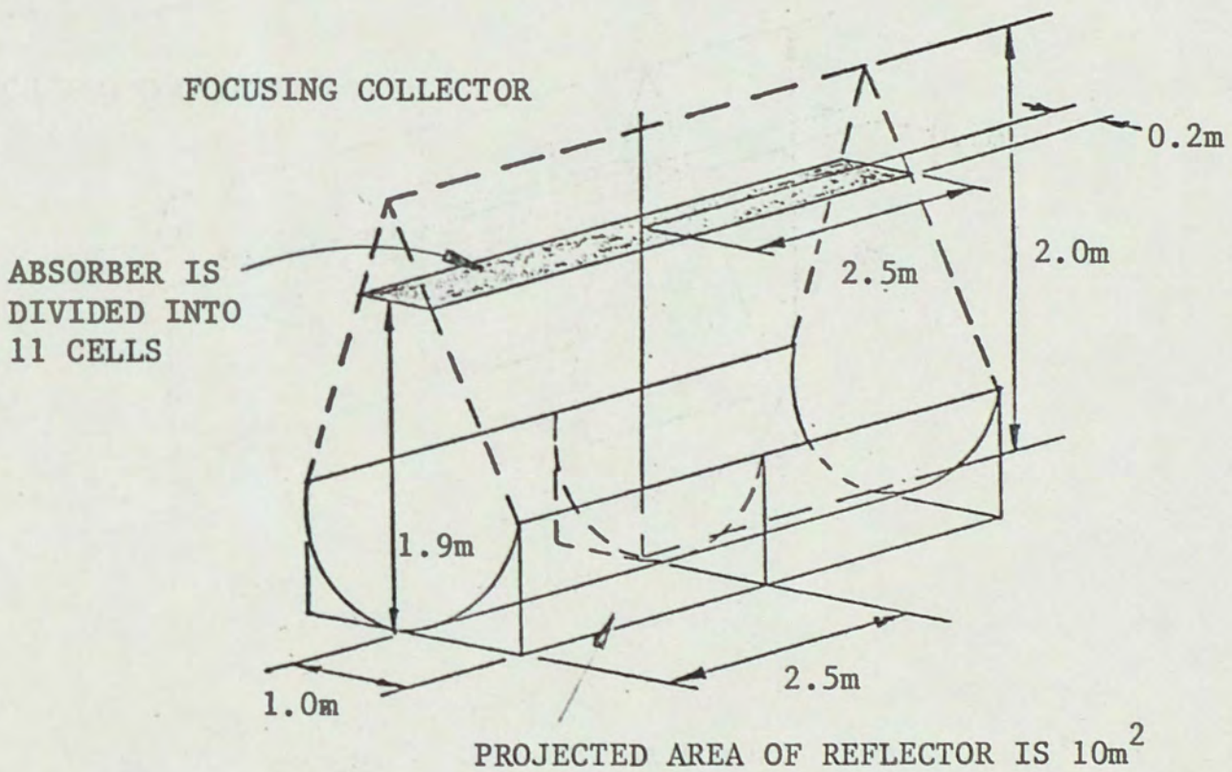

Figure 31. Collector Geometries Used for Performance Comparison

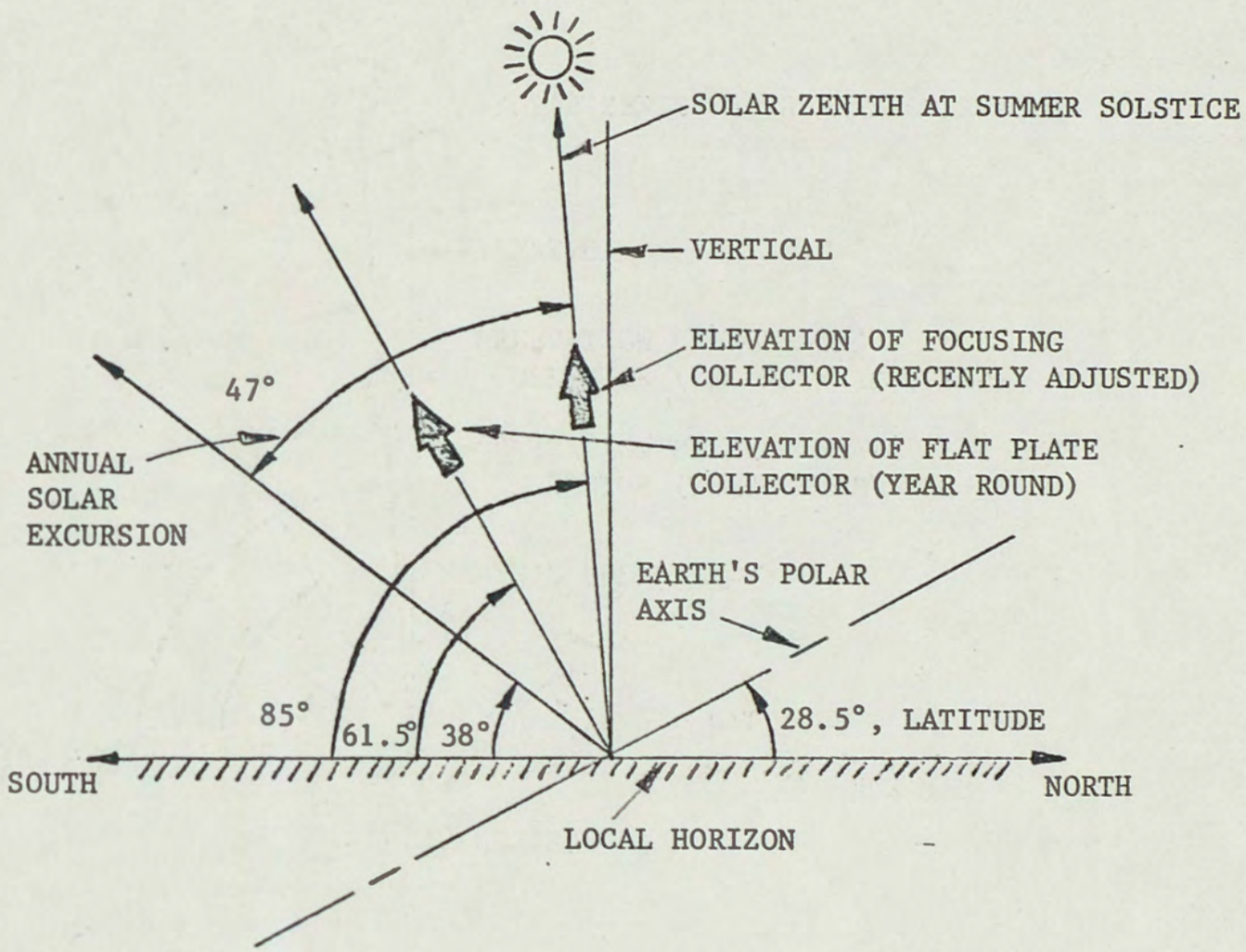

Figure 32. Collector Orientations Used in Analysis and Solar Zenith Angles

corresponding to the day of interest, the summer solstice.

Interestingly, at the time of year assumed, the sun rises and sets to the north of the collector, but reaches its zenith in the southern sky. This means that the collector cannot be oriented so that the solar track coincides exactly with the reflector's plane of symmetry in the case of the focusing system. This causes the pattern of focused energy to move along the collector y axis (see Figure 13) as well as its z axis, the primary direction of motion. At this time of year, the motion in the y direction is sufficient to move the focused energy entirely off the absorber plate in the early morning and late afternoon. At midmorning, as the sun crosses the local east-west axis, its focused image moves onto the absorber plate from the south, and remains on the plate until mid-afternoon, when the sun again moves into the northern sky. This "out-of-plane" motion of the sun is not too significant because it affects the collector energy gain only at low solar elevation angles. Here, the incident solar flux is fairly small, so its absence is not penalizing.

Materials and Radiation Properties

The portions of the collector structures whose radiation properties are of interest include the glass cover and the absorbent heat exchanger plate in the flat plate collector, and the reflector and absorber in the focusing system. The materials assumed for these components are summarized in Table 8 with the long wavelength radiation parameters required in the computer model. The short wavelength properties of these components were shown in Figure 15 and 16

TABLE 8

PROPERTIES OF MATERIALS CHOSEN FOR COLLECTORS

Collector Configuration	Surface	Material	Property	Symbol	Value
Flat Plate	Cover	Window Glass	Emissivity	ε_C	0.84 [4]
			Reflectivity	ρ_C	0.15 [4]
			Transmissivity	τ_C	0.01 [4]
			Selectivity	-	0.01 [4]
			Conductivity (w/m- C)	K	0.78 [9]
	Absorbent Plate	Flat Black Lacquer	Emissivity	ε_ρ	0.95 [9]
			Reflectivity	ρ_ρ	0.05 [9]
			Selectivity	-	1.0 [4]
Focusing	Reflector	Polished Aluminum	Reflectivity	ρ	0.95 [4]
			Emissivity	ε_R	0.05 [4]
	Absorbent Plate	Flat Black Lacquer	Emissivity	ε_ρ	0.95 [9]
			Selectivity	-	1.0 [4]

earlier in this paper. In Figure 15, the properties of window glass and flat black lacquer are shown. Note that no variation in absorbtivity with incidence angle has been assumed for the painted surface. A deliberately roughened surface of the heat exchanger plate would approximate this assumption [7]. In addition, no spectral selectivity has been assumed for the absorbent surfaces. The radiation properties for both the glass and the lacquer are based on experimental data [4].

Figure 16 shows the angular dependence of the reflectivity of a polished aluminum mirror and a rough absorber plate painted with black lacquer. The same assumptions have been made for the black surface as before. The shape of the aluminum reflectivity curve has been determined from theoretical electromagnetic considerations. Electromagnetic theory predicts the proportional angular dependence of material properties fairly well; absolute magnitudes are not generally very accurate, however. The curve shown in the figure was derived by scaling the theoretical curve so that the hemispherical reflectivity matched experimental data [7]. Note that the total reflectivity of aluminum for longwave radiation shown in Table 8 is somewhat higher than the values shown in Figure 16 for solar wavelengths.

Thermal Environment

Parameters required to define the local thermal environment seen by the collectors include the solar constant, the local temperature, T_∞, and the film coefficients for thermal convection. Coefficients, h and h_i, are required for exposed surfaces and those inside

the flat plate collector. In addition, atmospheric scattering parameters must be specified. These include the fraction of beam radiation transmitted by the atmosphere if the sun were directly overhead, f_{bo}, the air mass at sunrise or sunset m_{max}, giving the effect of the earth's curvature, and a curve defining the spatial distribution of diffuse radiation from the sky. Environmental parameters are summarized in Table 9.

The local temperature, T_{∞}, was chosen as a reasonable average air temperature for a summer day. The film coefficients used were obtained from detailed calculations assuming still air which were presented in Duffie and Beckman's Solar Energy Thermal Processes, in which flat plate collector losses were analyzed. The value for internal convection, h_i, assumes a spacing between the absorbing plate and the glass cover of 2.5 cm [3].

An accurate representation of atmospheric attenuation and scattering is most difficult and would require empirical data for support. The development of a detailed atmospheric model is beyond the scope of this paper, although provision has been made for a non-uniform diffuse energy distribution in the computer program. A simplified model was chosen for this analysis. The value for atmospheric transmission, 63% for a clear day, is a measured spectral total quantity. The value for maximum air mass chosen here assumed an effective atmospheric thickness of 10 miles as outlined in the "Atmospheric Effects" section of this paper. The distribution of diffuse radiation was simply treated as uniform. Although the atmosphere is recognized as a non-uniform source of radiation [8], the

TABLE 9

THERMAL ENVIRONMENT

Solar Constant		1350 w/m^2 [3]
Local Temperature, T_∞		30°C
Film Coefficients:		
	Outside, h	6 w/m^2-°C [3]
	Inside, h_i	3 w/m^2-°C [3]
Maximum Atmospheric Transmission, f_{bo}, for clear day		0.63 [8]
Maximum Air Mass		28
Diffuse Radiation Spatial Distribution		Uniform

effect of that non-uniformity was considered of secondary importance to this analysis.

Program Inputs

The inputs used for a specific collector comparison are shown in Table 10 as actual "card images". The upper block of data consists of the "one time" inputs describing both the flat plate and focusing systems. The parameters at the bottom of the table, including the descriptive titles, are repeated for each run. Two such runs are shown here. The bottom card containing the work "end" terminates program execution.

Typical Collector Behavior

Figures 33 and 34 show the thermal power associated with a day's operation for the flat plate and focusing collectors at typical operating temperatures. The upper curve is the energy actually striking the absorbent face of the collector. The lower curve is the energy transferred to the working fluid. The sudden rise and fall of the lower curve in the morning and afternoon coincide with the start and stop of the flow of working fluid. In Figure 34 the steps in this curve are due to sudden changes in the flow as the thermostats in the individual absorber cells open and close throughout the day. Important performance parameters for the two collectors are summarized in Table 11.

An interesting feature of Figure 33 is the peculiar behavior predicted for the thermal energy incident upon the flat plate collector immediately after sunrise and prior to sunset. The incident power is

TABLE 10

ACTUAL INPUTS FOR TYPICAL COLLECTOR
COMPARISON (CARD IMAGE)

```
 7
 0.   20.   40.   60.   70.   80.   90.
 0.04  0.05  0.06  0.07  0.07  0.05  0.0
 0.84  0.84  0.83  0.77  0.68  0.49  0.0
  0.01   13.
 0.95  0.05  0.84  0.15  0.01
 0.78
 5
 0.  50.   65.   80.   90.
 0.85 0.85  0.84  0.82  0.87
 0.05
 2
 0.    90.
 0.95   0.95
 0.95   1.0
  1350.
 0.63   28.
 2
 0.    180.
 1.    1.
   6.   3.
  30.
 4187.
 1000.
 10.   0.006
 5   1.0   2.5
 0.2   5   2.5
 2.   1.9
10 SQUARE METER FLAT PLATE COLLECTOR  JUNE 22  SETPOINT-80C
28.5  180.  61.5  0.   173
600  1  1  80.  85.  75.
10 SQUARE METER FOCUSSING COLLECTOR  JUNE 22  SETPOINT-100C
28.5  180.  85.  90.   173
600  1  2  100.  105.  90.
END
```

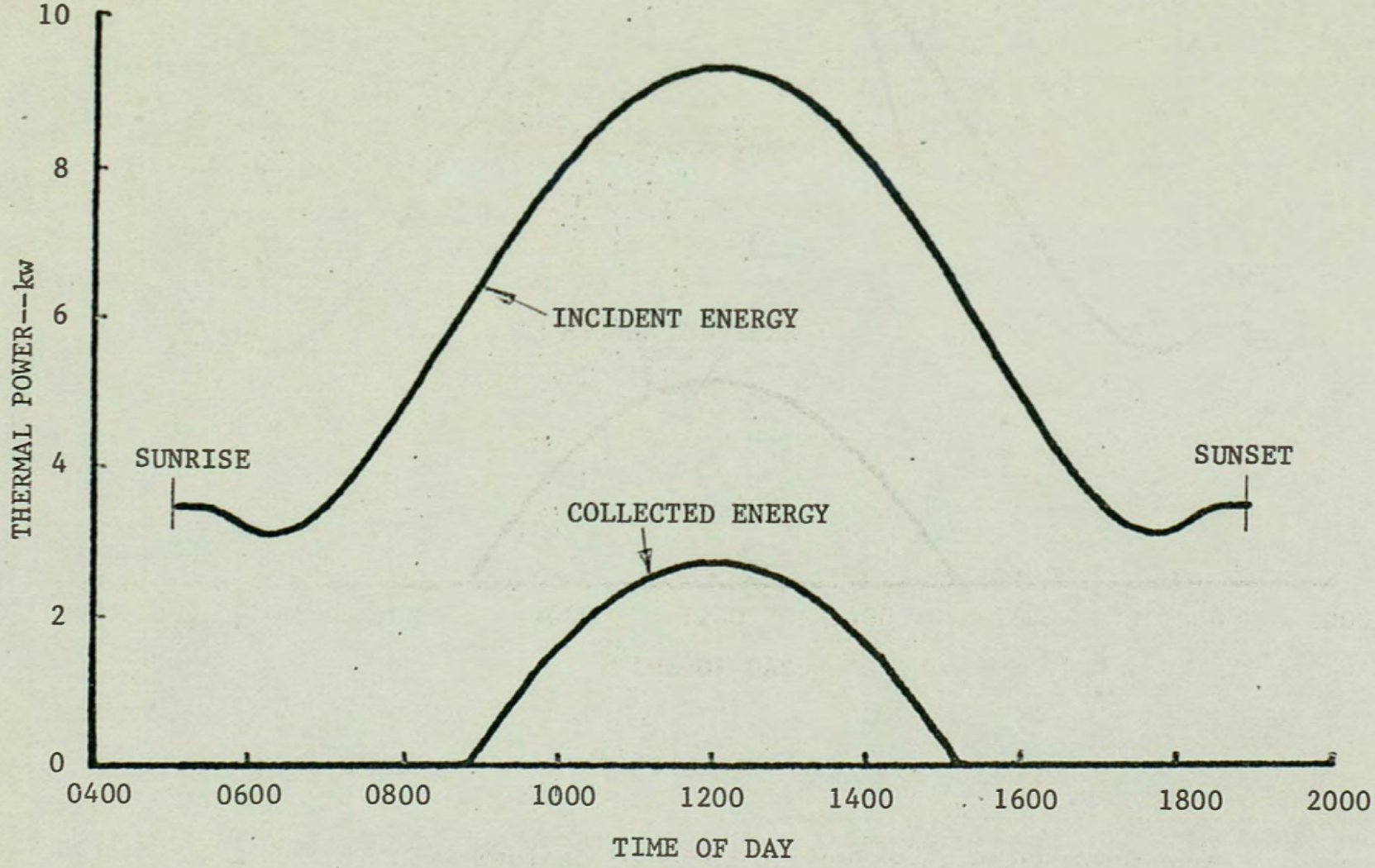

Figure 33. Typical Behavior of $10m^2$ Flat Plate Collector

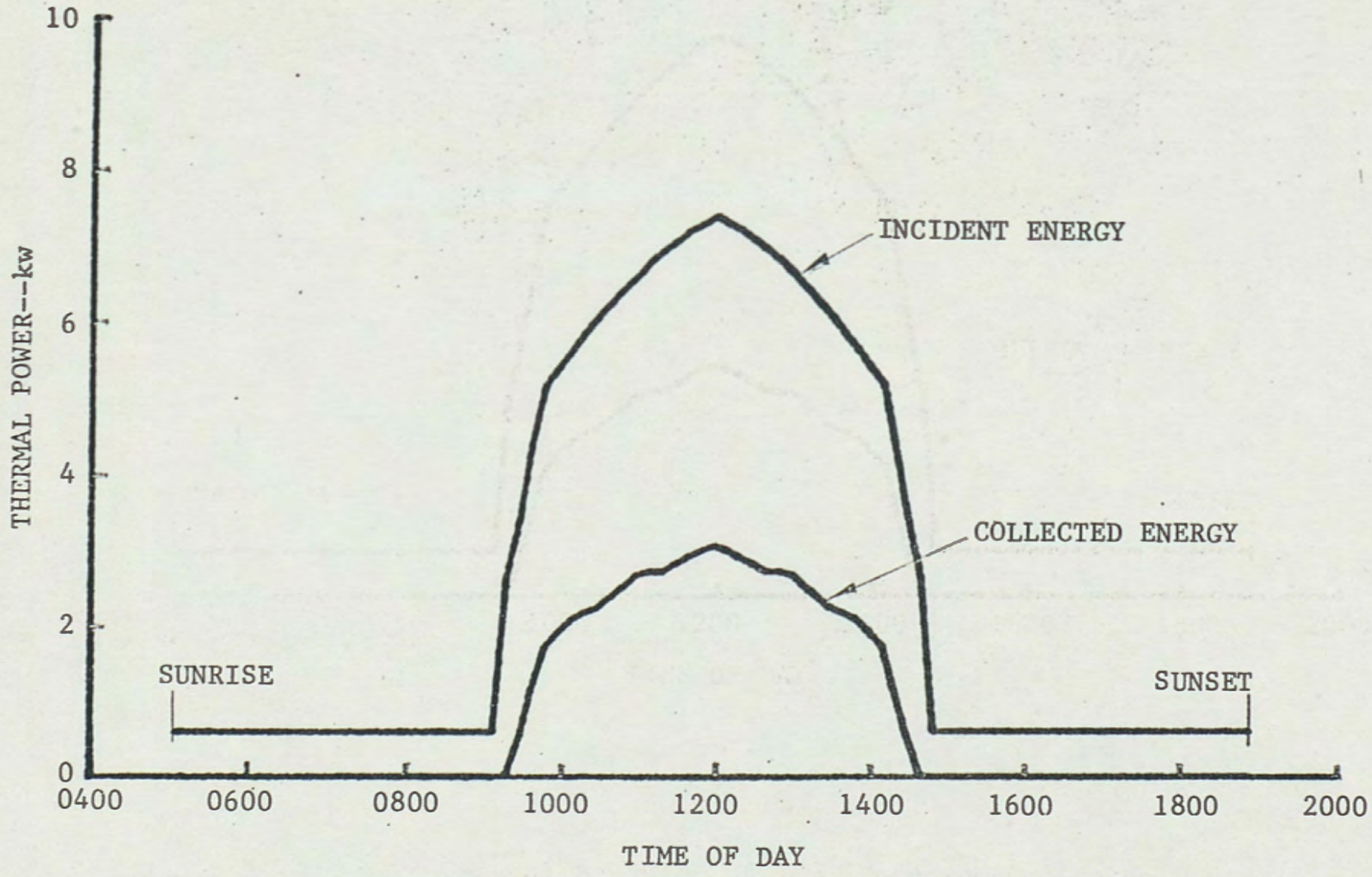

Figure 34. Typical Behavior of $10m^2$ Focusing Collector

TABLE 11

TYPICAL COLLECTOR PERFORMANCE PARAMETERS

Parameter	Flat Plate Collector	Focusing Collector
Operating Temperature	80°C	100°C
Time Fluid Flow Starts	0850	0920
Maximum Incident Power	9284w	7388w
Maximum Power Transferred to Fluid	2751w	3059w
Energy Incident on Absorbent Face from Sunrise to Sunset	82.2 kw-hr	37.4 kw-hr
Energy Incident on Absorbent Face During Fluid Flow	52.1 kw-hr	31.9 kw-hr
Energy Collected	11.5 kw-hr	11.8 kw-hr

Time of Sunrise: 0505

Time of Sunset: 1855

prediction to drop for a short time after sunrise before increasing as the solar elevation angle increases. Similar behavior is seen in reverse at sunset. This phenomenon is due to the assumption of uniform diffuse radiation from the sky in the computer model. At dawn and dusk, virtually all of the sun's radiation reaching the collector is diffuse and the collector intercepts this radiation. Since a uniform distribution has been assumed, the interception is fairly efficient. As the sun rises, the air mass through which the radiation must travel drops rapidly, decreasing the intensity of the diffuse radiation and increasing the beam radiation flux. The sun is at such a low elevation, however, that the collector cannot trap much of this beam radiation. Hence, the sun must reach a high enough point in the sky that the increasing beam flux "overtakes" the decreasing diffuse radiation before the incident energy curve is predicted to rise.

Figure of Merit Optimization

For a fair comparison of the collectors to be made, their temperatures should be chosen to reflect the respective optimal operating points where actual installations would be set to run. Prior to evaluating various possible operating temperatures, several assumptions were made. First, it was assumed that the temperature difference between the fluid entering the collector at T_{IN}, and the nominal exit temperature, the thermostat set point, T_O, would be a constant 10°C regardless of the operating point. It was further assumed that the absorption cycle boiler temperature, T_H, used in the

computation of the figure of merit, coincided with the fluid inlet temperature, T_{IN}. The region of linear thermostat throttling between the set point, T_O, and the saturation point, T_{OO}, was made a constant width, 5°C, regardless of operating point. Finally, the coolant was assumed to be water (pressurized where appropriate to prevent boiling) with the same maximum circulation rate, 1000 kg/hr, available for both the flat plate and focusing collectors. The refrigeration temperature, T_C, was simply taken to be 16°C (60°F) for all cases considered. Temperature control parameters are summarized in Table 12.

Substituting the appropriate quantities into the equation for ideal coefficient of performance derived for the figure of merit yields,

$$COP_i = \left(\frac{T_{IN}-T_\infty}{T_{IN}}\right)\left(\frac{T_C}{T_\infty-T_C}\right)$$

The variation in ideal COP with boiler temperature, T_{IN}, is shown in Table 13. Note that the ideal COP increases by a factor of four as the collector inlet temperature increases from 50°C to 125°C. This permits a substantial decrease in collected energy, Q_H, as the temperature increases for a given value of reversible cooling effect, Q_C, the figure of merit.

A number of computer runs were made with the input parameters previously described, in an attempt to find the optimum operating temperatures. The temperature range simulated for the flat plate collector thermostat set point was from 60°C to 95°C, representing air conditioner boiler temperatures from 50°C to 85°C. The set points

TABLE 12

TEMPERATURE CONTROL PARAMETERS

Refrigeration Temperature, T_C	16°C
Nominal Temperature Rise in Collector (T_O-T_{IN})	10°C
Region of Linear Thermostat Throttling (T_{OO}-T_O)	5°C
Coolant, Specific Heat	Water, 4187 J/kg-°C*
Maximum Coolant Flow Rate	1000 kg/hr

*Assumed to be exactly 1 BTU/lbm-°F

TABLE 13

COEFFICIENT OF PERFORMANCE OF
REVERSIBLE ABSORPTION CYCLE AIR CONDITIONER

Boiler Temperature ~ °C	COP
50	1.28
55	1.49
60	1.86
65	2.14
70	2.41
75	2.62
80	2.92
85	3.17
90	3.41
95	3.65
100	3.87
105	4.09
110	4.31
115	4.52
120	4.73
125	4.92

Refrigeration Temperature = 16°C (60°F)

Ambient Temperature = 30°C (86°F)

considered for the focusing collector ranged from 80°C to 120°C. For each set point, the thermal energy collected throughout a day's operation, Q_H, was obtained from the computer output. The ideal COP for a reversible system at various operating temperatures is shown in Table XIII. The reversible cooling effect, Q_C, is simply the product of Q_H and the appropriate COP.

The results of the computer runs are shown in Figure 35. It is evident from the figure that the optimum operating points for the two collectors are at distinctly different temperatures, about 72°C for the flat plate collector and 100°C for the focusing system. These temperatures represent absorption cycle boiler temperatures of 62°C and 90°C, respectively. The 90°C boiler temperature is realistic, although somewhat lower than conventional absorption cycle units use. The flat plate optimum, 62°C, is much too low for a lithium bromide absorption system [1]. Since no other working media are currently available for a practical air conditioner at these temperatures, the characteristics of the lithium bromide-water cycle must be considered constraints on the choice of system operating point [2].

The lowest realistic boiler temperature for the lithium bromide solution is about 77°C (170°F) [1]. This limit is shown in Figure 35, and corresponds to a collector operating temperature of 87°C. In the case of reversible refrigeration, this temperature constraint extracts some penalty from the flat plate collector performance because of its lower optimum temperature. A comparison of collector and reversible air conditioning performance is provided in Table 14.

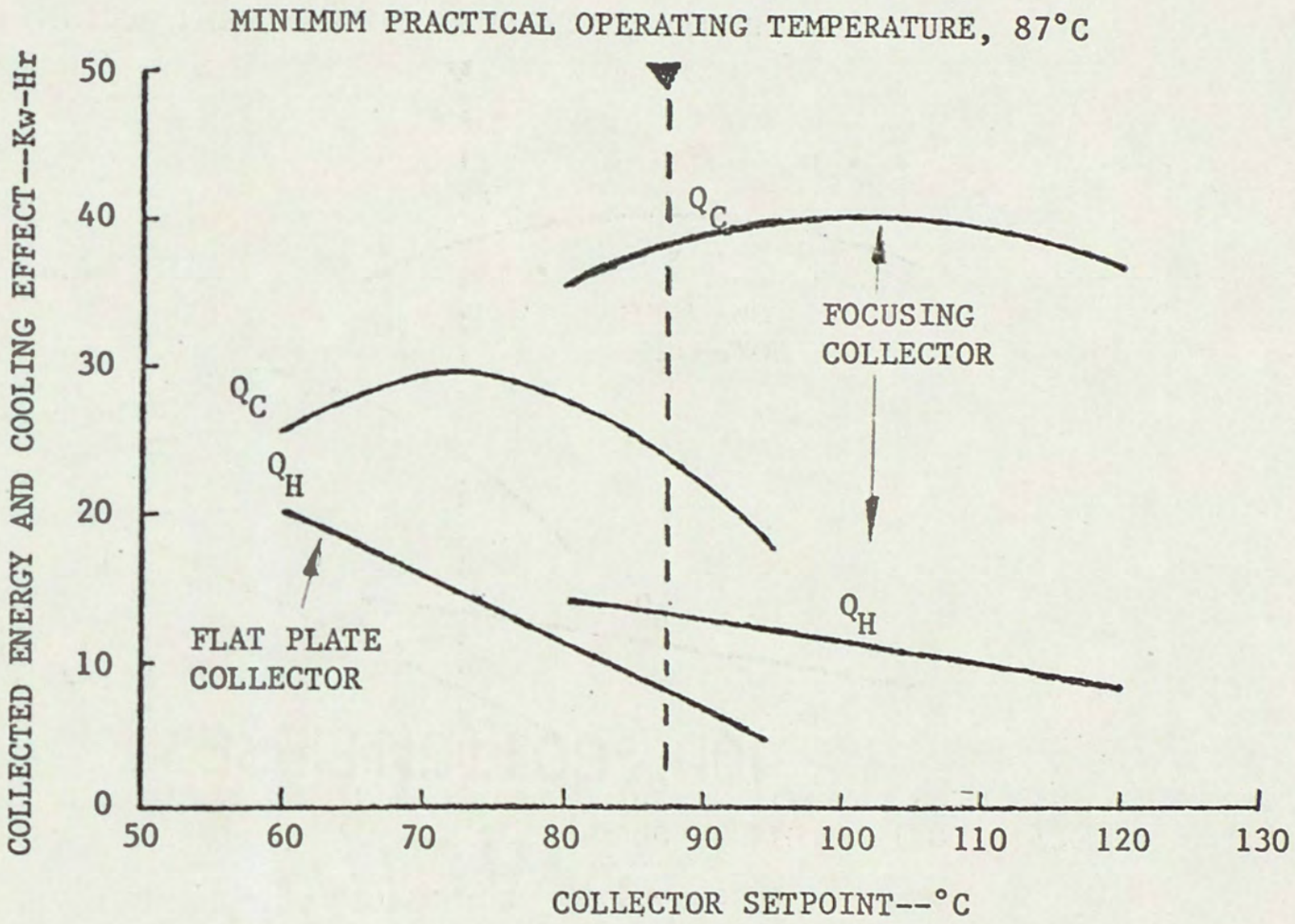

Figure 35. Flat Plate and Focusing Collector Cooling Performance Comparison (Reversible Cycle)

TABLE 14

COLLECTOR PERFORMANCE IN DRIVING REVERSIBLE ABSORPTION CYCLE AIR CONDITIONER

	Flat Plate Collector	Focusing Collector
Optimum Collector Operating Temperature	72°C	100°C
Minimum Practical Operating Temperature	87°C	87°C
Collected Energy, Q_H		
at Optimum Temperature	16 kw-hr	12 kw-hr
at Minimum Temperature	8 kw-hr	- *
Reversible Cooling Effect, Q_C		
at Optimum Temperature	30 kw-hr	40 kw-hr
at Minimum Temperature	24 kw-hr	- *

*No constraint

Results

It is obvious from Figure 35 that the performance of the focusing system is superior to that of the flat plate collector under the assumptions stated earlier. As shown in Table XIV, the difference in cooling effect is significant--slightly more than 30%, if the two optimum operating points are compared, or nearly a factor of two if the minimum operating temperature is used for the flat plate. A greater sensitivity of cooling effect to operating temperature for the flat plate than for the focusing collector is also evident in the figure. The lower sensitivity to temperature and the higher cooling performance suggest that the focusing collector is the better of the two configurations.

It should be recalled that the comparison summarized here assumes still air and a clear sky. The latter assumption strongly favors the focusing collector. Its inability to collect scattered radiation from the sky makes it particularly sensitive to any haze or clouds blocking the sun. On the other hand, the flat plate is an efficient collector of diffuse radiation which does not exhibit such a dramatic sensitivity. Hence, the results of this simple comparison represent the most optimistic situation for collector operation, and are not conservative. Clearly, the effect of expected weather patterns, including winds and cloudiness, must be considered in any definitive comparison.

A more basic limitation in this comparison is the assumption of reversibility in the computation of air conditioner COP and cooling effect. Actual coefficients of performance for absorption cycle air

conditioners seldom exceed unity [1], in contrast to the optimistic values shown in Table 13. Again, the choice of a collection configuration for an actual installation would require a more detailed analysis than presented here, including a realistic model of air conditioner COP.

V. CONCLUSIONS AND RECOMMENDATIONS

It is concluded from the collector comparison presented in this paper that the computer program functioned as intended. Performance parameters suitable for the comparison of a specific flat plate collector and a focusing arrangement were generated by the program. In addition, studies of collector geometry, materials, and operating temperature are possible extensions of the normal program function by appropriate variation of the input variables. If improvements in the accuracy of the program are required, refinements to the computer model could include making the local environmental parameters for temperature, convective heat loss, and the diffuse sky radiation pattern dynamic functions of time rather than constants as they are now specified. In addition, a more sophisticated heat exchanger model with some provision for thermal storage would improve the accuracy of the model in predicting transient, short-term behavior if this is of interest. Refinements of this kind were not considered necessary for the type of collection evaluation presented in this paper.

The comparison of flat plate and focusing collector performance clearly indicates a higher cooling potential for the focusing arrangement than for the flat plate in an idealized reversible refrigeration cycle. The performance advantage offered by the focusing collector under this assumption is at least 30%, and perhaps

nearly a factor of two if a realistic absorption cycle temperature constraint is imposed. This conclusion is restricted to operation on clear days since a parametric study of performance degradation due to cloudiness has not been undertaken here. The significant "clear day" advantage offered by the focusing collector suggests that a considerable reduction (perhaps 50%) in direct solar radiation could be tolerated before this advantage was lost.

Obviously, a definitive comparison of collector configurations will require consideration of expected weather conditions in the location of interest. Further, any detailed analysis must include a more accurate model of the intended air conditioning system than the simplified reversible cycle used in this comparison.

APPENDIX I.

COMPUTATION OF UNIT VECTOR NORMAL TO PARABOLIC CYLINDRICAL SURFACE

In general, the function, $F(x,y,z) = 0$, has a vector normal to its surface defined as follows:

$$\overline{V}_n = \begin{bmatrix} \frac{\partial F}{\partial x} \\ \frac{\partial F}{\partial y} \\ \frac{\partial F}{\partial z} \end{bmatrix} ,$$

where the partial derivatives are evaluated at the point of interest on the surface.

For the parabolic cylinder shown in Figure 36, $F(x,y,z) = x - Ky^2 = 0$.

Now,

$$\overline{V}_n = \begin{bmatrix} 1 \\ -2Ky \\ 0 \end{bmatrix}$$

The unit normal to the surface is just,

$$\overline{U}_n = \frac{1}{\zeta} \begin{bmatrix} 1 \\ -2Ky \\ 0 \end{bmatrix} ,$$

when $\zeta = \sqrt{1 + (2Ky)^2}$.

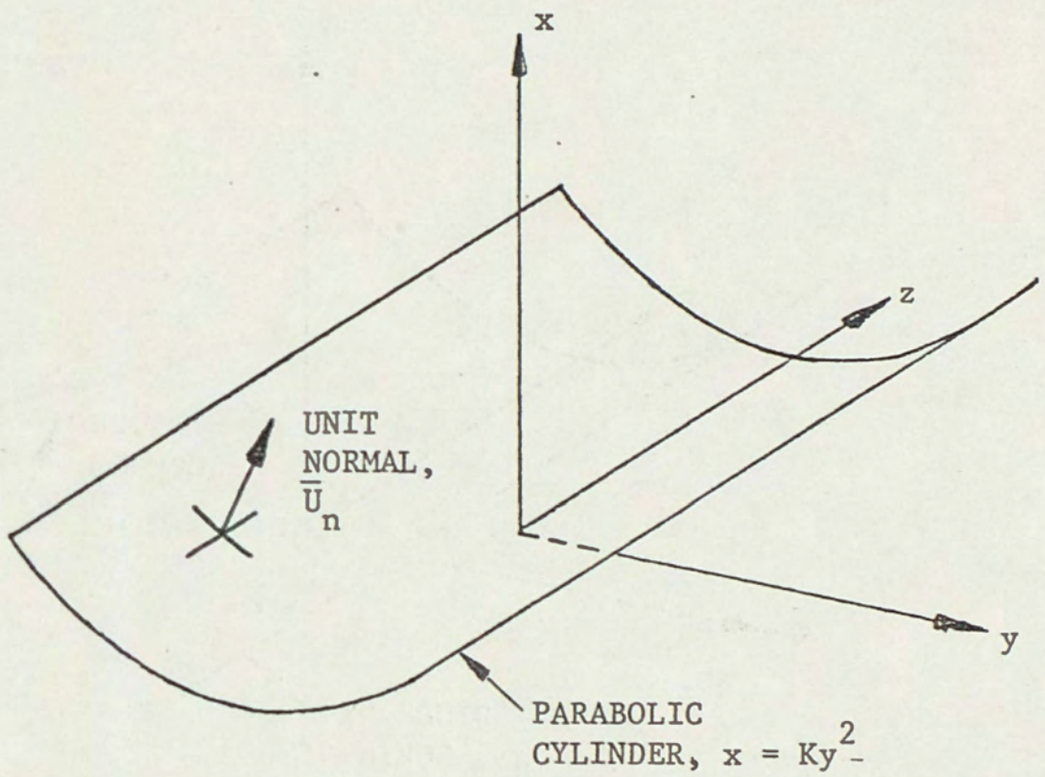

Figure 36. Normal to Parabolic Cylinder

APPENDIX II.

VECTOR REPRESENTATION OF SPECULAR REFLECTION

The reflecting surface shown in Figure 37 has a unit normal, $\overline{U}_n$, and an incident light ray represented by $\overline{U}_i$. The unit vector, $\overline{U}_r$, represents the reflected ray. In the figure, $\overline{U}_i'$ is simply the vector, $\overline{U}_i$, translated to the point of reflection. The angle of incidence, β, is the same as the angle of reflection. The vector, $\overline{V}$, is the component of $\overline{U}_i$ parallel to the normal $\overline{U}_n$. Clearly,

$$\overline{U}_r = \overline{U}_i' - 2\overline{V}$$

$$= \overline{U}_i - 2\overline{V},$$

and,

$$\overline{V} = (\overline{U}_i \cdot \overline{U}_n)\ \overline{U}_n.$$

Let, $\mu = -\overline{U}_i \cdot \overline{U}_n$. Now, $\overline{U}_r = \overline{U}_i + 2\mu\overline{U}_n$.

Note that μ is simply $\cos\beta$.

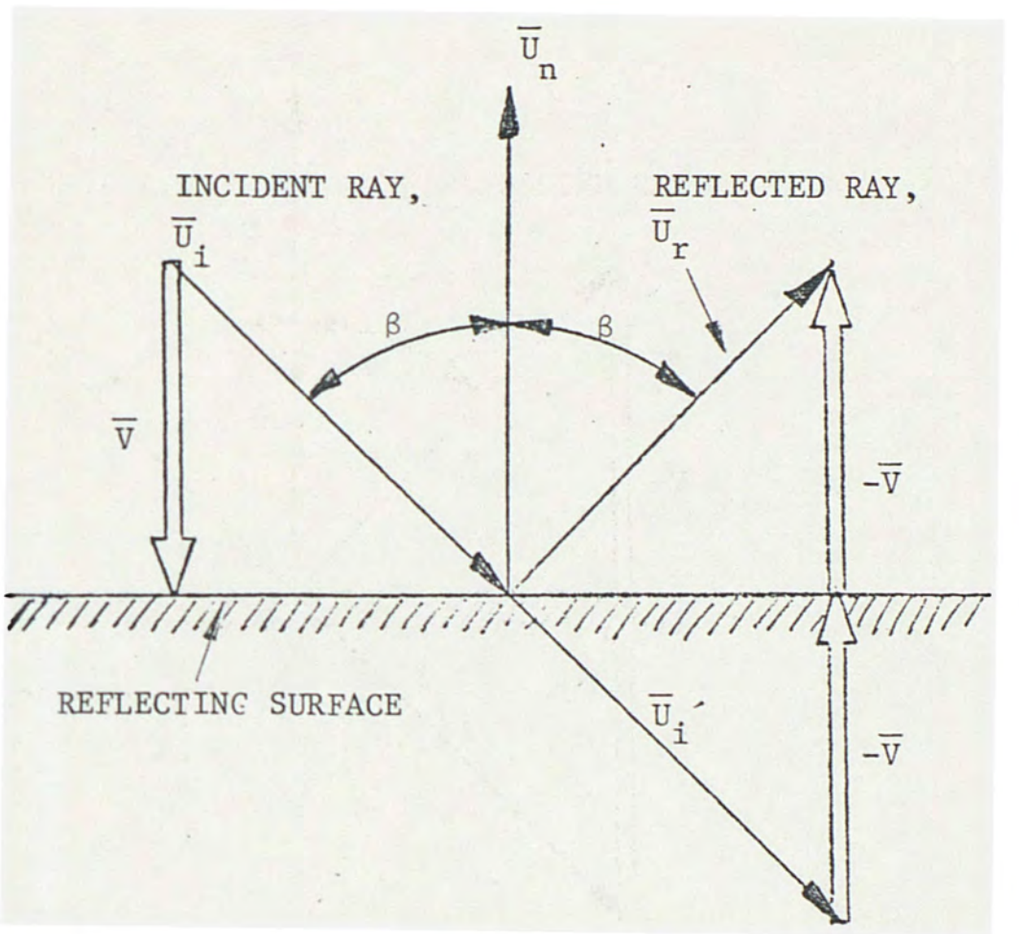

Figure 37. Vector Reflection

APPENDIX III.

INTERSECTION OF A REFLECTED RAY WITH A PLANE ABOVE A PARABOLIC REFLECTOR

In Figure 38, $\overline{U}_i$ describes the orientation of the incident ray, $\overline{U}_n$, the normal to the reflector, and $\overline{U}_r$, the reflected ray. $\overline{P}$ is the vector representing the coordinates of the point of intersection of $\overline{U}_r$ and the plane shown.

The incident ray strikes the reflector at $\overline{R}$; the plane is defined as $x = f$. From Appendix II,

$$\overline{U}_r = \overline{U}_i - 2(\overline{U}_i \cdot \overline{U}_n)\,\overline{U}_n.$$

Clearly, $\overline{P}$ can be found as follows:

$$\overline{P} = \overline{R} + m\overline{U}_r,$$

where m is a scalar representing the distance from the tip at $\overline{R}$ to $\overline{P}$. Rewriting this expression to show the individual components,

$$\begin{bmatrix} f \\ P_y \\ P_z \end{bmatrix} = \begin{bmatrix} R_x \\ R_y \\ R_z \end{bmatrix} + m \begin{bmatrix} U_{rx} \\ U_{ry} \\ U_{rz} \end{bmatrix}$$

Solving for the scalar multiplier, $m = (f - R_x)/U_{rx}$.

Substituting, the coordinates of the intersection are found:

$$\overline{P} = \begin{bmatrix} f \\ R_y + mU_{ry} \\ R_z + mU_{rz} \end{bmatrix}.$$

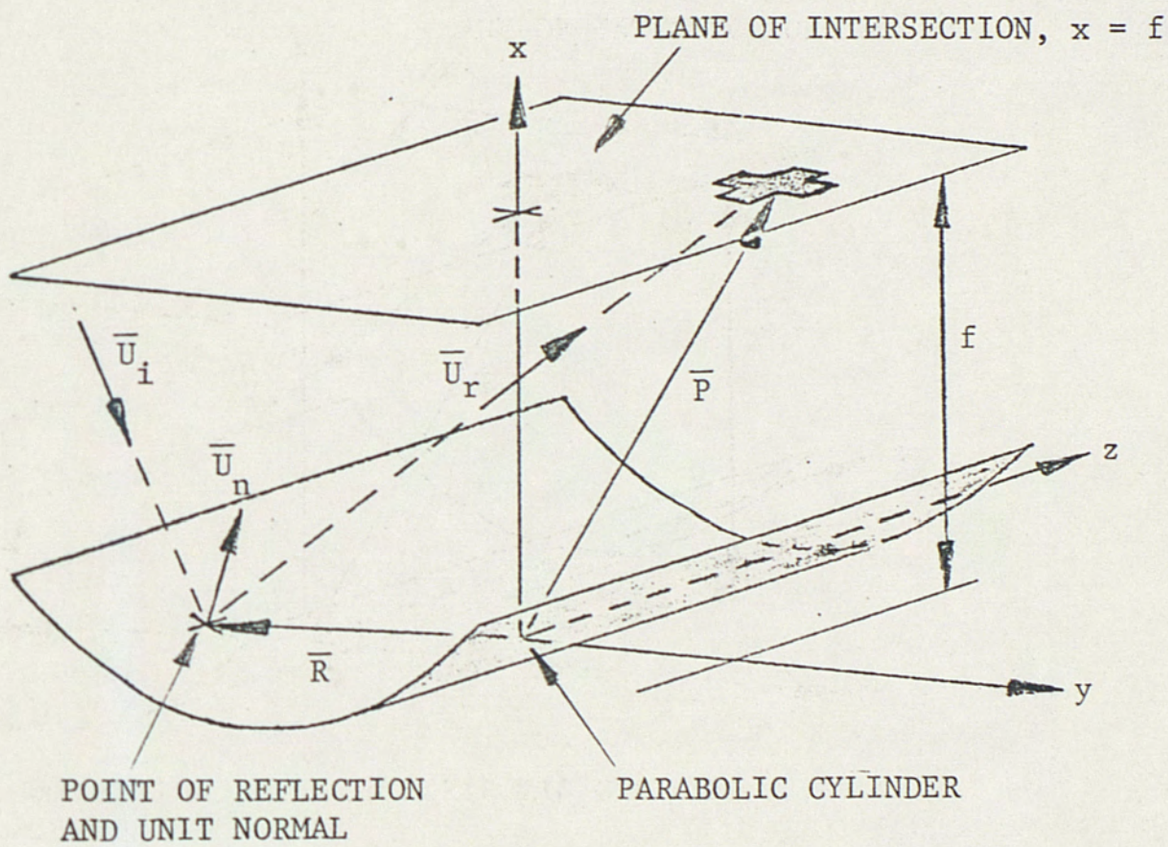

Figure 38. Intercept of Reflected Ray

APPENDIX IV.

BOUNDARY OF A SHADOW CAST ON A PARABOLIC REFLECTOR

Figure 39 shows a ray of light specified by unit vector, $\overline{U}_i$, grazing a boundary of an opaque plate above a parabolic reflector. The intersection of this ray with the reflector defines a point on the boundary of the shadow cast by the plate; the locus of such points is the shadow boundary. The vector $\overline{P}$ represents the coordinates of the point of contact between $\overline{U}_i$ and the plate. $\overline{R}$ is the corresponding set of shadow coordinates. The equation for the plane containing the plate is simply, $x = f$.

From the figure, $\overline{R} = \overline{P} + m\overline{U}_i$, where m is scalar representing the distance from the tip of $\overline{P}$ to $\overline{R}$. If the parabolic surface is defined as $x = Ky^2$,

$$\overline{R} = \begin{bmatrix} KR_y^2 \\ R_y \\ R_z \end{bmatrix}$$

Substituting this into the original expression for $\overline{R}$,

$$\begin{bmatrix} KR_y^2 \\ R_y \\ R_z \end{bmatrix} = \begin{bmatrix} f \\ P_y \\ P_z \end{bmatrix} + m \begin{bmatrix} U_{ix} \\ U_{iy} \\ U_{iz} \end{bmatrix}$$

This vector equation represents three simultaneous equations having the unknowns, m, R_y, and R_z. Manipulation yields,

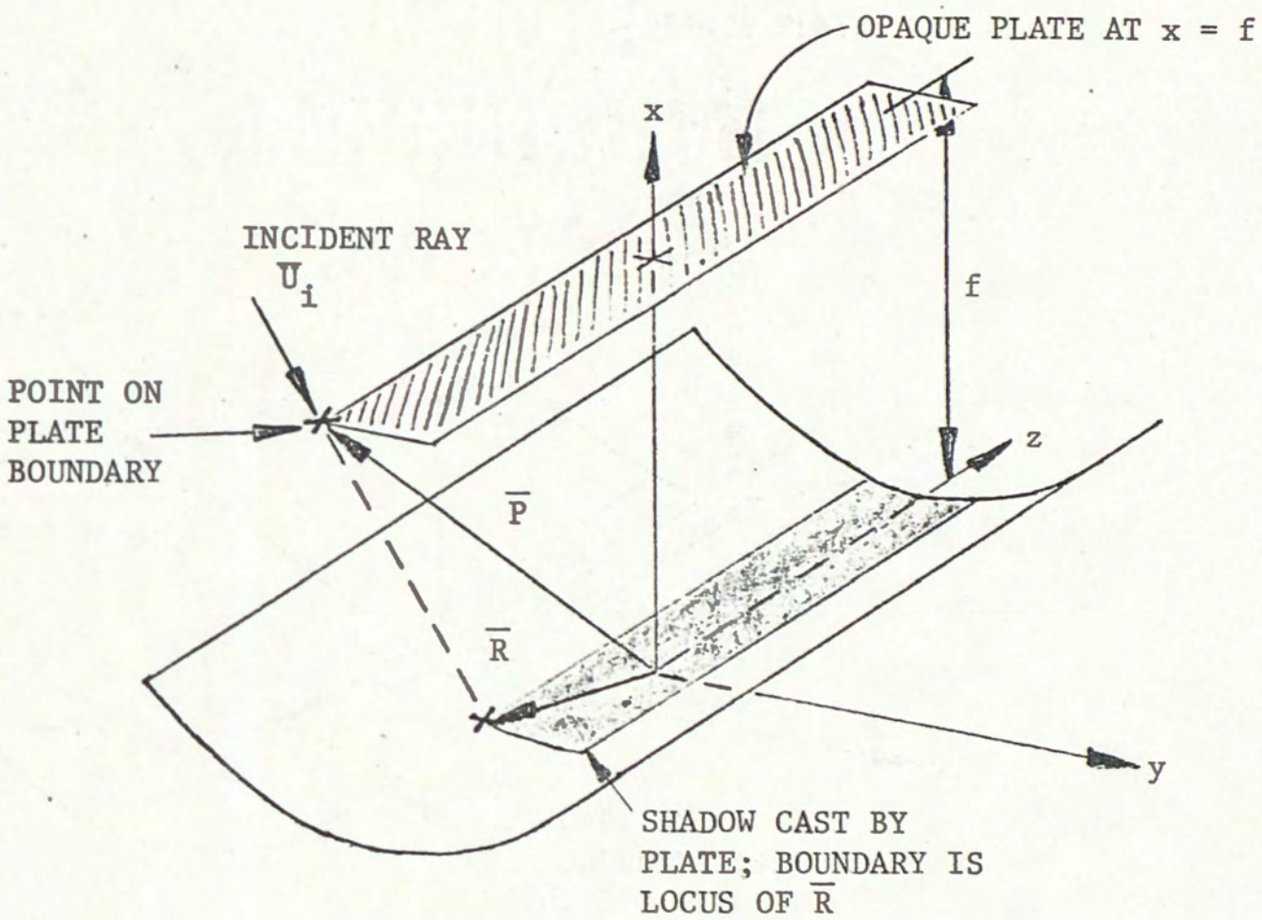

Figure 39. Shadow Cast on Reflector

$$K(P_y + mU_{iy})^2 = f + mU_{ix}$$

or,

$$KU_{iy}^2 m^2 + (2KP_yU_{iy} - U_{ix})\, m + (KP_y^2 - f) = 0.$$

The positive root of m is found for this equation and substituted into the vector equation:

$$\overline{R} = \begin{bmatrix} K(P_y + mU_{iy})^2 \\ P_y + mU_{iy} \\ P_z + mU_{iz} \end{bmatrix} .$$

APPENDIX V.

EQUIVALENT METRIC AND ENGLISH UNITS [9]

length	1 ft = 0.3048 m
mass	1 lbm = 0.4536 kg
energy	1 BTU = 1055 J 1 kw-hr = 3413 BTU
power	1 BTU/hr = 0.293 w
heat flux	1 BTU/hr-ft^2 = 3.1537 w/m^2
thermal conductivity	1 BTU/hr-ft-°F = 1.7303 w/m-°C
convective heat transfer efficient	1 BTU/hr-ft^2-°F = 5.6768 w/m^2-°C
Stefan-Boltzmann constant	0.1714×10^{-8} BTU/hr-ft^2-°R^4 = 5.669×10^{-8} w/m^2-°k^4

APPENDIX VI.

LISTING OF COMPUTER PROGRAM

```
      DOUBLE PRECISION TITLE(10),TERM
      COMMON /SOLP/ ISR,ISS,XLAT,DELT,ITIME,JTIME,UIA(3),AZ,EL
      COMMON /VECT/ UI3(3),UN(3),U(3),URC(3),UNR(3),UNA(3),
     *R(3),P(3),UO3(3)
      COMMON /OOTP/ XMU,BETA,XMUR,BETAR,XMUA,BETAB
      COMMON /GEOM/ AC,YR,ZR,YR,YA,ZA,ZAUP,ZALW,NA,F,FZ,XK
      COMMON /SURFP/ NAT,BTFP(10),AT(10),ALCOV(10),NRH,BTAR(10),RHO(10),
     *NAL,BTAB(10),ALPH(10),AES,FSLAB,FRP1,FRC1,FRP2,FRC2,FSEL,FSELC
      COMMON /ENV/ PSURF,WB,NDF,BETD(20),WD(20),WDENV,H,HI,
     * HA,HAC,HIAC,TINF
      COMMON /XFORM/ CBA(9)
      COMMON /STRAD/ NW,SETI,STAJ,UST(3),CW,NN,IBET,J
      COMMON/ABSBR/QDIN(21),TP(21),FI(21),QDNET(21),CONV(21),RAD(21)
      COMMON /THERM/ CPMDZ,TZ,TZZ,TIN
      COMMON /FPABSR/ TPL,FF,QDINF,TC,QDINC,CONVF,RADF
      COMMON /QNET/ CPMD,POUT,TOUT
      COMMON /STRT/ INIT1,INIT2,INIT3,INIT4
      DIMENSION JTIME(3),AWD(20)
      DATA SIGMA /5.669E-8/
      DATA PI,TPI /3.141592,6.282184/
      DATA TERM /3HEND     /
C    INITIALIZATION FLAGS
C    INIT1--SOLPOS
C    INIT2--CYLRF
C    INIT3--STER
C    INIT4--ABSB
C
C    ONE TIME INPUTS
C
C
C    SURFACE PROPERTIES
C
C    FLAT PLATE
      READ (5,*) NAT
      READ (5,*) (BTFP(I),I=1,NAT)
      READ (5,*) (ALCOV(I),I=1,NAT)
      READ (5,*) (AT(I),I=1,NAT)
      READ (5,*) FSEL,FSELC
      READ (5,*) EP,RHP,EC,RHC,TAUC
      READ (5,*) CNCOV
C    CYLINDER REFLECTOR
C                  REFLECTOR
      READ (5,*) NRH
      READ (5,*) (BTAR(I),I=1,NRH)
      READ (5,*) (RHO(I),I=1,NRH)
      READ (5,*) EHTR
C                  ABSORBER
      READ (5,*) NAL
      READ (5,*) (BTAB(I),I=1,NAL)
      READ (5,*) (ALPH(I),I=1,NAL)
      READ (5,*) EHT,FSLAB
C
C    ENVIRONMENT
C
      READ (5,*) SOLC
      READ (5,*) FSZ,AMASZ
      READ (5,*) NDF
      READ (5,*) (BETD(I),I=1,NDF)
      READ (5,*) (AWD(I),I=1,NDF)
      READ (5,*) H,HI
```

```
      READ (5,*) TINF
C
C   THERMAL PROPERTIES OF COOLANT, THERMOSTAT PARAMETERS
C
      READ (5,*) CP
      READ (5,*) XMDI
C
C   GEOMETRY
C
C   FLAT PLATE
      READ (5,*) AC,TCOV
C   CYLINDRICAL REFLECTOR
      READ (5,*) MR,YR,ZR
      READ (5,*) YA,NA,ZA
      READ (5,*) FZ,F
C
C
C
C   INITIALIZATION
C
      NA2=2*NA+1
      NW=200
      XMDZ=XMDI/3600.
      CPMDZ=XMDZ*CP
      CPMD=CPMDZ
      DAA=2.*YA*ZA/(NA+0.5)
      AES=DAA*EHT*SIGMA
      WDENV=(SIGMA*(TINF+273.)**4)/PI
      HA=H*DAA
      HAC=AC/(1./H+0.5*TCOV/CNCOV)
      HIAC=AC/(1./HI+0.5*TCOV/CNCOV)
      FRP1=EP*SIGMA*AC*(1.-RHC)/(1.-RHP*RHC)
      FRC1=EC*SIGMA*AC*(1.-RHP)/(1.-RHP*RHC)
      FRP2=EP*SIGMA*AC*TAUC/(1.-RHP*RHC)
      FRC2=EC*SIGMA*AC*(1.+RHP*TAUC-RHP*RHC)/(1.-RHP-RHC)
      GAM=0.5*(AMASZ*AMASZ-1.)
C   SCALE DIFFUSE RADIATION PATTERN
      SBL=0.
      AWDL=0.
      B=0.
      DARG=2./57.2958
      DO 5 I=2,180,2
      BETDI=I
      ARG=BETDI/57.2958
      SB=SIN(ARG)
      CALL LINT (NDF,BETDI,BETD(1),AWD(1),AWDI)
      B=B+0.5*(AWDI*SB+AWDL*SBL)*DARG
      SBL=SB
      AWDL=AWDI
    5 CONTINUE
      BB=AMAX1(B,0.001)
      A=SOLC/(TPI*BB)
      IF (B.EQ.0.) A=0.
      DO 6 I=1,NDF
      AWD(I)=A*AWD(I)
    6 CONTINUE
C
C
C
    2 CONTINUE
```

```
C
C    INPUTS FOR STACKED RUNS
C
      READ (5,90) TITLE
      IF (TITLE(1).EQ.TERM)  CALL EXIT
      WRITE (6,91)
      WRITE (6,90)
      WRITE (6,92) TITLE
      WRITE (6,90)
      WRITE (6,90)
      READ (5,*) XLATI,AZI,ELI,TILTI,NDAY
      DECLI=23.45*SIN(TP1*(284+NDAY)/365)
      WRITE (6,97) XLATI,AZI,ELI,TILTI,DECLI
      WRITE (6,91)
      AZC=AZI/57.2958
      ELC=ELI/57.2958
      TILTC=TILTI/57.2958
      CALL DCBA (AZC,ELC,TILTC,CBA)
      DO 11 I=1,3
      UN(I)=CBA(I)
      UDB(I)=CBA(3*I)
   11 CONTINUE
      XLAT=XLATI/57.2958
      DECL=DECLI/57.2958
      DELT=1.570796-DECL
      READ (5,*) IDTI,JPRINT,ISW,TZ,TZZ,TIN
      TPL=TIN
      TOUT=TIN
      WRITE (6,90)
      WRITE (6,90)
      IDT=0
      IDTP=JPRINT*IDTI
      IP=0
      EOUT=0.
      ESURF=0.
      INIT1=0
      INIT2=0
      INIT3=0
      INIT4=0
      ILABL=0
      CALL STER
C
C    START OF COMPUTATION LOOP
C
    1 CONTINUE
C   COMPUTE SOLAR POSITION, ORIENTATION OF INCIDENT RAY
      CALL SOLPOS
C    COMPUTE INTENSITY OF BEAM AND DIFFUSE COMPONENTS
C    OF RADIATION
      GUI=GAM*UIA(3)
      AMASS=SQRT(GUI*GUI+2.*GAM+1.)-GUI
      FB=FBZ**AMASS
      FD=1.-FB
      WB=SOLC*FB
      WDT=SOLC*FD
      DO 7 I=1,NDF
      WD(I)=AWD(I)*FD
    7 CONTINUE
C    PUT INCIDENT RAY IN  B  FRAME
      CALL ROT (CBA,UIA,UIB)
```

```
C   COMPUTE THERMAL GAINS
      IF (ISW.EQ.1) CALL FLPLC
      IF (ISW.EQ.2) CALL CYLRF
C   COOLANT MASS FLOW, KG/HR
      XMD=3600.*GPMD/GP
C   INCIDENT AND NET ENERGY (CUMULATIVE) EXPRESSED IN KW-HR
      IF (ITIME.NE.ISR) ESURF=ESURF+IDT*(PSURF+PSURFL)/7.2E6
      IF (ITIME.NE.ISR) EOUT=EOUT+IDT*(POUT+POUTL)/7.2E6
      II=MOD(ITIME,IDTP)
      IF (II.EQ.0) IP=0
      IF (ITIME.EQ.ISS) IP=0
      IF (IP.NE.0) GO TO 32
      ILABL=MOD(ILABL+1,3)
      IF (ILABL.NE.1) GO TO 20
      WRITE (6,90)
      WRITE (6,90)
      WRITE (6,83)
      WRITE (6,82) TITLE
      WRITE (6,83)
      WRITE (6,84)
      WRITE (6,90)
      IF (ISW.EQ.1) WRITE (6,85)
      IF (ISW.EQ.2) WRITE (6,86)
      WRITE (6,83)
   20 CONTINUE
      WRITE (6,90)
      WRITE (6,91) JTIME,AZ,EL
      WRITE (6,92) XMD,GPMD,POUT,TOUT,PSURF
      WRITE (6,96) EOUT,ESURF,WS,WDT
      WRITE (6,90)
      GO TO (21,31), ISW
   21 WRITE (6,95) TPL,QDINF,CONVF,RADF,FF,TC,QDINC
      GO TO 32
   31 WRITE (6,93) (TP(I),I=1,NA2)
      WRITE (6,93) (QDIN(I),I=1,NA2)
      WRITE (6,94) (FI(I),I=1,NA2)
      WRITE (6,93) (CONV(I),I=1,NA2)
      WRITE (6,93) (RAD(I),I=1,NA2)
      WRITE (6,93) (QDNET(I),I=1,NA2)
   32 CONTINUE
      IF (IP.EQ.0) IP=1
      IF (ITIME.EQ.ISS) GO TO 2
      PSURFL=PSURF
      POUTL=POUT
      IDT=MAXO(IDT,IDTI)
      IF (ITIME+IDT.GT.ISS) IDT=ISS-ITIME
      IF (ITIME.EQ.ISR) IDT=IDTI-MOD(ISR+IDTI,IDTI)
C   INCREMENT TIME
      CALL TIME (ITIME,JTIME,IDT)
      GO TO 1
   80 FORMAT (10A8)
   81 FORMAT (1H1)
   82 FORMAT (1X,10A8)
   83 FORMAT (40(24 /))
   84 FORMAT (1X,7(24 -),'HR:MN:SC',7X,'AZ',8X,'EL',/,
     *7X,'XMD',6X,'GPMD',6X,'POUT',6X,'TOUT',5X,'PSURF',/,
     *6X,'EOUT',5X,'ESURF',8X,'WB',7X,'WDT')
   85 FORMAT (7X,'TPL',5X,'QDINF',5X,'CONVF',6X,'RADF',8X,'FF',
     * 8X,'TC',5X,'QDINC')
   86 FORMAT (4X,'TP--1     2     3     4     .     .     .     .     .',/,
```

```
     *2X,'QDIN--1     2     3     4     .     .     .     .     .',/,
     *4X,'FI--1     2     3     4     .     .     .     .     .',/,
     *2X,'CONV--1     2     3     4     .     .     .     .     .',/,
     *3X,'RAD--1     2     3     4     .     .     .     .     .',/,
     *1X,'QDNET--1     2     3     4     .     .     .     .     .')
  90 FORMAT (1H )
  91 FORMAT (1X,7(2H -),I2,1H:,I2,1H:,I2,2F10.1)
  92 FORMAT (2F10.2,3F10.0)
  93 FORMAT (15F8.0)
  94 FORMAT (15F8.4)
  95 FORMAT (4F10.0,F10.3,2F10.0)
  96 FORMAT (2F10.3,2F10.0)
  97 FORMAT (5F15.3)
     END

     SUBROUTINE SOLPOS
C
C    COMPUTES SOLAR POSITION AS A FUNCTION OF
C    LATITUDE, TIME OF YEAR, AND TIME OF DAY
C
     COMMON /SOLP/ ISR,ISS,XLAT,DELT,ITIME,JTIME,UI(3),AZ,EL
     COMMON /STRT/ INIT1,INIT2,INIT3,INIT4
     DIMENSION UP(3),Q(3),UQ(3),UR(3),A(3),R(3),CAC(9)
     DIMENSION AMN(3),D(3),JTIME(3),UMN(3)
     DATA OMEGA /0.727221E-4/
     DATA D /0.,0.,1./
     DATA PI /3.141592/
     IF (INIT1.EQ.1) GO TO 1
C    COMPUTE  C  FRAME TO  A  FRAME TRANSFORMATION MATRIX
     UP(1)=COS(XLAT)
     UP(2)=0.
     UP(3)=-SIN(XLAT)
     CALL CROSS (D,UP,A)
     CALL CROSS (UP,A,AMN)
     AMNM=VMAG(AMN)
     CD=COS(DELT)
     CB=CD/UP(1)
     SB=SQRT(1.-CB*CB)
     A(1)=CB
     A(2)=SB
     A(3)=0.
     DO 3 I=1,3
     UMN(I)=AMN(I)/AMNM
     Q(I)=A(I)-CD*UP(I)
   3 CONTINUE
     QMAG=VMAG(Q)
     DO 6 I=1,3
     UQ(I)=Q(I)/QMAG
   6 CONTINUE
     XMU=DOT(UMN,UQ)
     ZETA=PI-ACOS(XMU)
C    COMPUTE TIMES OF SUNRISE AND SUNSET IN SECONDS
C    SOLAR ZENITH IS NOON
     ISR=43200-ZETA/OMEGA+0.5
     ISS=86400-ISR
     ITIME=ISR
     JTIME(1)=ITIME/3600
     JTIME(2)=(ITIME-3600*JTIME(1))/60
     JTIME(3)=MOD(ITIME,60)
     CALL CROSS (UP,UQ,UR)
```

```
      DO 2 I=1,3
      II=3*I-2
      IJ=3*I-1
      IK=3*I
      CAC(II)=UP(I)
      CAC(IJ)=UQ(I)
      CAC(IK)=UR(I)
    2 CONTINUE
      INIT1=1
    1 CONTINUE
      IDT=ITIME-ISR
      THET=OMEGA*IDT
C     COMPUTE SOLAR POSITION IN  D  FRAME
      R(1)=0.
      R(2)=RMAG*COS(THET)
      R(3)=-RMAG*SIN(THET)
C     COMPUTE SOLAR POSITION IN  A  FRAME
      CALL ROT (CAC,R,A)
      DO 4 I=1,3
      R(I)=CO*UP(I)+A(I)
    4 CONTINUE
      RMAG=VMAG(R)
C     COMPUTE ORIENTATION OF INCIDENT RAYS
      DO 5 I=1,3
      UI(I)=-R(I)/RMAG
    5 CONTINUE
      CALL ANGLE (R(1),R(2),AZ,H)
      CALL ANGLE (H,-R(3),EL,S)
      AZ=AZ*57.2958
      EL=EL*57.2958
      IF (EL.GT.180.) EL=0.
      RETURN
      END

      SUBROUTINE ROT (C,A,B)
C     VECTOR ROTATION OR COORDINATE TRANFORMATION
      DIMENSION C(9),A(3),B(3),I(3)
      DO 3 JJ=1,3
      DO 2 K=1 ,3
    2 I(K)=K+3*(JJ-1)
      SUM=0.0
      DO 1 K=1,3
      IK=I(K)
    1 SUM=SUM+C(  IK)*A(K)
    3 B(JJ)=SUM
      RETURN
      END

      SUBROUTINE CROSS (A,B,C)
C     VECTOR CROSS PRODUCT
      DIMENSION A(1),B(1),C(1)
      C(1)=A(2)*B(3)-A(3)*B(2)
      C(2)=A(3)*B(1)-A(1)*B(3)
      C(3)=A(1)*B(2)-A(2)*B(1)
      RETURN
      END

      SUBROUTINE ANGLE (X,Y,PHI,R)
C     CONVERTS X,Y TO R,THETA
      DIMENSION THETA(4)
```

```
      DATA THETA /0.,1.570796,3.141592,-1.570796/
      DATA PI2 /6.283184/
      PHI=0.0
      N=0
      R=SQRT(X*X+Y*Y)
      IF (X.GT.0.0.AND.ABS(X).GE.ABS(Y)) N=1
      IF (Y.GT.0.0.AND.ABS(Y).GT.ABS(X)) N=2
      IF (X.LT.0.0.AND.ABS(X).GE.ABS(Y)) N=3
      IF (Y.LT.0.0.AND.ABS(Y).GT.ABS(X)) N=4
      IF (N.EQ.0) RETURN
      IF ((MOD(N,2)).NE.0) PHI=THETA(N)+ATAN(Y/X)
      IF ((MOD(N,2)).EQ.0) PHI=THETA(N)-ATAN(X/Y)
      IF (PHI.GT.THETA(3)) PHI=PHI-2.*THETA(3)
      PHI=AMOD(PHI+PI2,PI2)
      RETURN
      END

      SUBROUTINE DCBA (PSI,THETA,PHI,CBA)
C   MATRIX FOR TRANSFORMATION FROM  A  TO  B  FRAME
      DIMENSION CBA(1)
      SPS=SIN(PSI)
      CPS=COS(PSI)
      STH=SIN(THETA)
      CTH=COS(THETA)
      SPH=SIN(PHI)
      CPH=COS(PHI)
      CBA(1)=CTH*CPS
      CBA(2)=CTH*SPS
      CBA(3)=-STH
      CBA(4)=-CPH*SPS+SPH*STH*CPS
      CBA(5)=CPH*CPS+SPH*STH*SPS
      CBA(6)=SPH*CTH
      CBA(7)=SPH*SPS+CPH*STH*CPS
      CBA(8)=-SPH*CPS+CPH*STH*SPS
      CBA(9)=CPH*CTH
      RETURN
      END

      FUNCTION VMAG (C)
C   COMPUTES VECTOR MAGNITUDE (A SCALAR)
      DIMENSION C(1)
      VMAG=SQRTI(C(1)*C(1)+C(2)*C(2)+C(3)*C(3))
      RETURN
      END

      FUNCTION SQRTI(X)
      X=AMAX1(X,0.)
      SQRTI=SQRT(X)
      RETURN
      END

      FUNCTION DOT(A,B)
C   VECTOR DOT PRODUCT
      DIMENSION A(1),B(1)
      DOT=A(1)*B(1)+A(2)*B(2)+A(3)*B(3)
      RETURN
      END

      SUBROUTINE TIME (ITIME,JTIME,IDT)
C   INCREMENTS TIME
```

```
C   CONVERTS SECONDS FROM MIDNIGHT TO HOURS, MINUTES, AND SECONDS
      DIMENSION JTIME(1)
      ITIME=ITIME+IDT
      JTIME(1)=ITIME/3600
      JTIME(2)=(ITIME-3600*JTIME(1))/60
      JTIME(3)=MOD(ITIME,60)
      RETURN
      END

      SUBROUTINE FLPLC
C
C   FLAT PLATE COLLECTOR MODEL--COMPUTES THERMAL
C   GAIN FROM DIFFUSE AND BEAM RADIATION
C
      COMMON/VECT/UI(3),UN(3),U(3),UR(3),UNR(3),UNA(3),R(3),P(3),UDB(3)
      COMMON /DOTP/ XMU,BETA,XMUR,BETAR,XMUA,BETAB
      COMMON /GEOM/ AC,YR,ZR,MR,YA,ZA,ZAUP,ZALW,NA,F,FZ,XK
      COMMON /SURFP /NAT,BTFP(10),AT(10),ALCOV(10),NRH,BTAR(10),RHO(10),
     *NAL,BTAB(10),ALPH(10),ALS,FSLAB,FRP1,FRC1,FRP2,FRC2,FSEL,FSELC
      COMMON /ENV/ PSURF,WB,NDF,BETD(20),WD(20),WDENV,H,HI,
     * HA,HAC,HIAC,TINF
      COMMON /XFORM/ CBA(9)
      COMMON /STRAD/ NW,BETI,BTAJ,UST(3),DW,NN,IBET,J
      COMMON /FPABSR/ TPL,FF,QDIN,TC,QDINC,CONVF,RADF
      COMMON /THERM/ CPMDZ,TZ,TZZ,TIN
      COMMON /QNET/ CPMD,POUT,TOUT
      COMMON /STRT/ INIT1,INIT2,INIT3,INIT4
      XMU=AMAX1(0.,-UI(1))
      BETA=ACOS1(XMU)*57.2958
      CALL LINT (NAT,BETA,BTFP(1),AT(1),ATI)
      CALL LINT (NAT,BETA,BTFP(1),ALCOV(1),ACI)
C   BEAM RADIATION
      PSURF=WB*XMU*AC
      PBM=PSURF*ATI
      PBMC=PSURF*ACI
      PDF=0.
      PDFC=0.
C   DIFFUSE RADIATION
      IBET=1
      J=0
      DO 1 I=1,NN
      CALL STER
      XX=AMAX1(0.,DOT(UST,UDB))
      IF (XX.LE.0.) GO TO 2
C   FROM GROUND
      WDI=WDENV
      GO TO 3
    2 XMU=DOT(UI,UST)
      BETAD=ACOS1(XMU)*57.2958
C   FROM SKY
      CALL LINT (NDF,BETAD,BETD(1),WD(1),WDI)
    3 CALL LINT (NAT,BETI,BTFP(1),AT(1),ATI)
      CALL LINT (NAT,BETI,BTFP(1),ALCOV(1),ACI)
      XMU=UST(1)
      DPSURF=WDI*XMU*DW*AC
      DPD=DPSURF*ATI
      DPDC=DPSURF*ACI
      IF (XX.GT.0.) DPD=DPD*FSEL
      IF (XX.GT.0.) DPDC=DPDC*FSELC
      PDF=PDF+DPD
```

```
      PDFC=PDFC+DPDC
C   THERMAL GAIN BEFORE LOSSES
      PSURF=PSURF+DPSURF
    1 CONTINUE
      QDIN=PBM+PDF
      QDINC=PBMC+PDFC
C   COMPUTE TEMPERATURE, LOSSES, AND NET THERMAL GAIN
      CALL FPABS
      RETURN
      END

      FUNCTION ACOS1(X)
      ACOS1=ACOS(SIGN(AMIN1(ABS(X),0.9999),X))
      RETURN
      END

      SUBROUTINE CYLRF
C
C   PARABOLIC CYLINDRICAL REFLECTOR MODEL--COMPUTES THERMAL
C   GAIN FROM DIFFUSE AND BEAM RADIATION
C
      COMMON/VECT/UI(3),UN(3),U(3),UR(3),UNR(3),UNA(3),R(3),P(3),UDB(3)
      COMMON /DOTP/ XMU,BETA,XMUR,BETAR,XMUA,BETAB
      COMMON /GEOM/ AC,YR,ZR,MR,YA,ZA,ZAUP,ZALW,NA,F,FZ,XK
      COMMON /AREA/ P1(3),P2(3),P3(3),P4(3),AMAP,AI,AF
      COMMON /SURFP/ NAT,BTFP(10),AT(10),ALCOV(10),NRH,BTAR(10),RHO(10),
     *NAL,BTAB(10),ALPH(10),AES,FSLAB,FRP1,FRC1,FRP2,FRC2,FSEL,FSELC
      COMMON /ENV/ PSURF,WB,NDF,BETD(20),WD(20),WDENV,H,HI,
     * HA,HAC,HIAC,TINF
      COMMON /SHDW/ RS1(3),RS2(3),RS3(3),RS4(3),BUS,BLS,XMS
      COMMON /ABSBR/  QDIN(21),TP(21),FI(21),QDNET(21),CONV(21),RAD(21)
      COMMON /THERM/ CPMDZ,TZ,TZZ,TIN
      COMMON /STRAD/ NW,BETI,BETAJ,UST(3),DW,NN,IBET,J
      COMMON /QNET/ CPMD,POUT,TOUT
      COMMON /STRT/ INIT1,INIT2,INIT3,INIT4
      DIMENSION YUR(23),YLR(23),NU(23),NL(23)
      IF (INIT2.EQ.1) GO TO 1
      INIT2=1
      UNA(1)=-1.
      UNA(2)=0.
      UNA(3)=0.
      UNR(3)=0.
C   COMPUTE NUMBER OF ABSORBER CELLS, SIZE, AREA
      NA2=2*NA+1
      NA1=NA+1
      DZA=ZA/(NA+0.5)
      DAA=2.*YA*DZA
      AREAP=4.*YA*ZA
C   COMPUTE NUMBER OF AREA ELEMENTS ON REFLECTOR
      MR2=2*MR+1
      MR4=MR2+2
      DY=YR/(MR+0.5)
C   COMPUTE BOUNDARIES OF AREA ELEMENTS ON REFLECTOR
      DO 20 I=1,MR2
      Y=DY*(I-MR-1)
      YUR(I)=Y+0.5*DY
      YLR(I)=Y-0.5*DY
   20 CONTINUE
C   COMPUTE COEFFICIENT FOR PARABOLA; IE, X=XK*Y**2
C   FZ IS FOCAL LENGTH
```

```
      XK=0.25/FZ
    1 CONTINUE
C     INITIALIZE THERMAL GAINS
      PSURF=0.
      DO 11 K=1,NA2
      QDIN(K)=0.
   11 CONTINUE
      P1(1)=F
      P2(1)=F
      P3(1)=F
      P4(1)=F
C     FIND OUTLINE OF SHADOW CAST BY ABSORBER ON REFLECTOR
C     RS'S ARE COORDINATES OF CORNERS OF SHADOW
      CALL SHADW
      YUR(MR2+1)=RS1(2)
      YUR(MR2+2)=RS3(2)
      YLR(MR2+1)=RS1(2)
      YLR(MR2+2)=RS3(2)
      CALL RANK (YUR,MR4,NU)
      CALL RANK (YLR,MR4,NL)
C     SUM UP THERMAL GAINS FOR EACH REFLECTOR ELEMENT
C     OUTSIDE OF ABSORBER SHADOW
      DO 2 I=1,MR4
      II=NU(I)
      IJ=NL(I)
      YU=YUR(II)
      YL=YLR(IJ)
      IF (YU.EQ.YL) GO TO 2
      YBAR=0.5*(YU+YL)
      ZETA=SQRT(1.+4.*XK*XK*YBAR*YBAR)
      ZU=ZR
      ZL=-ZR
      JJ=1
      IF (YBAR.GT.RS3(2).OR.YBAR.LT.RS1(2)) GO TO 7
      JJ=2
      ZUP=XMS*YBAR+BUS
      ZLW=XMS*YBAR+BLS
    7 CONTINUE
      DO 2 JI=1,JJ
      IF (JJ.EQ.1) GO TO 5
      IF (JI.NE.1) GO TO 6
      ZU=AMAX1(ZLW,-ZR)
      ZL=-ZR
      GO TO 5
    6 CONTINUE
      ZU=ZR
      ZL=AMIN1(ZUP,ZR)
    5 CONTINUE
      IF (ABS(ZU-ZL).LT.1.E-3) GO TO 2
      ZBAR=0.5*(ZU+ZL)
      DA=(YU-YL)*(ZU-ZL)
      UNR(1)=1./ZETA
      UNR(2)=-2.*XK*YBAR/ZETA
      R(1)=XK*YBAR*YBAR
      R(2)=YBAR
      R(3)=ZBAR
      CALL REFL (UNR,UI,UR,XMUR)
      IF (XMUR.EQ.0.) GO TO 2
      BETAR=ACOS1(XMUR)*57.2958
      CALL LINT (NRH,BETAR,BTAR(1),RHO(1),RHOI)
```

```
      XMUA=AMAX1(0.,-DOT(UR,UNA))
      IF (XMUA.EQ.0.) GO TO 2
C   COMPUTE COORDINATES OF CORNERS OF PROJECTIONS OF EACH
C   REFLECTOR AREA ELEMENT ON ABSORBER PLANE
C   SUM UP NUMBER OF CORNERS FALLING ON ABSORBER
      N=0
C   CORNER 1
      R(1)=XK*YL*YL
      R(2)=YL
      R(3)=ZL
      UNR(1)=1./SQRT(1.+4.*XK*XK*YL*YL)
      UNR(2)=-2.*XK*YL*UNR(1)
      CALL REFL (UNR,UI,UR,XMUR)
      CALL ABINT (R,UR,P1)
      IF (ABS(P1(2)).LE.YA.AND.ABS(P1(3)).LE.ZA) N=N+1
C   CORNER 2
      R(3)=ZU
      CALL REFL (UNR,UI,UR,XMUR)
      CALL ABINT (R,UR,P2)
      IF (ABS(P2(2)).LE.YA.AND.ABS(P2(3)).LE.ZA) N=N+1
C   CORNER 3
      R(1)=XK*YU*YU
      R(2)=YU
      UNR(1)=1./SQRT(1.+4.*XK*XK*YU*YU)
      UNR(2)=-2.*XK*YU*UNR(1)
      CALL REFL (UNR,UI,UR,XMUR)
      CALL ABINT (R,UR,P3)
      IF (ABS(P3(2)).LE.YA.AND.ABS(P3(3)).LE.ZA) N=N+1
C   CORNER 4
      R(3)=ZL
      CALL REFL (UNR,UI,UR,XMUR)
      CALL ABINT (R,UR,P4)
      IF (ABS(P4(2)).LE.YA.AND.ABS(P4(3)).LE.ZA) N=N+1
C
C
      IF (N.EQ.0) GO TO 2
C
      BETAB=ACOS1(XMUA)*57.2958
      CALL LINT (NAL,BETAS,BTAB(1),ALPH(1),ALPHI)
C   COMPUTE CONTRIBUTION OF EACH REFLECTOR ELEMENT
C   TO THERMAL GAIN OF EACH ABSORBER CELL
      DO 22 K=1,NA2
      ZZ=(K-NA1)*DZA
      ZAUP=ZZ+0.5*DZA
      ZALW=ZZ-0.5*DZA
      CALL AFAB
      PSURF=PSURF+W3*ZETA*DA*XMUR*AF
      DPS=W3*ZETA*DA*XMUR*RHOI*ALPHI*AF
      SOIN(K)=SOIN(K)+DPS
   22 CONTINUE
    2 CONTINUE
C   COMPUTE CONTRIBUTION OF DIFFUSE RADIATION
      P(1)=F
      P(2)=0.
      DO 24 K=1,NA2
      P(3)=(K-NA1)*DZA
      IBET=1
      J=0
      DO 24 KK=1,NN
      CALL STER
```

```
      DO 26 L=1,3
   26 UST(L)=-UST(L)
      CALL RFINT (XK,P,UST,R)
      IF (ABS(R(2)).GT.YR.OR.ABS(R(3)).GT.ZR) GO TO 27
C     FROM REFLECTOR
      WDI=EHTR*WDENV
      GO TO 28
   27 XX=AMAX1(0.,DOT(UST,UDS))
      IF (XX.LE.0.) GO TO 29
C     FROM GROUND
      WDI=WDENV
      GO TO 28
   29 XMU=DOT(UI,UST)
      BETAD=ACOS1(XMU)*57.2958
C     FROM SKY
      CALL LINT (NDF,BETAD,BETD(1),WD(1),WDI)
   28 CALL LINT (NAL,BETI,BTAB(1),ALPH(1),ALPHI)
      XMU=-UST(1)
      DPD=WDI*XMU*ALPHI*DW
      IF (XX.GT.0.) DPD=DPD*FSLAB
      PSURF=PSURF+WDI*XMU*DAA*DW
      QDIN(K)=QDIN(K)+DAA*DPD
   24 CONTINUE
C     COMPUTE TEMPERATURES, LOSSES, NET THERMAL GAIN
C     OF EACH CELL
      CALL ABSB
      RETURN
      END

      SUBROUTINE REFL (UN,UI,UR,XMU)
C     COMPUTES NEW ORIENTATION OF REFLECTED VECTOR
      DIMENSION UN(1),UI(1),UR(1)
      XMU=AMAX1(0.,-DOT(UN,UI))
      DO 1 I=1,3
    1 UR(I)=UI(I)+2.*XMU*UN(I)
      RETURN
      END

      SUBROUTINE ABINT (R,UR,P)
C     COMPUTES COORDINATES OF INTERSECTION OF VECTOR
C     WITH ABSORBER PLANE
      DIMENSION R(1),UR(1),P(1)
      A=(P(1)-R(1))/UR(1)
      P(2)=R(2)+A*UR(2)
      P(3)=R(3)+A*UR(3)
      RETURN
      END

      SUBROUTINE SHADW
C     COMPUTES COORDINATES OF CORNERS OF SHADOW CAST
C     BY ABSORBER PLATE ON REFLECTOR
      COMMON /VECT/ UI(3),UN(3),U(3),URC(3),UNR(3),UNA(3),
     *R(3),P(3),UDS(3)
      COMMON /GEOM/AC,YR,ZR,MR,YA,ZA,ZAUP,ZALW,NA,F,FZ,XK
      COMMON /SHDW/ RS1(3),RS2(3),RS3(3),RS4(3),BUS,BLS,XMS
      P(1)=F
      P(2)=-YA
      P(3)=-ZA
      CALL RFINT (XK,P,UI,RS1)
      P(3)=ZA
```

```
      CALL RFINT (XK,P,UI,RS2)
      P(2)=YA
      CALL RFINT (XK,P,UI,RS3)
      P(3)=-ZA
      CALL RFINT (XK,P,UI,RS4)
      XMS=(RS3(3)-RS2(3))/(RS3(2)-RS2(2))
      BUS=RS3(3)-XMS*RS3(2)
      BLS=BUS-2.*ZA
      RETURN
      END

      SUBROUTINE RFINT (XK,P,UI,RS)
C     COMPUTES COORDINATES OF INTERSECTION OF VECTOR
C     WITH REFLECTOR
      DIMENSION P(1),UI(1),RS(1)
      A=XK*UI(2)*UI(2)
      B=2.*XK*P(2)*UI(2)-UI(1)
      C=XK*P(2)*P(2)-P(1)
      IF (ABS(A).LT.1.E-5) GO TO 1
      D=SQRT(B*B-4.*A*C)
      XM1=(-B+D)/(2.*A)
      XM2=(-B-D)/(2.*A)
      XM=AMAX1(XM1,XM2)
      GO TO 2
    1 XM=C/UI(1)
    2 RS(2)=P(2)+XM*UI(2)
      RS(3)=P(3)+XM*UI(3)
      RS(1)=XK*RS(2)*RS(2)
      RETURN
      END

      SUBROUTINE RANK (X,M,N)
C     RANKS POINTS FROM MINIMUM TO MAXIMUM
      DIMENSION X(1),N(1)
      DO 2 I=1,M
    2 N(I)=I
      MM1=M-1
      DO 1 I=1,MM1
      IP1=I+1
      DO 1 J=IP1,M
      NI=N(I)
      NJ=N(J)
      IF (X(NI).LE.X(NJ)) GO TO 1
      N(I)=NJ
      N(J)=NI
    1 CONTINUE
      RETURN
      END

      SUBROUTINE AFAB
C
C     COMPUTES FRACTION OF AREA OF PROJECTION OF REFLECTOR
C     ELEMENT ON ABSORBER PLANE WHICH FALLS ON ABSORBER PLATE
C
      DOUBLE PRECISION ATOT
      COMMON /GEOM/ AC,YR,ZR,MR,YA,ZA,ZAUP,ZALW,NA,F,FZ,XK
      COMMON /AREA/ P1(3),P2(3),P3(3),P4(3),AMAP,AI,AF
      DIMENSION Y(3),Z(3),N(3)
      Y(1)=P1(2)
      Y(2)=-YA
```

```
      Y(2)=P3(2)
      Y(4)=YA
      Z(1)=P1(3)
      Z(2)=P2(3)
      Z(3)=P3(3)
      Z(4)=P4(3)
      IF(ABS(Y(3)-Y(1)).LT.1.E-4)Y(3)=Y(1)+SIGN(1.E-4,(Y(3)-Y(1)))
      DY=Y(3)-Y(1)
      SLU=(Z(3)-Z(2))/DY
      SLL=(Z(4)-Z(1))/DY
      A=Z(2)-SLU*Y(1)
      B=Z(1)-SLL*Y(1)
      IF (ABS(SLU).LT.1.E-5) SLU=SIGN(1.E-5,SLU)
      IF (ABS(SLL).LT.1.E-5) SLL=SIGN(1.E-5,SLL)
      Y(5)=(ZAUP-A)/SLU
      Y(6)=(ZALW-A)/SLU
      Y(7)=(ZAUP-B)/SLL
      Y(8)=(ZALW-B)/SLL
      CALL RANK (Y,8,N)
      ATOT=0.DO
      YLW=AMIN1(Y(1),Y(3))
      YUP=AMAX1(Y(1),Y(3))
      DO 10 I=1,7
      NN=N(I)
      NN1=N(I+1)
      DZ=0.
      DZ1=0.
      DZ2=0.
      IF (Y(NN).LT.-YA.OR.Y(NN1).GT.YA) GO TO 1
      DZ=ZAUP-ZALW
      IF ((Y(NN).GE.YLW.AND.Y(NN).LE.YUP).AND.
     * (Y(NN1).GE.YLW.AND.Y(NN1).LE.YUP)) GO TO 8
      GO TO 9
    9 DZ1=AMAX1(SLU*Y(NN)+A,ZAUP)-AMIN1(SLL*Y(NN)+B,ZALW)
     * -AMAX1(SLL*Y(NN)+B-ZAUP,0.)+AMIN1(SLU*Y(NN)+A-ZALW,0.)
      DZ2=AMAX1(SLU*Y(NN1)+A,ZAUP)-AMIN1(SLL*Y(NN1)+B,ZALW)
     * -AMAX1(SLL*Y(NN1)+B-ZAUP,0.)+AMIN1(SLU*Y(NN1)+A-ZALW,0.)
      DZ=0.5*(DZ1+DZ2)
      GO TO 9
    1 IF ((Y(NN).GE.YLW.AND.Y(NN).LE.YUP).AND.
     * (Y(NN1).GE.YLW.AND.Y(NN1).LE.YUP)) DZ=
     *0.5*(SLU-SLL)*(Y(NN)+Y(NN1))+A-B
    9 CONTINUE
      ATOT=ATOT+DZ*(Y(NN1)-Y(NN))
   10 CONTINUE
      DZMAP=0.5*(SLU-SLL)*(Y(1)+Y(3))+A-B
      AMAP=DZMAP*ABS(DY)
      AI=AMAP+2.DO*YA*(ZAUP-ZALW)-ATOT
      AF=AI/AMAP
      RETURN
      END

      SUBROUTINE STER
C
C    COMPUTES UNIT VECTOR AND SPACE ANGLES DEFINING
C    ELEMENTS OF HEMISPHERE
C
      COMMON /STRAD/ NW,BETI,ETAJ,UST(3),DW,NN,IBET,J
      COMMON /STRI/ INIT1,INIT2,INIT3,INIT4
      DIMENSION NETA(50),BET(50),DETA(50),DWB(50)
```

```
      DATA PI,TPI /3.141592,6.282184/
      IF (INIT3.EQ.1) GO TO 1
      INIT3=1
      DW=TPI/NW
      DBZ=SQRT(DW)
      DEZ=DBZ
      NBET=0.5*(PI/DBZ+1.)
      DBET=0.5*PI/NBET
      NN=0
      DO 2 I=1,NBET
      XI=I
      BET(I)=(XI-0.5)*DBET
      SBI=SIN(BET(I))
      NETA(I)=TPI*SBI/DEZ+0.5
      NETA(I)=MAXO(NETA(I),3)
      DETA(I)=TPI/NETA(I)
      DWB(I)=SBI*DBET*DETA(I)
      NN=NN+NETA(I)
    2 CONTINUE
      RETURN
    1 CONTINUE
    4 J=J+1
      IF (J.LE.NETA(IBET)) GO TO 5
      IBET=IBET+1
      J=0
      GO TO 4
    5 CONTINUE
      BETI=BET(IBET)*57.2958
      ETAR=(J-0.5)*DETA(IBET)
      ETAJ=ETAR*57.2958
      DW=DWB(IBET)
      SB=SIN(BET(IBET))
      UST(1)=COS(BET(IBET))
      UST(2)=SB*COS(ETAR)
      UST(3)=SB*SIN(ETAR)
      RETURN
      END

      FUNCTION ASIN1(X)
      ASIN1=ASIN(SIGN(AMIN1(ABS(X),0.9999),X))
      RETURN
      END

      SUBROUTINE ABSB
C
C   MAINTAINS ENERGY BALANCE BETWEEN INCIDENT ENERGY AND
C   LOSSES FOR FOCUSSING COLLECTOR ABSORBER
C
      COMMON /GEOM/ AC,YR,ZR,WR,YA,ZA,ZAUP,ZALW,NAB,FF,FFZ,XX
      COMMON /ABSBR/ QDIN(21),TP(21),F(21),QDNET(21),CONV(21),RAD(21)
      COMMON /THERM/ CPWDZ,TZ,TZZ,TIN
      COMMON /ENV/ PSURF,WB,NDF,BETD(20),WD(20),WDENV,H,HI,
     * HA,HAC,HIAC,TINF
      COMMON /SURFP/ NAT,RTFP(10),AT(10),ALCOV(10),NRH,RTAR(10),RHO(10),
     *NAL,RTAB(10),ALPH(10),AES,FSLAB,FRP1,FRC1,FRP2,FRC2,FSEL,FSELC
      COMMON /CNET/ CP4D,QDSUM,TOUT
      COMMON /STRT/ INIT1,INIT2,INIT3,INIT4
      DIMENSION TPI3(21)
      IF (INIT4.EQ.1) GO TO 6
      INIT4=1
```

```
      NA=2*NAB+1
      SUMX=NA*(TZZ-TZ)
      DO 1 I=1,NA
      TP(I)=TZZ
      TPI3(I)=(273.+TP(I))**3
    1 CONTINUE
    6 CONTINUE
      SUM=0.
      DO 2 I=1,NA
      SUM=SUM+AMIN1(AMAX1(TP(I)-TZ,0.),TZZ-TZ)
    2 CONTINUE
C   COMPUTE AMOUNT OF COOLANT THERMOSTAT MAKES AVAILABLE
      CPMD=CPMDZ*SUM/SUMX
      DENOM=AMAX1(SUM,0.01)
      SUMT=0.
      QDSUM=0.
C   COMPUTE FRACTION OF COOLANT AVAILABLE FLOWING
C   THROUGH INDIVIDUAL ABSORBER CELLS
      DO 3 I=1,NA
      F(I)=AMIN1(AMAX1(TP(I)-TZ,0.),TZZ-TZ)/DENOM
      QNET(I)=CPMD*F(I)*(TP(I)-TIN)
      QDSUM=QDSUM+QNET(I)
      CONV(I)=HA*(TP(I)-TINF)
      RAD(I)=AES*(TP(I)+273.)*TPI3(I)
      R=QNET(I)-QDIN(I)+CONV(I)+RAD(I)
      ZZ=AMAX1(TP(I)-TIN,0.)/DENOM
      IF (SUM.EQ.0.) ZZ=0.
      DTP=R/(CPMD*(ZZ+F(I))+HA+4.*AES*TPI3(I))
      SUMT=SUMT+DTP*DTP
C   CELL TEMPERATURES
      TP(I)=TP(I)-DTP
      TPI3(I)=(273.+TP(I))**3
    3 CONTINUE
      TEST=SQRT(SUMT)
      IF (TEST.GT.0.01) GO TO 6
      IF (SUM.EQ.0.) GO TO 5
C   COOLANT EXIT TEMPERATURE
      TOUT=QDSUM/CPMD+TIN
      RETURN
C   THERMOSTATS ARE ALL CLOSED--NO COOLANT FLOW
    5 QDSUM=0.
      TOUT=TIN
      RETURN
      END

      SUBROUTINE FPABS
C
C   MAINTAINS ENERGY BALANCE BETWEEN INCIDENT ENERGY AND
C   LOSSES FOR FLAT PLATE COLLECTOR
C
      COMMON /ENV/ PSURF,WB,NDF,BETD(20),WD(20),WDENV,H,HI,
     * HA,HAC,HIAC,TINF
      COMMON /FPABSR/ TPL,F,QDIN,TC,QDINC,CONV,RAD
      COMMON /THERM/ CPMDZ,TZ,TZZ,TIN
      COMMON /SURFP/ NAT,BTFP(10),AT(10),ALCOV(10),NRH,BTAR(10),RHO(10),
     *NAL,BTAB(10),ALPH(10),AES,FSLAB,FRP1,FRC1,FRP2,FRC2,FSEL,FSELC
      COMMON /QNET/ CPMD,QNET,TOUT
      IF (TPL.NE.TIN) GO TO 1
      TOUT=TZZ
      TC=TZ
```

```
      HHIAC=HAC+HIAC
      FRC21=FRC2+FRC1
      FRP21=FRP2-FRP1
    1 CONTINUE
C   COMPUTE AMOUNT OF COOLANT THERMOSTAT MAKES AVAILABLE
      F=AMIN1(AMAX1(TOUT-TZ,0.),TZZ-TZ)/(TZZ-TZ)
      CPMD=CPMDZ*F
      QDNET=CPMD*(TOUT-TIN)
      CONV=HIAC*(TOUT-TC)
      TO3=(TOUT+273.)**3
      TC3=(TC+273.)**3
      RAD=FRP1*TO3*(TOUT+273.)-FRC1*TC3*(TC+273.)
      RP=QDNET-QDIN+CONV+RAD
      ZZ=AMAX1(TOUT-TIN,0.)/(TZZ-TZ)
      DPP=CPMDZ*(ZZ+F)+HIAC+4.*FRP1*TO3
      DPC=-HIAC-4.*FRC1*TC3
      CONVC=HAC*(TC-TINF)-CONV
      RADC=FRC2*TC3*(TC+273.)+FRP2*TO3*(TOUT+273.)-RAD
      RC=-QDINC+CONVC+RADC
      DCP=-HIAC+4.*FRP21*TO3
      DCC=HHIAC+4.*FRC21*TC3
      DET=DPP*DCC-DCP*DPC
      DTO=(DCC*RP-DPC*RC)/DET
      DTC=(-DCP*RP+DPP*RC)/DET
C   GLASS COVER AND PLATE TEMPERATURE
      TC=TC-DTC
      TOUT=TOUT-DTO
      TEST=SQRT(DTO*DTO+DTC*DTC)
      IF (TEST.GT.0.001) GO TO 1
      TPL=TOUT
      IF (F.GT.0.) RETURN
C   THETMOSTAT IS CLOSED--NO COOLANT FLOW
      TOUT=TIN
      RETURN
      END

      SUBROUTINE LINT(N,X,A,B,Y)
C   LINEAR INERPOLATION FROM TABLES
      DIMENSION A(1),B(1)
      IF (N) 10,10,11
   11 DO 12 J=2,N
      I=J
      IF (X-A(J)) 13,13,12
   12 CONTINUE
   13 IF(A(I).EQ.A(I-1)) GO TO 19
      Y=B(I-1) + (X-A(I-1)) *(B(I)-B(I-1))/(A(I)-A(I-1))
      RETURN
   10 Y=0.0
      RETURN
   19 Y=B(I-1)
      RETURN
      END
```

REFERENCES

1. Chrysler Corporation. Space Division. "Development of a Solar Powered Residential Air Conditioner (Generator Optimization)." Final Report to George C. Marshall Space Flight Center in fulfillment of contract NASA-31437. March 1976.

2. Wood, Bernard D. Applications of Thermodynamics. Reading, Mass.: Addison-Wesley Publishing Co., Inc., 1969.

3. Duffie, John A., and Beckman, William A. Solar Energy Thermal Processes. New York: John Wiley and Sons, 1974.

4. Baumeister, Theodore D. Marks' Standard Handbook for Mechanical Engineers. 7th Ed. New York: McGraw-Hill Book Co., 1967.

5. Sears, Francis W., and Zemansky, Mark W. University Physics. 4th Ed. Reading, Mass.: Addison-Wesley Publishing Co., Inc., 1970.

6. Meyer-Arendt, Jurgen R. Introduction to Classical and Modern Optics. Englewood Cliffs, N.J.: Prentice-Hall, Inc., 1972.

7. Siegel, Robert, and Howell, John R. Thermal Radiation Heat Transfer. New York: McGraw-Hill Book Co., 1972.

8. Threlkeld, James L. Thermal Environmental Engineering. 2nd Ed. Englewood Cliffs, N.J.: Prentice-Hall, Inc., 1970.

9. Holman, J. P. Heat Transfer. 3rd Ed. New York: McGraw-Hill Book Co., 1972.

10. Angrist, Stanley W. Direct Energy Conversion. Boston, Mass.: Allyn and Bacon, Inc., 1976.